

Hillslope hydrological modeling

**the role of bedrock geometry and hillslope-stream
interaction**

promotoren: Prof. dr. ir. P.A. Troch
Professor of Hydrology and Water Resources
University of Arizona, USA

Prof. dr. ir. R. Uijlenhoet
Hoogleraar Hydrologie en Kwantitatief Waterbeheer
Wageningen Universiteit

co-promotor:
Drs. P.J.J.F. Torfs
Universitair docent, leerstoelgroep Hydrologie en
Kwantitatief Waterbeheer
Wageningen Universiteit

Samenstelling promotiecommissie:

prof. dr. ir. S.E.A.T.M. van der Zee, Wageningen Universiteit
prof. dr. ir. N.E.C. Verhoest, Universiteit Gent, België
prof. dr. ir. M.F.P. Bierkens, Universiteit Utrecht
prof. dr. S. Uhlenbrook, UNESCO-IHE Delft

Dit onderzoek is uitgevoerd binnen de onderzoekschool WIMEK-SENSE.

Hillslope hydrological modeling
**the role of bedrock geometry and hillslope-stream
interaction**

Kaka Shahedi

Proefschrift

ter verkrijging van de graad van doctor
op gezag van de rector magnificus
van Wageningen Universiteit,
Prof. dr. M.J. Kropff,
in het openbaar te verdedigen
op woensdag 18 juni 2008
des namiddags te vier uur in de Aula

Shahedi, Kaka

Hillslope hydrological modeling: the role of bedrock geometry and hillslope-stream interaction

Keywords: Hillslope hydrology, hydrological modeling, bedrock geometry, boundary condition, numerical solution

PhD-thesis, Hydrology and Quantitative Water Management group, Wageningen University and Research Center, Wageningen, The Netherlands.

ISBN: 978-90-8504-945-6

"... رب زدنی علما"

"... O my Lord!, advance me in knowledge."

(QS 20 Taahaa: 114)

***To my father N. Shahedi
who could not see this work completed
To my mother, my beloved family
and all my teachers***

Abstract

Shahedi, K. 2008. *Hillslope hydrological modeling: the role of bedrock geometry and hillslope-stream interaction*, Ph.D. thesis, Wageningen University, Wageningen, The Netherlands.

This thesis focuses on hillslope subsurface flow as a dominant control on the hydrological processes defining the catchment response to rainfall. Due to the difficulties associated with the three-dimensional equations, both in complexity and regarding the computational demand, focus is on 1D physically-based hillslope groundwater flow models. The main core of this research is to study how the simulated hillslope response, and specifically runoff generation, is affected by different simplifying assumptions concerning hillslope geometry and boundary conditions.

Several generalizations have been made to incorporate the complexity of bedrock geometry in models of the hillslope hydrological response. In order to handle and compare these different models, a general and flexible numerical algorithm has been developed. Through the proposed numerical scheme several applications of these models are performed: (a) to investigate the role of the hillslope lower boundary condition on the groundwater response, (b) to study the role of bedrock geometry on the hillslope hydrological response, and (c) to approximate the hillslope response using the quasi-steady state approximation. Evaluation of the numerical scheme shows that it is flexible and capable to handle all these different models, which have been applied for different purposes, and that the mass balance is preserved.

Evaluation of the developed models leads to the following general conclusions: (a) A head-discharge relationship as the hillslope lower boundary condition is a proper approach to model the coupled hillslope-stream system; (b) The recession characteristics of hillslopes depend on their bedrock profiles and local minima and maxima in the curved bedrock profile influence the groundwater head for small rainfall intensities; (c) The quasi-steady state approximation proves to be a simple but adequate method (both as a model and regarding computation time) to simulate the groundwater dynamics of hillslopes.

In summary, this thesis aims to understand theoretically how hydrological processes (subsurface flow and water table dynamics) react to bedrock complexity and the hillslope lower boundary condition. The presented numerical scheme can be applied in many investigations of hillslope hydrology because of its generality and flexibility.

Keywords: *Hillslope hydrology, hydrological modeling, bedrock geometry, boundary condition, numerical solution.*

Acknowledgement

Above all, I would like to express my gratitude and praises to great Allah for all good graces and mercies He granted me, *Alhamdulillah*. I would like to extend my thanks to all people whom Allah made available to ease my stay and to support and guide my family and me during our stay in the Netherlands. Therefore, I consider my work is incomplete without these acknowledgments.

First, I am grateful of the Ministry of Science, Research, and Technology (MSRT) of Iran for granting me a four-year scholarship to follow my PhD study abroad.

I am deeply indebted to my first promoter, Prof. Dr. Peter Troch for giving me the opportunity to do my PhD in the Hydrology and Quantitative Water Management group. I appreciate his inspiring guidance which kept me on the right way to the planned destination of PhD promotion. Your comprehensive guidelines and support in all steps of my research enabled me to follow and finally get the job done. Thank you for everything.

My special thanks go to my second promoter, Prof. Dr. Remko Uijlenhoet for his intellectual ideas, and valuable guidance. Dear Remko, you gave all due attention to my work especially in final stages of my PhD despite the limited time you had. I deeply thank you.

I would like to extend my sincere appreciation to the person most involved in this dissertation, my daily supervisor Drs. Paul Torfs, for his brilliant guidance, excellent ideas, and invaluable support. Dear Paul, without your guidance the study would have been far more difficult and perhaps even impossible. I will not forget your help, and I deeply thank you for everything.

I would like to express my sincere gratitude to Prof. Dr. Rik Leemans (Director of WIMEK) who helped me when I was involved in some problems during my PhD project.

I sincerely acknowledge Dr. Emiel van Loon, who was the first person in the HWM group with whom I communicated. He arranged all preliminary affairs before my arrival to the Netherlands.

I would like also to thank all colleagues and staff members in the HWM group (especially Arno, Hidde, Patrick, and Ruud) and my roommates (Ali, Anne, Claudia, Marie, Pieter and Darina) for providing a nice atmosphere for work and discussion. I learned a lot from you and enjoyed all the conversations we had on work, life and personal matters. My special thanks go to Henny and Annemarie, always ready to translate so many letters which I was receiving in the Dutch language.

I would like to take the opportunity to express my gratitude to all members of the Iranian student community here in Wageningen. My special thanks go to Majid, Vahedberdi, Mohammad Reza, Mostafa, Morteza, Mahdi, Mahmud, Mohammadali, Reza, Afshin, Hedayat and their families. I would also like to thank Mohammad Kazem to help on the layout of the book. Having so many Iranian friends here, I and my family rarely felt homesick.

I would like to thank our friends, Afshin, Mercedeh, Mohsen and Sara who were always ready to help during our stay in here. Dear friends, we will not forget your valuable helps.

Finally, last but not least, I am extremely grateful to my wife Oghol Bibi and my children Ainaz, Mohammad Reza, and Mohammad Hanif. I am quite sure that it would not have been possible to accomplish my PhD, without benefiting from their patience, tolerance, good willing, and emotional support. My dears, I would like to say THANK YOU for everything.

Kaka Shahedi, Wageningen, 18th June 2008

Contents

Part	Title	Page
Chapter 1	Introduction	
1.1	Background	3
1.2	Objectives	4
1.3	The hillslope models	5
1.3.1	The Dupuit model	7
1.3.2	The Boussinesq equation	9
1.3.3	The extended Boussinesq equation	13
1.3.4	Bedrock with general geometry	13
1.3.5	The extended Boussinesq based on the slanted Dupuit assumption	14
1.3.6	The extended Boussinesq based on the curved Dupuit assumption	17
1.3.7	Remark on the position of the groundwater table	20
1.4	Parameterization of boundary conditions	21
1.5	Conclusions	22
1.6	Outline of thesis	22
Chapter 2	The numerical solution algorithm	
2.1	Introduction	27
2.2	The general steady state equation	27
2.2.1	The hillslope steady state equations	28
2.3	Linearization	30
2.3.1	Solution of the non-linear equations	30
2.4	Construction of linearization	31
2.4.1	Taylor approximation	32
2.4.2	Ad hoc method	32
2.4.3	Other linearization methods	33
2.5	Spatial discretization	33
2.5.1	Discretization of internal flux	34
2.5.2	Discretization of external flux	34
2.6	Discrete equations	35
2.6.1	The balance equations	35
2.6.2	The boundary conditions	35
2.6.3	Total system of equations	36
2.7	Solution procedure of the general unsteady equations	36

Part	Title	Page
Chapter 3	The role of hillslope lower boundary condition on groundwater response	
3.1	Introduction	43
3.1.1	The downhill boundary condition and the backwater effect	43
3.2	Modeling setup	45
3.2.1	Boundary conditions	45
3.2.2	Short discussion on the third type of boundary condition	46
3.3	Numerical simulations	48
3.3.1	Examples of non-linear equations for the lower boundary condition	49
3.3.2	Taylor approximation	49
3.3.3	Ad hoc method	50
3.3.4	Piecewise linear boundary condition	51
3.4	Results and discussion	51
3.4.1	Mass balance check	52
3.4.2	Comparison of the outflow hydrographs of model 1 and model 2	52
3.4.3	Construction of the $Q-h$ boundary condition	53
3.4.4	Effect of the boundary condition	54
3.4.5	Numerical instability and time step choice	55
3.4.6	The length of temporal period	55
3.5	Conclusions	61
Chapter 4	The role of bedrock geometry on hillslope hydrological response	
4.1	Introduction	65
4.2	Governing equations	66
4.2.1	The differential equations	66
4.2.2	Bedrock geometry	66
4.2.3	Initial and boundary conditions	67
4.2.4	Parameters	67
4.3	Numerical simulation setup	68
4.4	Problems associated with numerical solution	70
4.5	Results and discussion	71
4.5.1	Influence of rainfall intensity on groundwater flux	71
4.5.2	Influence of different types of bedrock profiles	73
4.5.3	Bedrock profile and groundwater flux	76
4.5.4	Influence of bedrock profile convexity and concavity	78

Part	Title	Page
4.6	Conclusions	83
Chapter 5	Lumping the hillslope hydrological model through a quasi-steady state approach	
5.1	Introduction	87
5.2	Setup	88
5.3	Solution procedure of QSS approximation	89
5.3.1	Steady state storage-discharge relation	89
5.3.2	QSS approximation	89
5.4	Results and discussion	91
5.4.1	Storage-outflow ($S - Q$) relationship	91
5.4.2	QSS approximation in different cases	92
5.4.3	Effect of time step	96
5.4.4	The mass balance check	96
5.4.5	Further test of QSS approximation	100
5.5	Conclusions	100
Chapter 6	Summary and conclusions	
6.1	Overview	105
6.2	Ideas for future research	106
	Appendices	109
	References	118
	Curriculum vitae	123
	SENSE certificate	124
	Summary in Dutch	126
	Summary in Persian	127

List of symbols

Symbol	Description	Dimension	Formula
A	Matrix of the coefficients of the equations	-	Section 2.6.3
A_{md}, A_{ld}, A_{ud}	Main diagonal, lower diagonal and upper diagonal elements of matrix A	-	Appendix D
b	Vector of known right hand side	-	Section 2.6.3
b, b'	Elevation of bedrock measured vertically and its derivative	L, (-)	Sections 1.3.5, 1.3.6, 2.2.1.4, and 2.2.1.5.
BC_L, BC_R	Left and right hand side boundary conditions	L or L ³ /T	-
f	Effective drainable porosity	-	$f = \theta_s - \theta_r$ where θ_s is saturated soil moisture content, and θ_r is the residual soil moisture.
h	Vector of unknown variable	-	Section 2.6.3
h	Water table height	L	-
$h(x_L, t),$ $h(x_R, t)$	Head terms of boundary condition	L	-
\hat{h}	Used to solve non-linear set of equations by relaxation factor	L	Section 2.3.1
i, j	Index for space and time, respectively	-	-
K_u	Unsaturated hydraulic conductivity	L/T	-
K_s	Saturated hydraulic conductivity	L/T	-
L	Hillslope length	L	-
M, U, L, Z	Vectors constructed to calculate h	-	Appendix D
N	External flux (recharge)	L/T	-
N_{nl}	Non-linear external flux	L/T	Equation 2.3
q_x	Specific discharge in 'x' direction	L/T	$q_x = -K \cdot \nabla \phi$
q_y	Specific discharge in 'y' direction	L/T	$q_y = -K \cdot \nabla \phi$
q_z	Specific discharge in 'z' direction	L/T	$q_z = -K \cdot \nabla \phi$
q_0, q_l, q_r	Three terms to calculate flux	L/T	Equation 2.52
Q	Total flux through a vertical unit-width surface (e.g., in Dupuit assumption)	L ² /T	$= q_x(x, t) \int_0^{h(x, t)} dZ$ $= -K_s(x) h(x, t) \frac{\partial h}{\partial x}(x, t)$
Q_{nl}	Non-linear internal flux	L ³ /T	Equation 2.2

Symbol	Description	Dimension	Formula
$Q(x_L, t),$ $Q(x_R, t)$	Flux terms of boundary condition	L^3/T	-
t	time	T	-
$\hat{t}, \hat{h}, \hat{Q}, \hat{N}$	Used to solve non-linear set of equations in unsteady case	T, L, L^3/T , L/T	Section 2.7
w	Hillslope width function	L	exB equation
x	Horizontal coordinate	L	-
y	Horizontal distance from slope center	L	-
Z	Coordinate perpendicular to the 'X' axis in a sloping bed	L	$z = Z \cos i$
z	As vertical coordinate (positive upward)	L	-
α	Constant coefficient	-	Appendix B
β	Bedrock slope angle	-	-
α_b, β_b	Constant coefficients	-	Chapter 3
$\alpha_L, \beta_L, \gamma_L$	Elements to construct left side boundary condition	$1/L, T/L^3, -$	Equation 2.45
$\alpha_R, \beta_R, \gamma_R$	Elements to construct right side boundary condition	$1/L, T/L^3, -$	Equation 2.45
δ, δ'	Implicitness factor of numerical solution in unsteady case	-	Section 2.7
ε		-	Chapter 1
ζ	Elevation (curved Dupuit assumption)	L	-
η	Transformed variable of h	-	Appendix B
θ	Soil moisture content	-	$\theta = \frac{V_w}{V_s}$
κ_B	Bedrock profile curvature	-	$\beta(x) = \frac{d\beta}{dx}(x) = \kappa_B(x)$
λ	Angle (circle)		Section 1.3.7
ϕ	Total (piezometric) head	L	$\phi = z + \frac{p}{\gamma}$
ψ	pressure head	L	$\psi = \frac{p}{\gamma}$
ω_r	Relaxation factor	-	Section 2.3.1
ω	Constant slope angle	-	-

Chapter 1

Introduction

1.1 Background

Catchment hydrological processes control runoff generation and its transportation to the catchment outlet. Catchments as a management unit of landscapes play a key role in decision making and natural resources management. Hence, exploring the hydrological processes underlying catchment responses is an important issue.

Hillslopes can be considered as the basic elements of catchments (Hilberts, 2006). To explore the mechanism of catchment hydrological processes, many studies have focused on hillslope hydrology (e.g., Troch et al., 2003; Berne et al., 2005). Hillslope hydrology involves several mechanisms for runoff generation: infiltration excess runoff or Hortonian flow (Horton, 1933), saturation excess runoff originating from the variable source area concept (e.g., Hewlett and Hibbert, 1967; Freeze, 1972; Dunne et al., 1975), return flow (Dunne and Black, 1970), and macropore flow (Beven and Germann, 1982). Studies especially since the 1960's improved the understanding and mathematical description of water flow processes.

Mathematical models of hillslope flow processes were presented in two prominent books edited by Kirkby (1978) and Anderson and Brooks (1996). Neither of these references presents models to account for the 3-D hillslope form while still using simple flow equations (Troch et al., 2003). This motivated Troch et al. (2003) to derive the hillslope-storage Boussinesq (hsB) equation based on the Boussinesq equation and soil moisture storage capacity function of Fan and Bras (1998), which reduces the 3-D soil mantle into a 1-D drainable pore space profile. The major advantage of this formulation is that the interaction between hillslope shape and hydrological response can be quantified easily (Hilberts, 2006).

The hillslope geometry influences the hydrological response due to the role of geometry in defining the domain and boundary conditions of moisture storage (Troch et al., 2003). Studies of the spatial variability of subsurface flow (e.g., Anderson and Burt, 1978; Huff et al., 1982; McDonnell, 1990; Woods et al., 1997) indicate the importance of topography. McDonnell et al. (1996) and Freer et al. (1997) claimed that for describing the water flow paths the bedrock surface topography may be more important than the surface topography. Recharge-induced groundwater flow over a plane sloping bed has been the subject of continuing development since the classic works of Dupuit (1863) and Boussinesq (1877) (Chapman, 2005). For the original application to the location of drains on a sloping impermeable bed, the assumption of a plane bed was appropriate, but at the scale of more recent applications in hillslope hydrology, a plane bed must be seen as a poor representative of a typical hillslope profile (Chapman and Ong, 2006). Troch et al. (2003) and Hilberts et al. (2004) demonstrated that (numerical) solutions of the hsB equation are able to account explicitly for plan shape (by the hillslope width function) and profile curvature (local bedrock slope angle and hillslope soil depth function) of the hillslope.

However, most simplified hydraulic groundwater models (e.g., Hilberts et al., 2004; Chapman and Ong, 2006) which consider the geometry of the bedrock profile, are based on the standard

(classic*) Dupuit assumption; they do not account for complexity of the bedrock profile. Thus, simple but physically realistic alternative parameterizations are needed that represent hydrological processes at the hillslope and catchment scales, and that account for complex bedrock profiles and different types of boundary conditions.

1.2 Objectives

The objective of this thesis is to study how simulated hillslope response, and specifically runoff generation, is affected by different simplifying assumptions concerning hillslope geometry and boundary conditions. Assuming that runoff processes are mainly driven by topography, catchments can be divided into different hillslopes (Figure 1.1). The procedures that can be used to perform such a division into hillslopes remain undiscussed in this work; we refer the reader to Fan and Bras (1998) and Bogaart and Troch (2006) for more information on this subject. However, in this work we will assume that the hillslopes are chosen in such a way that the groundwater flow through each slope is essentially one-dimensional downhill.

The ultimate goal of this line of research is to make a rainfall-runoff model for the entire catchment. Each hillslope is thought to contribute independently to this process: all the rain falling on a particular hillslope will be transformed by that same hillslope model into discharge to its corresponding river section. The study of some of these hillslope processes will form the subject of this work. The channel routing process is beyond the scope of this thesis. We want these hillslope models to be both practical and as much as possible physically based. The practical consideration results in the choice of a one-dimensional representation. To give the models a physical base a hydraulic groundwater flow model will be used, for which as much as possible information will be derived from the topography alone.

Even with these restrictions many different models can be formulated, as will be shown in Section 1.3. All these models have their own geometrical-physical assumptions, resulting in mathematical differential equations that differ in complexity. One of the objectives of this work is to compare these models. As all these differential equations are non-linear, they can only be solved numerically. In order to be able to compare these different models, as independent from the numerical aspects as possible, a general numerical scheme will be used that allows within one and the same framework to study the solutions of different differential equations, including the consequences of different forms of linearization. Chapter 2 will present this numerical approach. In the following chapters (3, 4, and 5) this methodology will then be used to compare the different hillslope models.

* For non-standard Dupuit assumption see Sections 1.3.5 and 1.3.6.

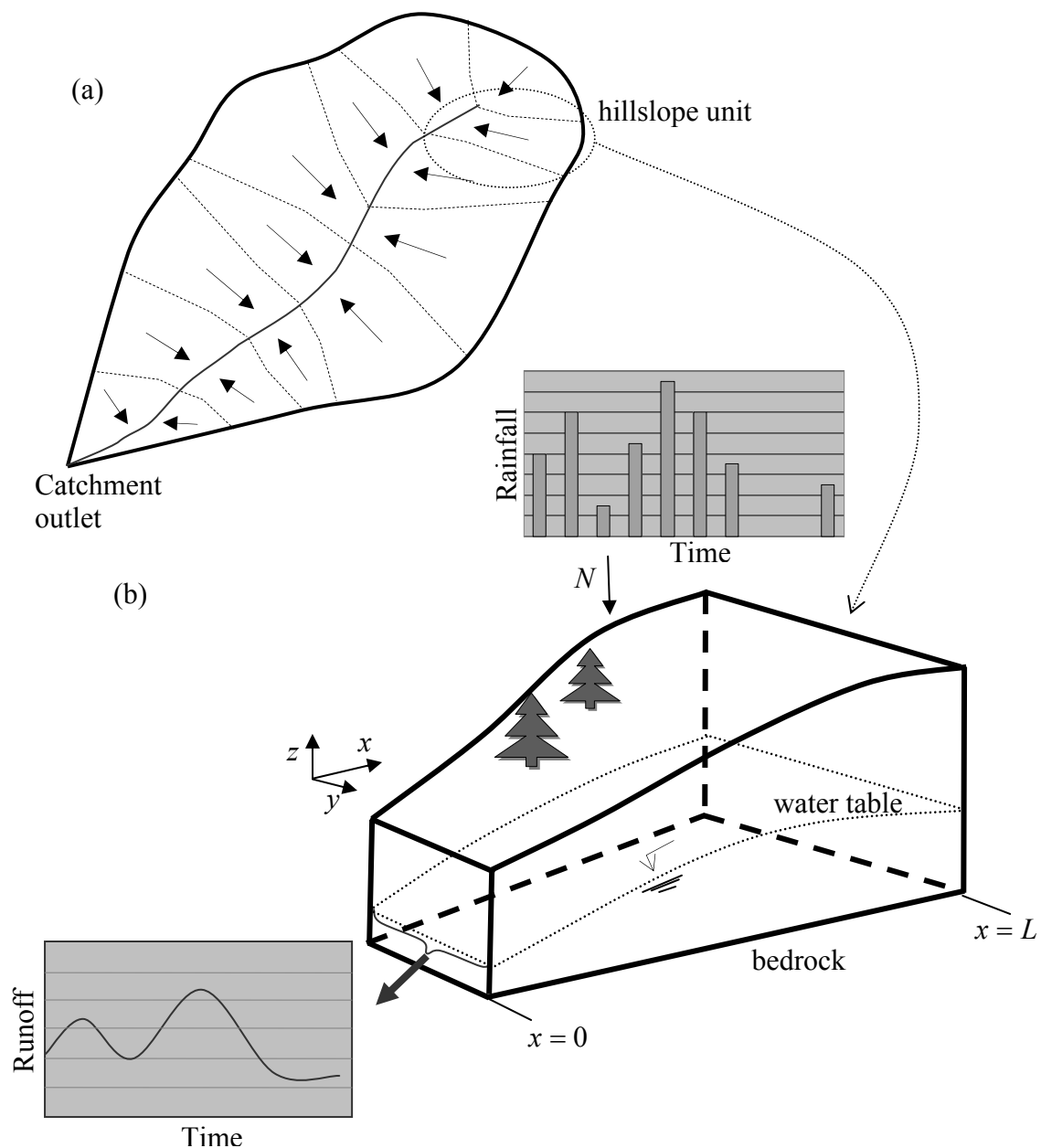


Figure 1.1: A schematic view of (a) a catchment with its hillslope units (arrows show general flow direction into stream), and (b) input and output of a hillslope unit.

1.3 The hillslope models

If we neglect overland flow, the whole hillslope process can be described by a combined saturated-unsaturated groundwater model. The fundamental equation for this is the Darcy equation:

$$\begin{pmatrix} q_x \\ q_y \\ q_z \end{pmatrix} = -K(x, y, z, \Psi) \begin{pmatrix} \frac{\partial \Psi}{\partial x} \\ \frac{\partial \Psi}{\partial y} \\ \frac{\partial(\Psi + z)}{\partial z} \end{pmatrix} \quad (1.1)$$

In this formula:

- q_x, q_y, q_z are the specific discharge components of the water flow through the soil in the x, y and z directions.
- $\Psi(x, y, z)$ is the pressure head.
- $K(x, y, z, \Psi)$ is the soil hydraulic conductivity that is assumed to be isotropic.

Combing the Darcy with the continuity equation results in the Richards equation:

$$\frac{\partial \theta(\Psi)}{\partial t} = \frac{\partial q_x}{\partial x} + \frac{\partial q_y}{\partial y} + \frac{\partial q_z}{\partial z} \quad (1.2)$$

where θ is the soil moisture content.

These equations are too difficult for a hillslope model as introduced in the previous section:

- They are three-dimensional, and require as such a considerable numerical effort to be solved. This three-dimensionality is in contrast with the conceptual view that the flow through the hillslope is dominantly one-dimensional downhill.
- The inclusion of the unsaturated zone also introduces unwanted complexity. Due to the high non-linearity of the unsaturated flow, much of the numerical effort to solve these equations will be spent on this part. The fact that the unsaturated flow will be mostly vertical also makes that it does not form the dominant part in the one-dimensional downhill runoff process.

In the remaining part of this thesis, both the overland flow and the unsaturated flow will be neglected. As only saturated groundwater will be considered, we will express all pressure-related terms in the total head: $\phi(t, x, y, z) = \Psi(t, x, y, z) + z$ and consider only z lower than the saturated groundwater table. The Darcy formula now reads:

$$\begin{pmatrix} q_x \\ q_y \\ q_z \end{pmatrix} = -K_s(x, y, z) \begin{pmatrix} \frac{\partial \phi}{\partial x} \\ \frac{\partial \phi}{\partial y} \\ \frac{\partial \phi}{\partial z} \end{pmatrix} \quad (1.3)$$

where K_s is the saturated conductivity.

Also these three-dimensional groundwater models are considered to be too complex to be an efficient hillslope model. This section presents various one-dimensional approximations, varying in the underlying assumptions.

The next sub-section introduces a very basic one-dimensional saturated groundwater model, the so called Dupuit model. Where the full Richards model was too complex, this model is too

simple to serve as a hillslope model. Here it is used as a starting point, and subsequent sections will relax the most unrealistic assumptions.

1.3.1 The Dupuit model

The simple Dupuit model that will be used as the starting point for the other derivations can be introduced with the help of Figure 1.2. The left of this figure shows a section of the river which will eventually drain all water from the model. This river section is assumed to be straight (in the y -direction) and to have a constant (both in time and space) horizontal water level h_R . The area draining into this river section is modelled as a rectangle orthogonal to the river section (in the x -direction) with a length L . The line $z = 0$ is both the bottom of the river and the impermeable boundary underneath the phreatic groundwater table. The soil physical properties are assumed to be uniform and isotropic.

Due to the assumed uniformity in the y -direction, pressure and groundwater table do not depend on y , and there is no flux in that direction, so that the Darcy equation simplifies to:

$$\begin{pmatrix} q_x \\ q_z \end{pmatrix} = -K_s(x, z) \begin{pmatrix} \frac{\partial \phi}{\partial x} \\ \frac{\partial \phi}{\partial z} \end{pmatrix} \quad (1.4)$$

A Dupuit model is defined by accepting the following equivalent statements:

- All flow is horizontal.
- There is no flux in the vertical direction, i.e. $q_z = 0$.
- Groundwater head is constant in the vertical: $\frac{\partial \phi}{\partial z} = 0$, and thus also $\phi(t, x, z) = h(t, x)$.

Figure 1.3 illustrates the flux aspects of the Dupuit assumption. It also illustrates (Figure 1.3.b) that the Dupuit assumptions are in many cases acceptable in a large part of the domain, but are seldom satisfied throughout the whole domain: near the extremes (outlet and hillslope divide) flow lines tend to have a vertical component. In this work the modeling will be done by accepting them valid throughout the whole domain, as illustrated by Figure 1.3.c. In the following sections the uniform validity of the assumptions will be accepted without discussion.

With this Dupuit assumption and neglecting the possible dependency on y and z , the flux is

given by:

$$q_x(x, y, z, t) = -K_s(x) \frac{\partial \phi}{\partial x}(x, z) = -K_s(x) \frac{\partial h}{\partial x}(x) \quad (1.5)$$

With the help of this, the volume balance for a vertical slice through x (see Figure 1.3.c) can be written as:

$$\begin{aligned} \frac{\partial}{\partial t} \int_0^{w(x)} dy \int_0^{h(x,t)} dz f(x, y, z) &= -\frac{\partial}{\partial x} \int_0^{w(x)} dy \int_0^{h(x,t)} dz q_x(x, y, z, t) + \int_0^{w(x)} dy N(x, y, t) \\ \Leftrightarrow \frac{\partial}{\partial t} \int_0^{w(x)} dy \int_0^{h(x,t)} dz f &= -\frac{\partial}{\partial x} \int_0^{w(x)} dy \int_0^{h(x,t)} dz \left(-K_s(x) \frac{\partial h}{\partial x}(x, t) \right) + \int_0^{w(x)} dy N(x, y, t) \end{aligned}$$

$$\Leftrightarrow w(x) f \frac{\partial h}{\partial t}(x, t) = \frac{\partial}{\partial x} \left(w(x) K_s(x) h(x, t) \frac{\partial h}{\partial x}(x, t) \right) + w(x) N(x, t) \quad (1.6)$$

where f is effective drainable porosity*, w is width, and N represents external flux.

The boundary conditions are given by the water level of the river and the fact that the right hand side is a water divide:

$$\begin{cases} h(t, 0) = h_R \\ q_x(t, L) = 0 \end{cases} \quad (1.7)$$

This model maybe useful as part of a runoff model for flat catchments, but certainly lacks some important properties in order to be generally applicable:

- The “flat bottom” is not realistic in many cases.
- The Dupuit assumption should be adjusted for non-flat-bottom cases.
- The rectangular shape is unrealistic for almost all cases.
- The lower boundary condition is unrealistically simple.

In the following sections, we will relax these restrictions and replace them by more general ones, this however without changing the one-dimensionality of the model.

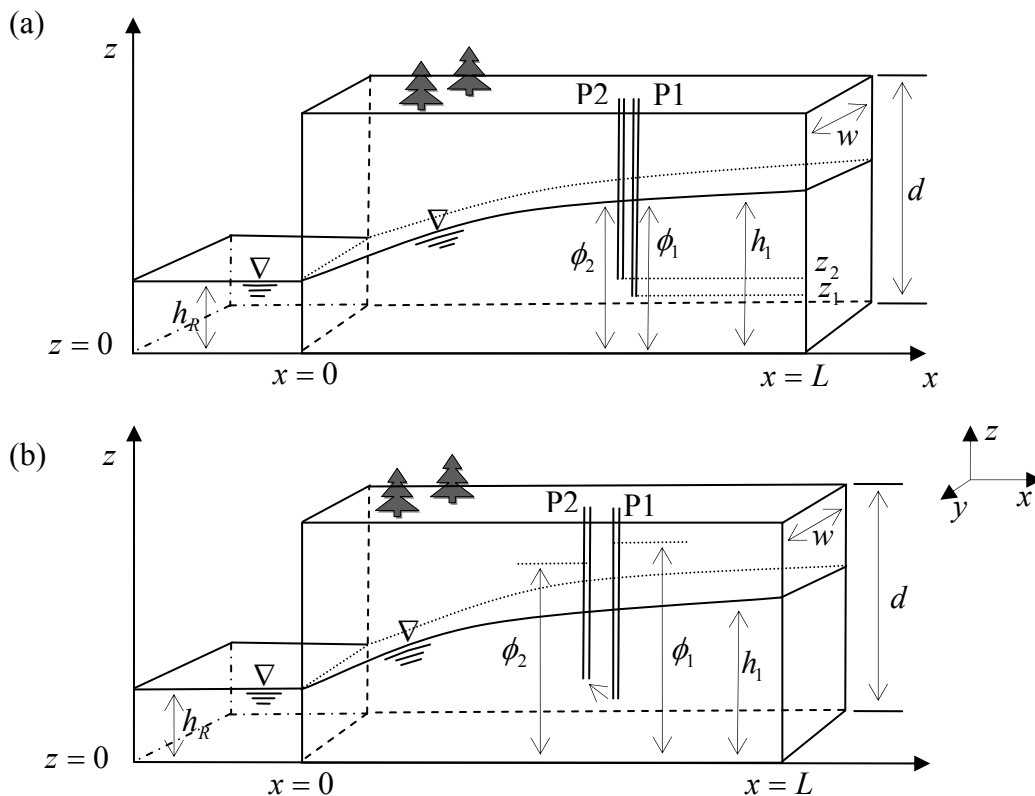


Figure 1.2: Schematic views of a hillslope satisfying the Dupuit assumption (a) and one where this is not the case (b). P1 and P2 are thought to be observation wells at the same spot in the plane but at different depths. When the Dupuit assumption is satisfied as in (a), they will yield the same potentials. In the non-Dupuit case this is no longer the case, and a higher potential from the deeper observation well as in (b) suggests an upward flux.

* The word ‘effective’ refers to the fact that above the saturated zone, the soil is partly saturated.

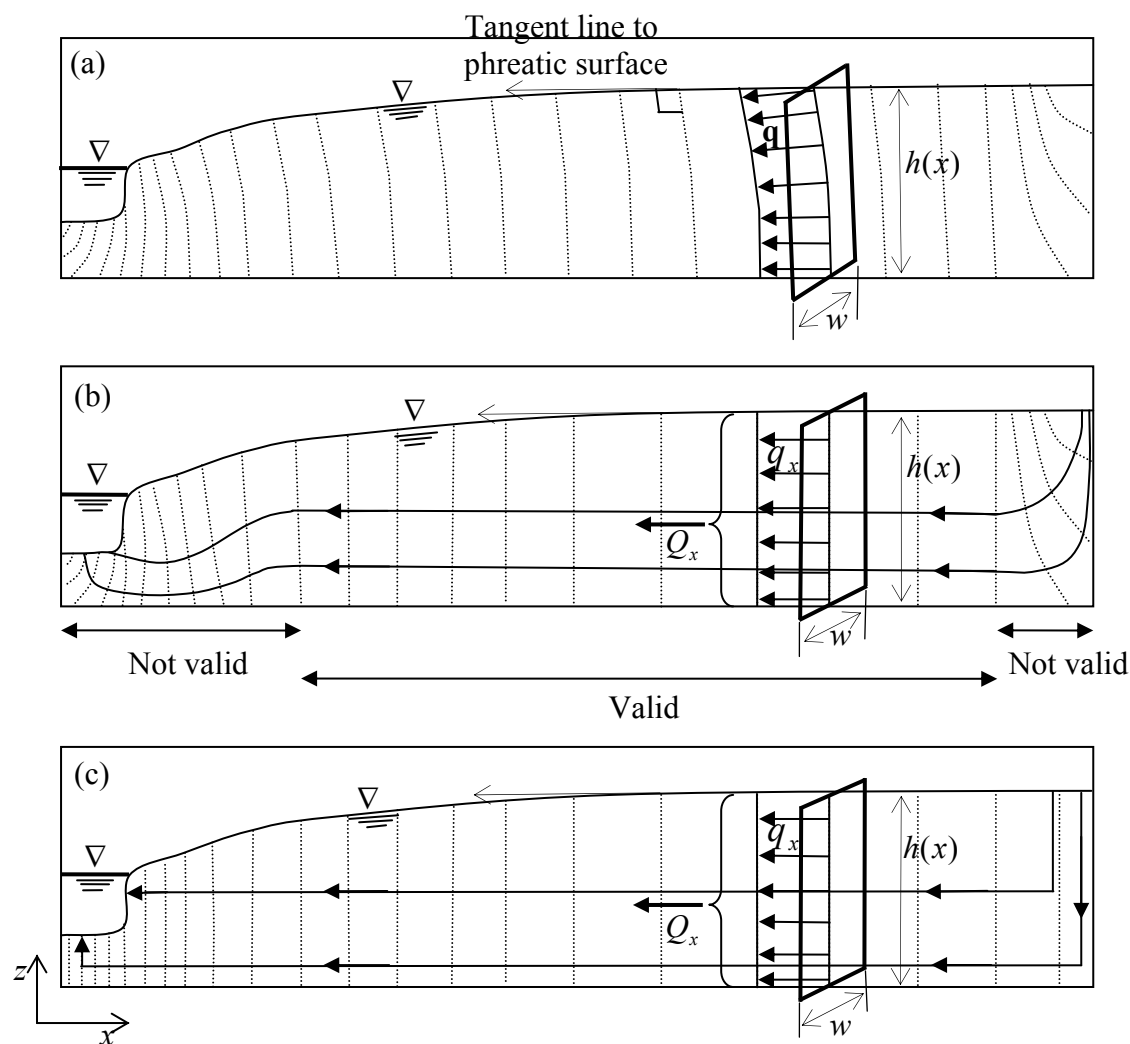


Figure 1.3: (a) View of regional flow system in a phreatic aquifer in non-Dupuit situation ($\mathbf{q} = \begin{pmatrix} q_x \\ q_z \end{pmatrix}$), which is added for comparison with 'b' and 'c', (b) flow system in a phreatic aquifer (where Dupuit assumption is valid, equipotentials are vertical, flow is horizontal, and specific discharge is uniform along the vertical), and (c) whole flow domain is under the Dupuit assumption except for left and right end point (Adapted from Bear and Verruijt, 1987).

1.3.2 The Boussinesq equation

The first assumption to be relaxed in the previous model is the flat bedrock bottom which will be replaced by one with a constant slope. For catchments where the rainfall runoff is driven by topography, this is certainly an important aspect. We may expect that in first order approximation the flow direction will follow that slope, so also this should change compared to the previous model. But in all other aspects the model of this section, e.g. the uniformity in the y -direction, will be similar to the Dupuit model. The resulting model is commonly known as the Boussinesq model (Boussinesq, 1877).

The equations will be derived starting from the notations as introduced in Figure 1.4. One of the important choices to be made in this context is the direction of the x -axis. It is tempting to choose this along the bedrock: the X in the figure. The direction orthogonal to this will be denoted by Z . As in the following sections even more general bedrock geometries will be introduced, and as we want to compare the models on the basis of their physical behavior and not their mathematical parameterization, this is not the choice of this work. So all the equations that follow, are expressed in terms of a fixed horizontal x -axis*. Similar remarks can be made for the z -axis.

We denote the (constant) angle of the bedrock by β . The elevation of the bedrock at any point x is thus given by $x \tan(\beta)$.

The Boussinesq model is defined by accepting the following equivalent statements:

- 1- All flow follows the bedrock, so is in the X -direction.
- 2- The groundwater head is constant in the Z -direction $\left(\frac{\partial \phi}{\partial Z} = 0\right)$ and there is no flow in this direction, i.e. $q_z = 0$.

Figure 1.4 illustrates the translation of these principles into formulas. Starting from a point x on the horizontal axis, all points on the line in the Z -direction on top of the bedrock point vertically above the x -point will have the same potential. The length along that line in the Z -direction starting from the bedrock to the groundwater table will be denoted by $h(t, x)$. At the groundwater surface, potential equals vertical elevation⁺:

$$\phi(x) = x \tan(\beta) + h(x) \cos(\beta) \quad (1.8)$$

Following Darcy, the flux in the X -direction is calculated by calculating the change of potential in that direction, so by:

$$\begin{aligned} q_x(x, t) &= -K_s(x) \lim_{\varepsilon \rightarrow 0} \left(\frac{\phi(x + \cos(\beta) \varepsilon, t) - \phi(x, t)}{\varepsilon} \right) \\ &= -K_s(x) \cos(\beta) \frac{\partial \phi}{\partial x}(x, t) \end{aligned} \quad (1.9)$$

Substitution of Equation 1.8 in Equation 1.9 results in:

$$\begin{aligned} q_x(x, t) &= -K_s(x) \cos(\beta) \left(\cos(\beta) \frac{\partial h}{\partial x}(x, t) + \tan(\beta) \right) \\ &= -K_s(x) \left(\cos^2(\beta) \frac{\partial h}{\partial x}(x, t) + \sin(\beta) \right) \end{aligned} \quad (1.10)$$

Total discharge through a surface in the Z -direction (perpendicular to the underlying impermeable layer as seen in Figure 1.5.a) is:

$$Q(x, t) = q_x(x, t) w(x) \int_0^{h(x, t)} dZ = -K_s(x) w(x) h(x, t) \left(\cos^2(\beta) \frac{\partial h}{\partial x}(x, t) + \sin(\beta) \right) \quad (1.11)$$

* This choice generates equations which differ from the ‘ x ’ choice, as e.g., in Hilberts, 2006.

⁺ Note that ‘ $\phi(x)$ ’ is not measured in a vertical above ‘ x ’. See also Section 1.3.7.

To derive the differential equation, we consider a control volume between two equipotential lines at $x - \frac{\Delta x}{2}$ and $x + \frac{\Delta x}{2}$ (see Figure 1.5.c). The length of this control volume along the X -axis is given by $\Delta X = \frac{\Delta x}{\cos(\beta)}$. For this control volume, the following balance terms can be calculated:

- The change in storage is given by: $f w(x) \Delta t \frac{\partial h}{\partial t}(x, t) \frac{\Delta x}{\cos(\beta)}$, (1.12)

where f stands for the effective drainable porosity.

- The net internal flow is given by:

$$\Delta t \left\{ Q \left(x + \frac{\Delta x}{2} \right) - Q \left(x - \frac{\Delta x}{2} \right) \right\} \approx \Delta t \Delta x \frac{\partial Q}{\partial x}(x, t) \quad (1.13)$$

- As there is no explicit modeling of the unsaturated zone, one has to replace the process by which the rain reaches the saturated groundwater by a kind of conceptual model. First we do assume that the transport from the surface to the groundwater is immediate, as was also done in the Dupuit model. To determine the part of the rainfall that reaches the control volume, one can make different choices as illustrated by Figures 1.5.b, 1.5.c, and 1.5.d. One may assume that the flow through the unsaturated zone occurs along saturated equipotential lines, as done in Figure 1.5.b. Another plausible assumption may be that the flow is completely vertical, as suggested by Figure 1.5.c. The third option is inspired by pure mathematical convenience: the rainfall falling in vertical column above the control volume reaches the groundwater oriented in the z -direction above that control volume. In principle, each choice leads to a different formula. However, as we may assume that the hillslopes are chosen in such a way that the spatial variation of rainfall over the hillslope is very limited, the different choices lead to minimal effective rainfall differences. For that reason, we will continue with the mathematically most tractable option (d), where the net recharge is given by:

$$\Delta t \Delta x N(t) w(x) \quad (1.14)$$

It should be mentioned that the only way to make a physically justified choice is to do that on the basis of unsaturated zone modeling, which is beyond the scope of this work. In principle it is possible to work all three choices out mathematically similar to what is done in Figure 1.13 (and even numerically as in Chapter 2). However, for this work we chose the simplest option.

Bringing all balance terms for uniform width (w) together and dividing by $w \Delta x \Delta t$ results in the Boussinesq equation

$$f \frac{1}{\cos(\beta)} \frac{\partial h(x, t)}{\partial t} = \frac{\partial}{\partial x} \left(K_s(x) h(x, t) \left(\cos^2(\beta) \frac{\partial h}{\partial x}(x, t) + \sin(\beta) \right) \right) + N(t) \quad (1.15)$$

when $\beta = 0$, Equation 1.15 reduces to the Dupuit model (Equation 1.6) with unit width.

1.3.3 The extended Boussinesq equation

Troch et al. (2003) generalized the Boussinesq equation to account for complex hillslope geometry (e.g., convergent and divergent plan shapes), relaxing the constant width assumption for each x , and replacing this by a space-dependent width $w(x)$ which is derived from the geometry of the hillslope (see Figure 1.6).

Following a similar reasoning as in the previous section, one obtains the following formula for the discharge:

$$Q(x,t) = -K_s(x) w(x) h(x,t) \left(\cos^2(\beta) \frac{\partial h}{\partial x}(x,t) + \sin(\beta) \right) \quad (1.16)$$

And by that at the following differential equation:

$$\frac{f}{\cos(\beta)} w(x) \frac{\partial h}{\partial t}(x,t) = \frac{\partial}{\partial x} \left(K_s(x) w(x) h(x,t) \left(\cos^2(\beta) \frac{\partial h}{\partial x}(x,t) + \sin(\beta) \right) \right) + N(t) w(x) \quad (1.17)$$

Where it is tacitly assumed that h is a representative water table height*. This equation is very closely related to the hsB equation proposed by Troch et al. (2003)*. When $\beta = 0$, Equation 1.17 reduces to the Dupuit model (Equation 1.6).

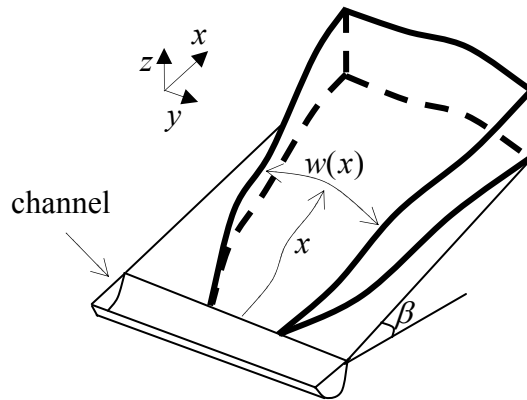


Figure 1.6: Conceptualization of a convergent hillslope (adapted from Troch et al., 2003).

1.3.4 Bedrock with general geometry

In the following section, the assumption that the bedrock has a constant slope will be relaxed.

This will be done in two steps:

- in the first model, which will be called the *slanted Dupuit* here, we do consider a general bedrock geometry, but the flow direction will still be assumed constant throughout the hillslope.
- in the second model, called the *curved Dupuit* here, even that last assumption will be relaxed and the flow will be considered to be parallel to the local bedrock slope.

From these two models, because one model is a special case of the other, the most complex one is most capable to approximate the true groundwater table. As done above, all equations

* Representative here means that the flux calculated with Equation 1.17 is a good approximation of the average flux over the y -direction.

* The difference being here that the Equation 1.17 is defined in terms of head instead of storage.

will be derived within a fixed coordinate system (x, y, z) . In the spirit of the one-dimensional hillslope concept, all variations in the y -direction (including convergence and divergence) will be neglected and only variation in the downhill x -direction will be considered including the dependence of the hillslope width on x . As a consequence, a general bedrock is described by giving for each x its elevation with respect to an arbitrary datum, i.e. the function $b(x)$. Some other geometrical characteristics will be useful in what follows:

- the derivative $b'(x)$.
- the local slope angle $\beta(x)$, defined by $\beta(x) = \text{atan}(b'(x))$.
- the local tangential length, i.e. the length traveled over the bedrock per unit x :

$$\|B'(x)\| = \frac{1}{\cos(\beta(x))} \quad (1.18)$$

- the local curvature, which is the change of the bedrock slope angle, defined by:

$$\beta'(x) = \frac{d\beta}{dx}(x) = \kappa_B(x) \quad (1.19)$$

which can be defined as $\kappa_B(x) = \frac{1}{R_c}$, where R_c is radius of curvature.

The curvature can be negative or positive, which depends on whether the curve is convex or concave, respectively (see Figure 1.7).

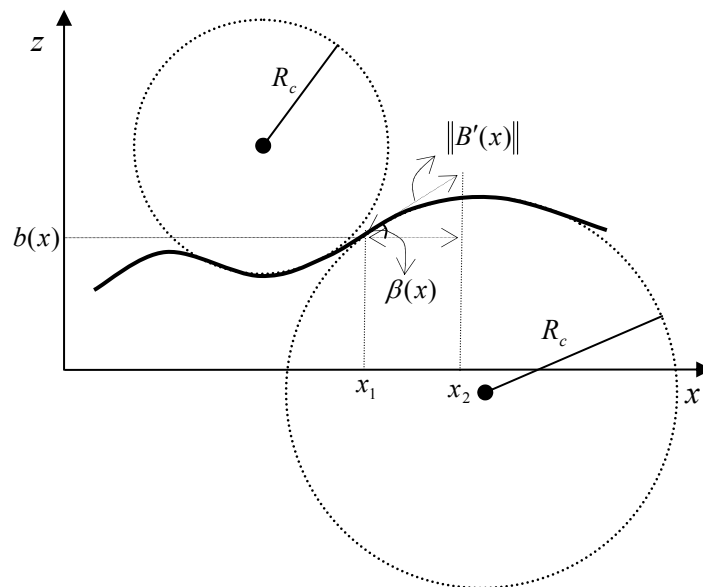


Figure 1.7: Definition of bedrock geometry and its characteristics.

1.3.5 The extended Boussinesq equation based on the slanted Dupuit assumption

The basic assumptions for the slanted Dupuit model are (see also Figure 1.8)

- all variations in the y -direction are neglected.
- the geometry of the bedrock may be general, resulting e.g. in a non-constant slope $\beta(x)$.

- there is one constant flow direction throughout the whole hillslope which will be denoted by X , which is assumed as representative of the average flow direction. The angle of this constant direction with the horizontal will be denoted by ω .
- the groundwater head is constant in the Z -direction ($\frac{\partial \phi}{\partial Z} = 0$) and there is no flow in this direction ($q_z = 0$).

In the slanted Dupuit model the water level $h(x)$ is defined as the water level above the bedrock at position x measured in the Z -direction. The potential along a Z -line is constant and given by the following formula (see Figure 1.8):*

$$\phi(x) = \cos(\omega)h(x) + b(x) \quad (1.20)$$

and the hydraulic gradient becomes:
$$\frac{\partial \phi}{\partial x}(x) = \cos(\omega) \frac{\partial h}{\partial x}(x) + b'(x) \quad (1.21)$$

Equation 1.21 indicates that the potential change follows from changes in the bedrock and/or changes in the groundwater head.

As the direction of the flux by assumption is given by X , whole flux vector is determined by calculating its magnitude. To derive a formula, consider two equipotential lines separated by a small distance ε in the X -direction, as in Figure 1.9.a. The difference in x -coordinates of these two lines is given by (see Figure 1.9.b):

$$\Delta x = \cos(\beta(x)) \frac{\varepsilon}{\cos(\beta(x) - \omega)} \quad (1.22)$$

The flux at any point on the equipotential line in the X -direction is given by the Darcy equation:

$$\begin{aligned} q_x(x) &= -K_s(x) \lim_{\varepsilon \rightarrow 0} \left(\frac{\phi(x + \Delta x) - \phi(x)}{\varepsilon} \right) \approx -K_s(x) \frac{\cos(\beta(x))\varepsilon}{\varepsilon \cos(\beta(x) - \omega)} \frac{\partial \phi}{\partial x}(x) \\ &= -K_s(x) \frac{\cos(\beta(x))}{\cos(\beta(x) - \omega)} \frac{\partial \phi}{\partial x}(x) \end{aligned} \quad (1.23)$$

The total flux through a slice in the Z -direction is then given by:

$$Q(x) = q_x(x) \int_0^{w(x)} dy \int_0^{h(x)} dZ = -\frac{K_s(x) w(x) h(x) \cos(\beta(x))}{\cos(\beta(x) - \omega)} \left(\cos(\omega) \frac{\partial h}{\partial x}(x) + b'(x) \right) \quad (1.24)$$

* Note that ' $\phi(x)$ ' is not measured in a vertical above ' x '. See also Section 1.3.7.

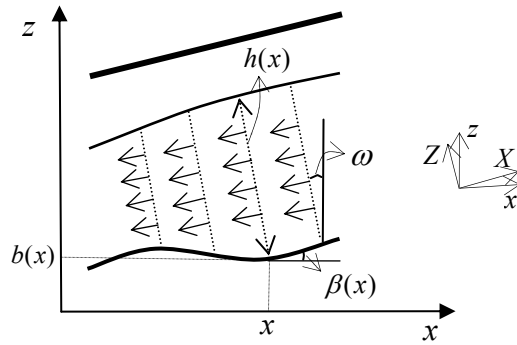


Figure 1.8: Schematic view of groundwater flow under slanted Dupuit assumption (arrows represent flux vectors and dashed lines are equipotential lines).

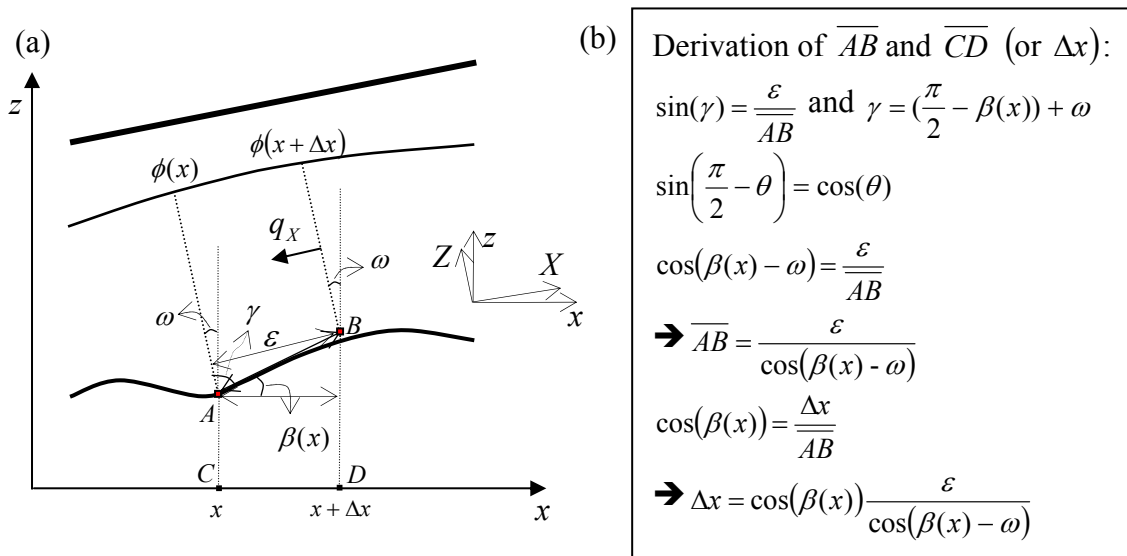


Figure 1.9: (a) Schematic view of geometry under slanted Dupuit assumption (non-vertical dashed lines are equipotential lines), and (b) Derivation of \overline{AB} and \overline{CD} (or Δx).

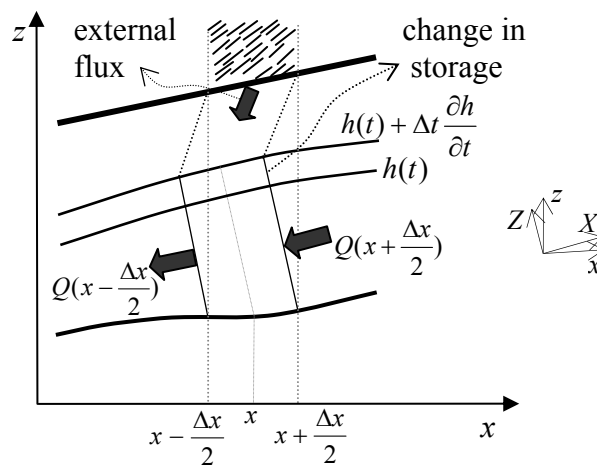


Figure 1.10: Control volume (in slanted Dupuit) and mass balance terms.

To derive the flow equation, two nearby equipotential lines are considered (see Figure 1.10). In a similar way to the previous section, using the fact that the length of this control volume along the X -direction equals $\frac{\Delta x}{\cos(\beta(x))}$, the balance terms become:

- change in storage $f w(x) \frac{1}{\cos(\beta(x))} \Delta t \frac{\partial h}{\partial t}(x, t) \Delta x$. (1.25)

- net internal flux

$$\Delta t \left\{ Q \left(x + \frac{\Delta x}{2} \right) - Q \left(x - \frac{\Delta x}{2} \right) \right\} \approx \Delta t \Delta x \frac{\partial Q}{\partial x}(x, t) \quad (1.26)$$

- for the net external flux we assume again that all the rainfall falls on the soil between two vertical lines above the bottom, which is instantaneously transferred vertically to the flux domain between two equipotential lines resulting in $\Delta t \Delta x N(t) w(x)$.

Assembling the mass balance equation using above mentioned balance terms, and dividing the result by $\Delta t \Delta x$ gives:

$$f w(x) \frac{1}{\cos(\beta(x))} \frac{\partial h}{\partial t}(x, t) = - \frac{\partial Q}{\partial x}(x, t) + N(t) w(x) \quad (1.27)$$

Substitution of Equation 1.24 in Equation 1.27 results in the flow equation:

$$f w(x) \frac{1}{\cos(\beta(x))} \frac{\partial h}{\partial t}(x, t) = \frac{\partial}{\partial x} \left(\frac{K_s(x) w(x) h(x, t) \cos(\beta(x))}{\cos(\beta(x) - \omega)} \left(\cos(\omega) \frac{\partial h}{\partial x}(x, t) + b'(x) \right) \right) + N(t) w(x) \quad (1.28)$$

When $\beta(x) = \omega = \beta$ (for all x), Equation 1.28 reduces to the extended Boussinesq equation (Equation 1.17).

1.3.6 The extended Boussinesq equation based on the curved Dupuit assumption

In this section we replace the condition of a constant flow direction by the assumption that at every point the flow will be parallel to the bedrock. This model will be called the curved Dupuit model. Using the notations of Figure 1.11, the model can be defined by the following:

- All flow follows the bedrock profile, so $\beta(x) = \omega(x)$. The local flow direction will be denoted by $X(x)$.
- The direction orthogonal to the bedrock at x will be denoted by $Z(x)$. This direction also defines the equipotential lines ($\frac{\partial \phi}{\partial Z} = 0$), and there will be no flow in the Z -direction ($q_z = 0$).

The groundwater head $h(x)$ is measured as the elevation of the groundwater table above the bedrock measured in the $Z(x)$ direction (see Figure 1.11). Along this equipotential line, the potential is given by

$$\phi(x) = \cos(\beta(x)) h(x) + b(x) \quad (1.29)$$

The derivative of ϕ with respect to x is then (see also Equation 1.19):

$$\frac{\partial \phi}{\partial x}(x) = \cos(\beta(x)) \frac{\partial h}{\partial x}(x) - \sin(\beta(x)) \kappa_B(x) h(x) + b'(x) \quad (1.30)$$

To calculate the flux, we consider two equipotential lines separated by a distance ε (measured along the bedrock) in the X -direction as in Figure 1.12.a. As shown in this figure, the difference in x -coordinates of the bedrock base points of these two lines is given by $\Delta x = \cos(\beta(x)) \varepsilon$.

The flux at any point on the equipotential line in the X -direction is given by the Darcy equation:

$$\begin{aligned} q_X(x, Z) &= -K_s \lim_{\varepsilon \rightarrow 0} \left(\frac{\phi(x + \varepsilon \cos(\beta(x))) - \phi(x)}{\text{distance along streamline at elevation } Z} \right) \\ &= -K_s \lim_{\varepsilon \rightarrow 0} \left(\frac{\varepsilon \cos(\beta(x)) \frac{\partial \phi}{\partial x}(x)}{\text{distance along streamline at elevation } Z} \right) \end{aligned} \quad (1.31)$$

Since equipotential lines are perpendicular to the bedrock and the bedrock is in general curved, equipotential lines will not be parallel, and the distance between them will change as a function of elevation above the bottom. As we have assumed the equipotential lines to be straight, this dependency will be linear. As worked out in Figure 1.12.c, one can write distance as $(1 - Z\kappa_B(x))\varepsilon$. Using this in the formula above results in:

$$\begin{aligned} q_X(x, Z) &\approx -K_s(x) \frac{\varepsilon \cos(\beta(x))}{\varepsilon (1 - Z\kappa_B(x))} \left(\frac{\partial \phi}{\partial x}(x) \right) \\ &= -K_s(x) \frac{\cos(\beta(x))}{1 - Z\kappa_B(x)} \left(\frac{\partial \phi}{\partial x}(x) \right) \end{aligned} \quad (1.32)^*$$

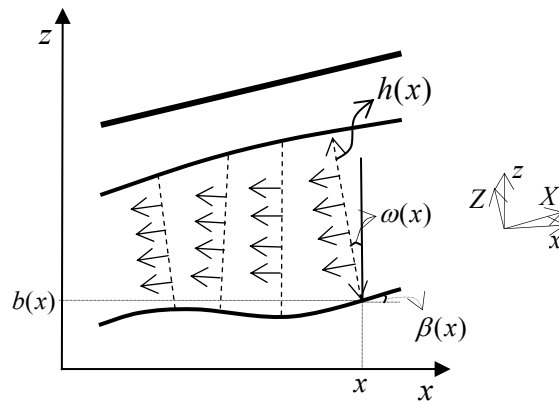


Figure 1.11: Schematic view of groundwater flow under curved Dupuit assumption (arrows represent flux vectors, dashed lines are equipotential lines, angles are $\beta(x)$, and $\omega(x)$).

* By the local linearity of the bedrock curve, the ε in the denominator and the distance in the numerator will be equal when the limit is taken for ε approaching zero.

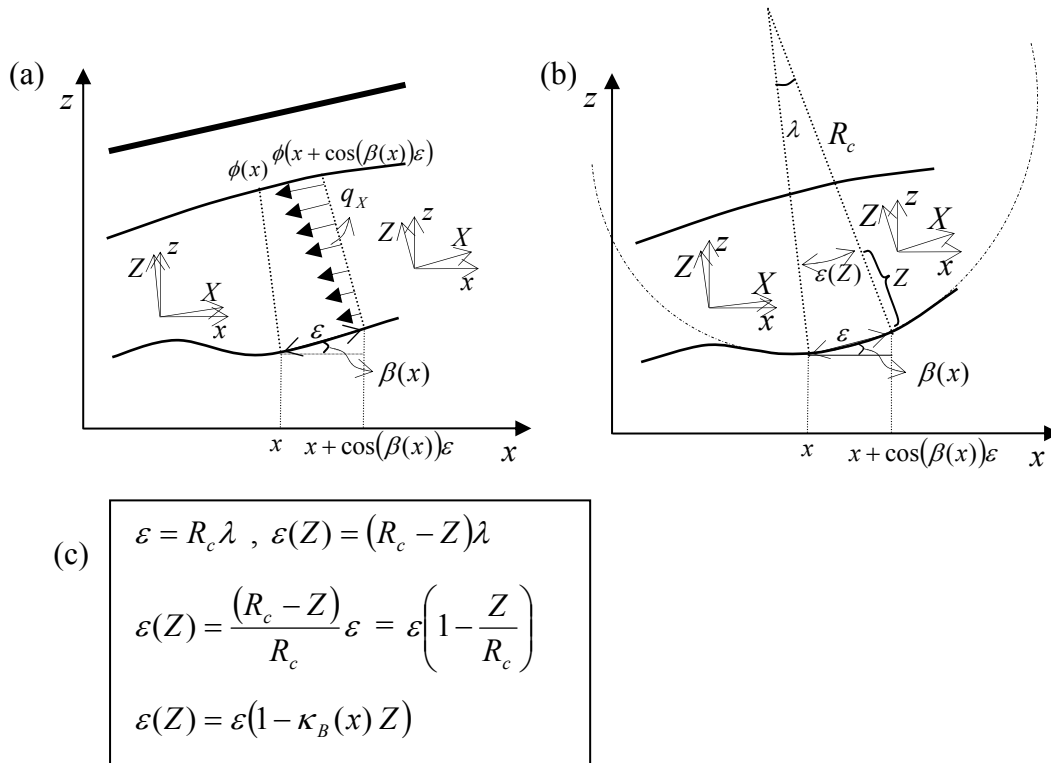


Figure 1.12: (a) Schematic view of geometry under curved Dupuit assumption (arrows are flux vectors); (b) calculation of distance between equipotential lines; and (c) derivation of distance at elevation Z .

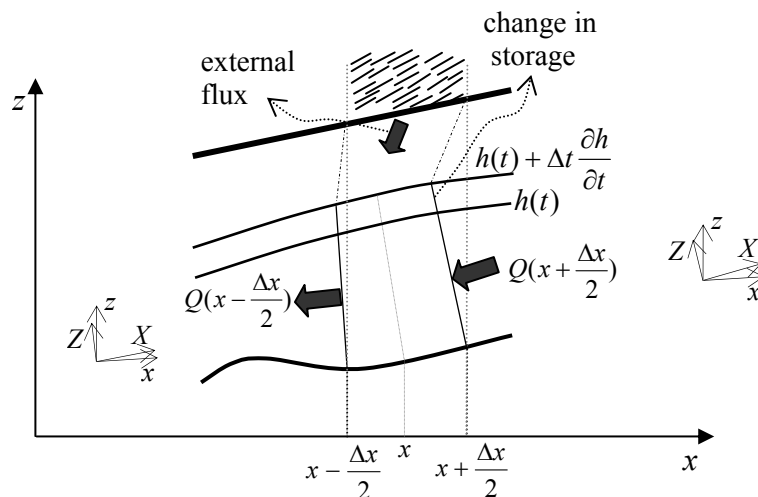


Figure 1.13: Control volume (in curved Dupuit case) and mass balance terms.

The total flux through a slice orthogonal to the bedrock can then be calculated as follows:

$$\begin{aligned}
 Q(x) &= \int_0^{w(x)} dy \int_0^{h(x)} q_x(x, Z) dZ \\
 &= -K_s(x) w(x) \cos(\beta(x)) \frac{\partial \phi}{\partial x}(x) \int_0^{h(x)} dZ \frac{1}{1 - Z \kappa_B(x)} \\
 &= K_s(x) w(x) \cos(\beta(x)) \frac{1}{\kappa_B(x)} \frac{\partial \phi}{\partial x}(x) \ln(1 - h(x) \kappa_B(x))
 \end{aligned} \tag{1.33}$$

To derive the flow equation, a control volume is considered as in Figure 1.13. The width of this control volume along the X -direction at the phreatic surface is $\frac{\Delta x}{\cos(\beta(x))} (1 - h(x) \kappa_B(x))$

where the storage change occurs. This results in the following balance terms:

- The change in storage is given by

$$f w(x) \Delta t \frac{\partial h}{\partial t}(x, t) \Delta x \frac{1}{\cos(\beta(x))} (1 - h(x, t) \kappa_B(x)) \tag{1.34}$$

- The net internal flux can be calculated using Equation 1.26.
- The net external flux can be calculated using the approach presented in Figure 1.13 (following the arguments in Section 1.3.2). Regarding tangential length of the bedrock and width function, the total external flux is given by: $\Delta t \Delta x w(x) N(t)$ (1.35)

Combining these terms and dividing the result by $\Delta t \Delta x$ gives:

$$f \frac{1}{\cos(\beta(x))} w(x) (1 - h(x, t) \kappa_B(x)) \frac{\partial h}{\partial t}(x, t) = -\frac{\partial Q}{\partial x}(x, t) + w(x) N(t) \tag{1.36}$$

Substitution of Equation 1.33 in Equation 1.36 results in the flow equation as follows:

$$\begin{aligned}
 f w(x) \frac{1}{\cos(\beta(x))} (1 - \kappa_B(x) h(x, t)) \frac{\partial h}{\partial t}(x, t) &= -\frac{\partial}{\partial x} \left(\frac{K_s(x) w(x) \cos(\beta(x))}{\kappa_B(x)} \ln(1 - h(x, t) \kappa_B(x)) \right. \\
 &\quad \left. + \left(\cos(\beta(x)) \frac{\partial h}{\partial x}(x, t) + b'(x) - \sin(\beta(x)) \kappa_B(x) h(x, t) \right) \right) + N(t) w(x)
 \end{aligned} \tag{1.37}$$

In the special case where in the curved Dupuit assumption ω is constant, β is also constant and curvature term is $\kappa_B(x) = 0$, Equation 1.37 reduces to the extended Boussinesq equation (Equation 1.17).

1.3.7 Remark on the position of the groundwater table

The definitions of the groundwater table position determined by $h(x)$ in the sections above is rather complicated: one first has to find the point on the bedrock above x , then one has to follow the equipotential line starting in that point over a length $h(x)$, to arrive at the point $\{x - \sin(\omega(x))h(x), b(x) + \cos(\omega(x))h(x)\}$. Figure 1.14 illustrates this procedure and shows also that for many practical situations (where $\omega(x)$ is limited) the graph thus obtained does not differ significantly from the graph obtained by plotting $\{x, h(x) + b(x)\}$, unless one is

interested in local details (However, discharge and the differential equations are locally defined).

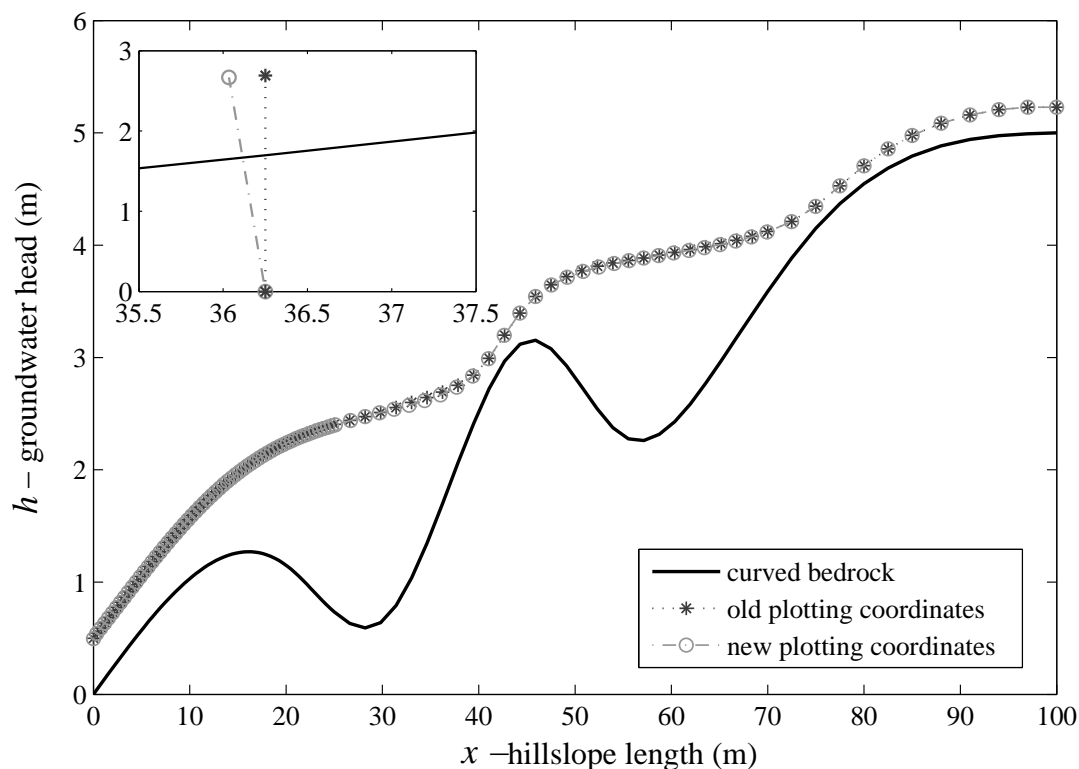


Figure 1.14: The effect of different definitions for the position of the groundwater table. Inset shows local effect.

1.4 Parameterization of boundary conditions

To solve a differential equation, initial values and boundary conditions are required. For the initial value, we will always use a steady state solution. Our hillslope equations, as they are in essence second order differential equations in space, need two spatial boundary conditions. Technically, these boundary conditions are usually given as functional relations between state h , state change $\frac{\partial h}{\partial t}$ and discharge Q at that point.

As we will assume the upper boundary to be a water divide, the boundary condition at that point is simply given by $Q = 0$ that is called Neumann boundary condition. For the lower outflow point, a given head will often be used (Dirichlet boundary condition). Chapter 3 however will discuss more general formulations where more complex discharge-head relations are considered as a replacement for the hillslope-river interaction (see also Figure 1.15). This type of boundary condition is generally called Cauchy boundary condition.

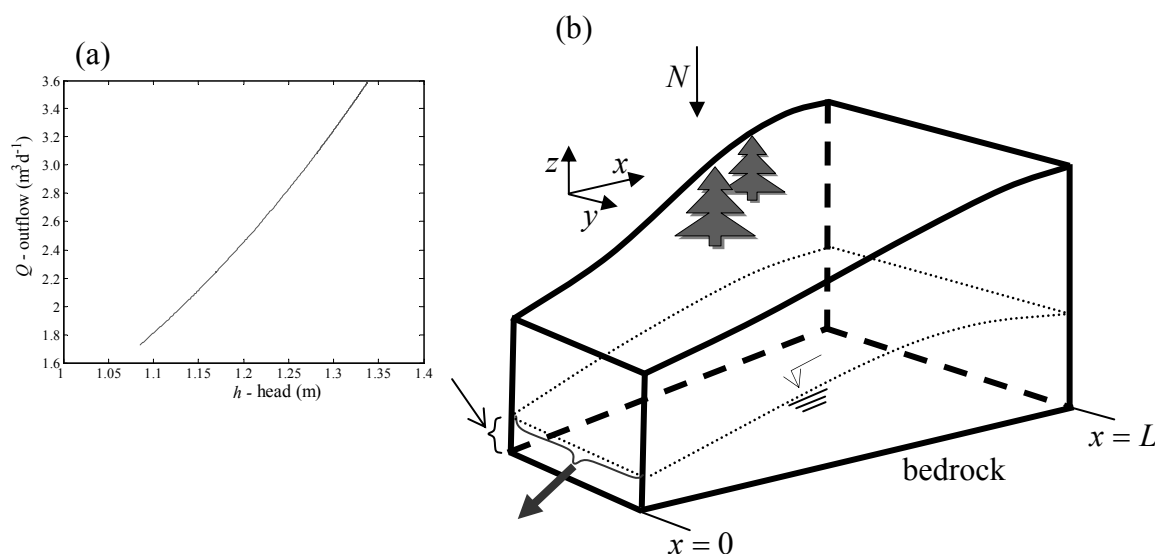


Figure 1.15: Conceptualization of imposing mixed boundary condition (Cauchy boundary condition): (a) A head-flux curve for hillslope; and (b) the hillslope system uses head-flux relationship as boundary condition.

1.5 Conclusions

Different types of partial differential equations with different levels of complexity and non-linearity were presented in Section 1.3. To solve these flow equations, the system under study should be constrained by proper boundary conditions that correspond to identifiable hydrological features. Imposing real hydrological boundaries calls for appropriate parameterizations. In order to handle all of these equations, a general and flexible numerical solution algorithm is required. This algorithm enables us to compare the results of different types of flow equations, which have been parameterized differently.

1.6 Outline of thesis

In **Chapter 2** the numerical solution algorithm is presented. The differential equations presented in section 1.3 are complex and non-linear to be solved analytically. To solve these different flow equations, we need a uniform, flexible and robust numerical solution algorithm. This algorithm can handle different types of flow equations based on different linearization methods in both steady and unsteady states.

Chapter 3 describes application of the proposed algorithm to study the role of the hillslope lower boundary condition on the hydrological response. Interest is focused on the hillslope-stream interaction and the discharge hydrograph resulting from water leaving at the hillslope lower boundary. Investigation of the backwater effect is carried out by imposing a time-varied boundary condition at the lower end of the hillslope. Our final target is to replace the reservoir

system in the coupled case with a discharge-head relationship to simplify modeling of the hillslope-stream interaction.

Chapter 4 presents the results of application of the generalized extended Boussinesq equation based on the curved Dupuit assumption to investigate the role of bedrock profile geometry on hydrological response. The obtained flow equation is solved in both steady and unsteady states using the algorithm defined in Chapter 2.

In **Chapter 5** a semi-stationary approach is applied to calculate the hydrological response of a hillslope. Then the hillslope model is replaced by a lookup table, which includes storage versus outflow in the steady state. In this approach the dynamics of the soil water is treated as a stream of transitions between steady state situations, called the ‘quasi’ or ‘pseudo’ steady state approach (e.g., Basha and Maalouf, 2005; van Walsum et al., 2006). For the boundary condition, a proper boundary condition such as presented in Chapter 3 is applied. At the end the results of the semi-stationary approach are compared with those of transient calculations for different cases.

In **Chapter 6** the findings of the thesis are presented and concluding remarks are summarized. Finally suggestions for future research are given.

Chapter 2

The numerical solution algorithm

2.1 Introduction

The differential equations presented in the previous chapter are certainly too complex and non-linear to be solved analytically. This chapter describes a numerical technique to solve them. Of course, there are many different numerical methods for this type of problem. As the models are spatially one-dimensional, spatial discretization is not an issue*. As the models are all highly non-linear, many different choices of numerical schemes can be considered to tackle this particular problem. In this work, however, we prefer to describe one single technique that can handle all the equations in a uniform way.

Non-linear equations are generally solved by iteratively solving a sequence of linear approximations, in the hope that these converge to the solution of the non-linear problem. Iterative schemes such as the Picard, Newton, secant, and relaxation methods have been proposed for this purpose (e.g., Mehl, 2006; Burden and Faires, 1997). In this work, only the Picard method will be used. Convergence problems will be handled by classical relaxation.

The numerical technique that will be presented in this chapter will however be very flexible in terms of choice of linearization (see Section 4). The numerical scheme will also be very physically oriented: at all numerical stages, fluxes will be calculated and mass balances will be preserved. A last conscious choice made was to let the numerical treatment of the spatial distribution prevail over that of time changes. This can be seen from the fact that first solutions for the steady state problem will be developed and solutions for the transient case will be derived from these.

The different aspects and characteristics of the proposed algorithm are described in this chapter. In the next section, a general formulation of the partial differential equations to be solved and some examples are presented. Section 3 explains the general linearization procedure and the iterative use of these in solving non-linear equations. Section 4 deals with different examples of linearization methods. Spatial discretization schemes and derivation of the discrete equations are presented in Sections 5 and 6, respectively. The time stepping method and solution method of the unsteady flow equations is given in Section 7.

2.2 The general steady state equation

The numerical technique that will be described in this chapter will be able to handle the following general system of steady state equations for $x_L \leq x \leq x_R$ (x_L and x_R stand for the

$$x - \text{coordinates of the left and right boundary conditions): } -\frac{\partial Q(x)}{\partial x} + N(x) = 0 \quad (2.1)$$

$$Q(x) = Q_{nl} \left(x, h(x), \frac{\partial h}{\partial x}(x) \right) \quad (2.2)$$

$$N(x) = N_{nl}(x, h(x)) \quad (2.3)^*$$

* Here only the position of the nodes is important. In the 2D case, the form of the discretization (rectangular, triangular, etc.) plays an important role.

* This 'h' dependency may not occur in many places, but for an example see Section 6.2.

$$\begin{cases} 0 = BC_L(h(x_L), Q(x_L)) \\ 0 = BC_R(h(x_R), Q(x_R)) \end{cases} \quad (2.4)$$

In this:

- $h(x)$ is the unknown state function that should be found by solving the equations.
- Q_{nl} is the given non-linear function (of three arguments) that enables to calculate the internal flux at any point x as a function of position x , state at that point $h(x)$ and gradient of the state at that point.
- N_{nl} is the given non-linear function (of two arguments) that enables one to calculate the external flux at any point x as a function of position x and state $h(x)$ at that point.
- BC_L and BC_R are two given functions of two arguments: state and flux, respectively. These functions represent the boundary conditions.

This general steady state problem is thus determined by giving four functions: Q_{nl} , N_{nl} , BC_L and BC_R . These functions may be highly non-linear in general. Linearization of these functions will be needed. For this, it will be handy to introduce a general abstract notation for their arguments. If needed, we will denote the arguments $x, h, \frac{\partial h}{\partial x}$ and Q^* by a_1, a_2, a_3 and a_4 , respectively. Abstract arguments are introduced to focus on the functional form of Q_{nl} as this will be the base for linearization. Hence, Q_{nl} is a given non-linear function of three real arguments: $Q_{nl}(a_1, a_2, a_3)$, N_{nl} is a given non-linear function of two real arguments $N_{nl}(a_1, a_2)$, BC are given functions of two real arguments $BC(a_2, a_4)$. We will call the equations linear if all four functions are linear in the arguments a_1, a_2, a_3 and a_4 .

2.2.1 The hillslope steady state equations

In this section, we will show that the steady state form of all hillslope models of the previous chapter is captured by the general steady state equation above. The discussion of the boundary conditions will be postponed to Chapter 3.

2.2.1.1 The Dupuit equation

The steady state form of the Dupuit equation (see 1.3.1) can be written as

$$\frac{\partial}{\partial x} \left(K_s(x) w(x) h(x) \frac{\partial h}{\partial x}(x) \right) + N(x) w(x) = 0 \quad (2.5)^\wedge$$

which is of the general form above with the following choices:

$$Q_{nl}(a_1, a_2, a_3) = -K_s(a_1) w(a_1) a_2 a_3 \quad (2.6)$$

* A notation list is presented in list of symbols.

^\wedge In this equation, the partial derivative is still used and this is for visual comparison with the other equations. Although strictly spoken they should be replaced by the ordinary differential symbol.

$$N_{nl}(a_1, a_2) = N(a_1) w(a_1) \quad (2.7)$$

2.2.1.2 The Boussinesq equation

The steady state form of the Boussinesq equation (see 1.3.2) can be written as

$$\frac{\partial}{\partial x} \left(K_s(x) h(x) \left(\cos^2(\beta) \frac{\partial h}{\partial x}(x) + \sin(\beta) \right) \right) + N(x) = 0 \quad (2.8)$$

which is of the general form above with the following choices:

$$Q_{nl}(a_1, a_2, a_3) = -K_s(a_1) a_2 (\cos^2(\beta) a_3 + \sin(\beta)) \quad (2.9)$$

$$N_{nl}(a_1, a_2) = N(a_1) \quad (2.10)$$

2.2.1.3 The extended Boussinesq equation

The steady state form of the extended Boussinesq equation (see 1.3.3) can be written as

$$\frac{\partial}{\partial x} \left(K_s(x) w(x) h(x) \left(\cos^2(\beta) \frac{\partial h}{\partial x}(x) + \sin(\beta) \right) \right) + N(x) w(x) = 0 \quad (2.11)$$

which is of the general form above with the following choices:

$$Q_{nl}(a_1, a_2, a_3) = -K_s(a_1) w(a_1) a_2 (\cos^2(\beta) a_3 + \sin(\beta)) \quad (2.12)$$

$$N_{nl}(x) = w(a_1) N(a_1) \quad (2.13)$$

2.2.1.4 The extended Boussinesq equation based on the slanted Dupuit assumption

The steady state form of the extended Boussinesq equation based on the slanted Dupuit assumption (see 1.3.5) can be written as

$$\frac{\partial}{\partial x} \left(\frac{K_s(x) w(x) h(x) \cos(\beta(x))}{\cos(\beta(x) - \omega)} \left(\cos(\omega) \frac{\partial h}{\partial x}(x) + b'(x) \right) \right) + N(x) w(x) = 0 \quad (2.14)$$

which is of the general form above with the following choices:

$$Q_{nl}(a_1, a_2, a_3) = \frac{-K_s(a_1) w(a_1) \cos(\beta(a_1)) a_2}{\cos(\beta(a_1) - \omega)} (\cos(\omega) a_3 + b'(a_1)) \quad (2.15)$$

$$N_{nl}(a_1) = N(a_1) w(a_1) \quad (2.16)$$

2.2.1.5 The extended Boussinesq equation based on the curved Dupuit assumption

The steady state form of the extended Boussinesq equation based on the curved Dupuit assumption (see 1.3.6) can be written as

$$\begin{aligned} & -\frac{\partial}{\partial x} \left(\frac{K_s(x) w(x) \cos(\beta(x))}{\kappa_B(x)} \ln(1 - h(x) \kappa_B(x)) \left(\cos(\beta(x)) \frac{\partial h}{\partial x}(x) + b'(x) - \sin(\beta(x)) \kappa_B(x) h(x) \right) \right) \\ & + N(x) w(x) = 0 \end{aligned} \quad (2.17)$$

which is of the general form above with the following choices:

$$\begin{aligned} Q_{nl}(a_1, a_2, a_3) &= \frac{K_s(a_1) w(a_1) \cos(\beta(a_1))}{\kappa_B(a_1)} \ln(1 - a_2 \kappa_B(a_1)) \\ & \cdot (\cos(\beta(a_1)) a_3 + b'(a_1) - \sin(\beta(a_1)) \kappa_B(a_1) a_2) \end{aligned} \quad (2.18)$$

$$N_{nl}(a_1) = N(a_1)w(a_1) \quad (2.19)$$

2.3 Linearization

The differential Equation 2.1 is called linear if the functions involved (Q_{nl} , N_{nl} , BC_L and BC_R) are linear in their arguments, involving their dependency on $h, \frac{\partial h}{\partial x}$ and Q , and thus in their dependency on a_2, a_3 and a_4 (as introduced in Section 2.2). All the presented hillslope examples are non-linear according to this definition.

In order to be solvable, one has to approximate the non-linear differential equation by a linear one. To be concrete, this means that one has to approximate the non-linear functions involved by linear ones.

In this work, a very general and flexible definition of linearization will be used. For the function Q_{nl} for example this definition reads as follows:

During the solution procedure, we will construct a sequence ($n=1,2,3,\dots$) such that $a_i^{(n)} \xrightarrow{n \rightarrow \infty} a_i$ where $i=2,3$. Based on this we approximate the function Q_{nl} by $Q_{nl}^{(n)}$:

$$Q_{nl}^{(n)}(a_1, a_2, a_3) \approx Q_a(a_1, a_2^{(n)}, a_3^{(n)}) + Q_b(a_1, a_2^{(n)}, a_3^{(n)}) a_2 + Q_c(a_1, a_2^{(n)}, a_3^{(n)}) a_3 \quad (2.20)$$

Because we want $Q_{nl}^{(n)} \rightarrow Q_{nl}$, we should require

$$Q_{nl}(a_1, a_2, a_3) = Q_a(a_1, a_2, a_3) + Q_b(a_1, a_2, a_3) a_2 + Q_c(a_1, a_2, a_3) a_3 \quad (2.21)$$

By definition any set of functions Q_a, Q_b and Q_c in Equation 2.21 will be called a (general) linearization of the function Q_{nl} in this work. In a similar way linearizations for the other functions are defined.

A linearization of the N_{nl} function consists of two functions N_d and N_e such that:

$$N_{nl}(a_1, a_2) = N_d(a_1, a_2) + N_e(a_1, a_2) a_2 \quad (2.22)$$

For left and right hand side boundary conditions, three functions (continuously differentiable) of two arguments should be given:

$$\begin{cases} BC_L(a_2, a_4) = \gamma_L(a_2, a_4) + \alpha_L(a_2, a_4) a_2 + \beta_L(a_2, a_4) a_4 \\ BC_R(a_2, a_4) = \gamma_R(a_2, a_4) + \alpha_R(a_2, a_4) a_2 + \beta_R(a_2, a_4) a_4 \end{cases} \quad (2.23)$$

In Section 2.4 several examples of linearizations will be provided, but first we will argue that the general definition above is sufficient to define an iterative approximation scheme of the differential equation.

2.3.1 Solution of the non-linear equations

Let any linearization be given, then a sequence of approximations is recursively defined as follows. Given $h^{(n)}$, $h^{(n+1)}$ is found as the solution of the following linear differential equation:

$$-\frac{\partial Q^{(n+1)}}{\partial x} + N^{(n+1)} = 0 \quad (2.24)$$

$$Q^{(n+1)}(x) = Q_a \left(x, h^{(n)}(x), \frac{\partial h^{(n)}}{\partial x}(x) \right) + Q_b \left(x, h^{(n)}(x), \frac{\partial h^{(n)}}{\partial x}(x) \right) h^{(n+1)}(x) \\ + Q_c \left(x, h^{(n)}(x), \frac{\partial h^{(n)}}{\partial x}(x) \right) \frac{\partial h^{(n+1)}}{\partial x}(x) \quad (2.25)$$

$$N^{(n+1)}(x) = N_d(x, h^{(n)}(x)) + N_e(x, h^{(n)}(x)) h^{(n+1)}(x) \quad (2.26)$$

$$\begin{cases} \gamma_L(h^{(n)}(x_L), Q^{(n)}(x_L)) + \alpha_L(h^{(n)}(x_L), Q^{(n)}(x_L)) h^{(n+1)}(x_L) + \beta_L(h^{(n)}(x_L), Q^{(n)}(x_L)) Q^{(n+1)}(x_L) = 0 \\ \gamma_R(h^{(n)}(x_R), Q^{(n)}(x_R)) + \alpha_R(h^{(n)}(x_R), Q^{(n)}(x_R)) h^{(n+1)}(x_R) + \beta_R(h^{(n)}(x_R), Q^{(n)}(x_R)) Q^{(n+1)}(x_R) = 0 \end{cases} \quad (2.27)$$

If the sequence $\{h^{(n)}\}$ converges then its limit $h^{(\infty)}(x) = \lim_{n \rightarrow \infty} h^{(n)}(x)$ is the solution of the non-linear differential equation. This follows immediately from the definition of linearization as can be seen as follows:

$$Q^{(\infty)}(x) = Q_a \left(x, h^{(\infty)}(x), \frac{\partial h^{(\infty)}}{\partial x}(x) \right) + Q_b \left(x, h^{(\infty)}(x), \frac{\partial h^{(\infty)}}{\partial x}(x) \right) h^{(\infty)}(x) \\ + Q_c \left(x, h^{(\infty)}(x), \frac{\partial h^{(\infty)}}{\partial x}(x) \right) \frac{\partial h^{(\infty)}}{\partial x}(x) = Q_{nl} \left(x, h^{(\infty)}(x), \frac{\partial h^{(\infty)}}{\partial x}(x) \right) \quad (2.28)$$

There is of course no guarantee that the sequence constructed above does converge. If it does not, or the convergence is very slow, one can try to improve this by the well known method of relaxation. For this, given $h^{(n)}$, one first constructs a candidate $\widehat{h}^{(n+1)}$ by solving the differential equation as given above, but takes as next approximation $h^{(n+1)}(x) = \omega_r h^{(n)}(x) + (1 - \omega_r) \widehat{h}^{(n+1)}(x)$. A proper choice of ω_r in general depends on the problem and the linearization*.

For practical purposes, any iterative procedure has to be complemented with a stopping criterion. In this work the standard approach of stopping when no significant change in $h^{(n)}$ is observed or the maximum number of iterations is exceeded is chosen. The latter is usually interpreted as a sign of non-convergence.

2.4 Construction of linearization

Examples of linearization procedures for the internal flux Q_{nl} will be given in this section. The external flux and boundary condition can be treated similarly.

The linearization techniques that follow, focus on the functional dependency of the non-linear functions of the second and third argument. For that reason we use here abstract arguments as introduced in Section 2.2, and these arguments are considered as independent of each other. At

* For the linear diffusion equation one may expect $1 < \omega < 2$. In the examples of this work, $0.5 < \omega_r < 0.95$ proved to be most efficient.

the end these arguments are replaced by others which are dependent (as $h(x)$, $\frac{\partial h}{\partial x}(x)$). But this dependency is again neglected for the construction of the linearization.

2.4.1 Taylor approximation

Let a_1, a_2 and a_3 be given, then for $\hat{a}_2 \approx a_2$ and $\hat{a}_3 \approx a_3$ a linear Taylor approximation (Kreyszig, 1983) results in (\hat{a}_i is general argument around which linearization is performed):

$$Q_{nl}(\hat{a}_1, \hat{a}_2, \hat{a}_3) \approx Q_{nl}(\hat{a}_1, a_2, a_3) + \frac{\partial Q_{nl}}{\partial a_2}(\hat{a}_1, a_2, a_3)(\hat{a}_2 - a_2) + \frac{\partial Q_{nl}}{\partial a_3}(\hat{a}_1, a_2, a_3)(\hat{a}_3 - a_3) \quad (2.29)^*$$

and in the following linearization:

$$Q_a(a_1, a_2, a_3) = Q_{nl}(a_1, a_2, a_3) - a_2 \frac{\partial Q_{nl}}{\partial a_2}(a_1, a_2, a_3) - a_3 \frac{\partial Q_{nl}}{\partial a_3}(a_1, a_2, a_3) \quad (2.30)$$

$$Q_b(a_1, a_2, a_3) = \frac{\partial Q_{nl}}{\partial a_2}(a_1, a_2, a_3) \quad (2.31)$$

$$Q_c(a_1, a_2, a_3) = \frac{\partial Q_{nl}}{\partial a_3}(a_1, a_2, a_3) \quad (2.32)$$

For the Dupuit equation (see 2.2.1.1) one can derive:

$$Q_{nl}(a_1, a_2, a_3) = -K_s(a_1) w(a_1) a_2 a_3 \quad (2.33)$$

$$\frac{\partial Q_{nl}}{\partial a_2}(a_1, a_2, a_3) = -K_s(a_1) w(a_1) a_3 \quad (2.34)$$

$$\frac{\partial Q_{nl}}{\partial a_3}(a_1, a_2, a_3) = -K_s(a_1) w(a_1) a_2 \quad (2.35)$$

And thus using Equations 2.30 through 2.32, we have:

$$Q_a(a_1, a_2, a_3) = K_s(a_1) w(a_1) a_2 a_3 \quad (2.36)$$

$$Q_b(a_1, a_2, a_3) = -K_s(a_1) w(a_1) a_3 \quad (2.37)$$

$$Q_c(a_1, a_2, a_3) = -K_s(a_1) w(a_1) a_2 \quad (2.38)$$

More examples are shown in Appendix A.

2.4.2 Ad hoc method

There are other ways to linearize the PDE. One of them is a method which we like to call the ad hoc method in this work. The inspiration for this method is the observation that the non-linearity of the total discharge is the product of the thickness of the layer, the width of the hillslope and the Darcy flux, and that both terms separately are linear. In the ad hoc method focus is on the dependency on the flux. For the Dupuit equation (see 2.2.1.1) this results in:

* Only linearity with respect to a_2 and a_3 plays a role, as discussed in Section 2.3.

$$Q_a(a_1, a_2, a_3) = 0 \quad (2.39)$$

$$Q_b(a_1, a_2, a_3) = 0 \quad (2.40)$$

$$Q_c(a_1, a_2, a_3) = -K_s(a_1) w(a_1) a_2 \quad (2.41)$$

More examples are presented in Appendix A.

2.4.3 Other linearization methods

In what follows even other types of linearization will be used. In Chapter 4 e.g. non-linear transformations of the state as $h = \eta^2$ and $h = e^\eta$ will be used to handle specific numerical problems, notably positiveness of h . Formulation of the linearization approaches in this context is presented in Appendix B and used in Chapter 4. The choice of the proper linearization method is left as part of the research.

2.5 Spatial discretization

This section discusses the numerical solution of the linear steady state form of the general equations, which will form the basis for the general solution procedure (see Section 2.6).

Generally, the linear form of Equations 2.1, 2.2, 2.3, and 2.4 is:

$$-\frac{\partial Q(x)}{\partial x} + N(x) = 0 \quad (2.42)$$

$$Q(x) = a(x) + b(x) h(x) + c(x) \frac{\partial h}{\partial x}(x) \quad (2.43)$$

$$N(x) = d(x) + e(x) h(x) \quad (2.44)$$

$$\begin{cases} \alpha_L h(x_L) + \beta_L Q(x_L) + \gamma_L = 0 \\ \alpha_R h(x_R) + \beta_R Q(x_R) + \gamma_R = 0 \end{cases} \quad (2.45)$$

where $a(x)$, $b(x)$, $c(x)$, $d(x)$ and $e(x)$ are linear coefficients of the equations and the subscripts L and R indicate left ($x_L = 0$) and right ($x_R = L$) boundaries, respectively.

The differential equation (Equation 2.42) equals an integral equation:

$$Q(x_1) - Q(x_2) + \int_{x_1}^{x_2} N(x) dx = 0 \quad \forall x_1 < x_2 \quad (2.46)$$

The flow domain is discretized by choosing two types of grids: *base nodes* or *primary points* and *dual points* (see Figure 2.1). At base nodes $x_b[i]$, the state function h will be approximated and a discrete mass balance will be formulated (see Figure 2.2). Note that these points can be freely distributed through space and they are not necessarily equidistant. To see the effect of the local density of grids, we refer the reader to Appendix C.

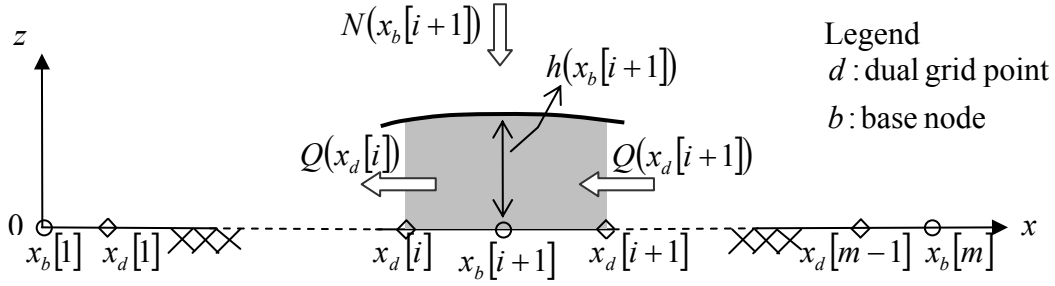


Figure 2.1: Definition of a cell between two dual points and terms of the mass balance.

The dual points are situated in the middle between the base points:

$$x_d[i] = \frac{x_b[i] + x_b[i+1]}{2} \quad (2.47)$$

In these dual points the internal fluxes will be approximated. The values for the external flux are again approximated in the base points.

2.5.1 Discretization of internal flux

For the calculation of the internal flux at the dual nodes, values for the state and the state gradient are needed. These values should be approximated by using the state values on the neighboring base nodes:

$$h(x_d[i]) \approx \frac{h(x_b[i]) + h(x_b[i+1]))}{2} \quad (2.48)$$

$$\frac{\partial h(x_d[i])}{\partial x} \approx \frac{h(x_b[i+1]) - h(x_b[i]))}{x_b[i+1] - x_b[i]} \quad (2.49)$$

Using Equations 2.48 and 2.49, the flux of Equation 2.43 can be approximated:

$$Q(x_d[i]) = a(x_d[i]) + b(x_d[i]) \frac{h(x_b[i]) + h(x_b[i+1]))}{2} + c(x_d[i]) \left(\frac{h(x_b[i+1]) - h(x_b[i]))}{x_b[i+1] - x_b[i]} \right) \quad (2.50)$$

For what follows, it is handy to rewrite this in the following form (note: $Q(x_d[i]) = Q[i]$):

$$Q[i] = q_0(x_d[i]) + q_l(x_d[i])h(x_b[i]) + q_r(x_d[i])h(x_b[i+1])) \quad (2.51)$$

where the coefficients involved in this equation are defined as:

$$\begin{cases} q_0(x_d[i]) = a(x_d[i]) \\ q_l(x_d[i]) = \frac{b(x_d[i])}{2} - \frac{c(x_d[i])}{x_b[i+1] - x_b[i]} \\ q_r(x_d[i]) = \frac{b(x_d[i])}{2} + \frac{c(x_d[i])}{x_b[i+1] - x_b[i]} \end{cases} \quad (2.52)$$

2.5.2 Discretization of the external flux

The total external flux over the interval around a base node $x_b[i]$ limited by its two neighboring dual nodes is approximated by:

$$\begin{aligned}
N(x_d[i]) &= \int_{x_d[i]}^{x_d[i+1]} N(x) dx \\
&\approx \int_{x_d[i]}^{x_d[i+1]} (d(x_b[i+1]) + e(x_b[i+1])h(x_b[i+1])) dx \\
&= (d(x_b[i+1]) + (e(x_b[i+1])h(x_b[i+1]))) (x_d[i+1] - x_d[i]) \\
&= (d(x_b[i+1]) + e(x_b[i+1])h(x_b[i+1])) \left(\frac{x_b[i+2] - x_b[i]}{2} \right)
\end{aligned} \tag{2.53}$$

For what follows, we also introduce the following notation (note: $N(x_d[i]) = N[i]$):

$$N[i] = N_0(x_b[i+1]) + N_1(x_b[i+1])h(x_b[i+1]) \tag{2.54}$$

$$\text{with } N_0(x_b[i+1]) = d(x_b[i+1]) \left(\frac{x_b[i+2] - x_b[i]}{2} \right) \tag{2.55}$$

$$N_1(x_b[i+1]) = e(x_b[i+1]) \left(\frac{x_b[i+2] - x_b[i]}{2} \right) \tag{2.56}$$

2.6 Discrete equations

2.6.1 The balance equations

With the help of the approximations above, we can now define a typical finite volume discrete mass balance for each interval between two dual nodes (see Figure 2.2): the difference between the internal flux entering at the left and leaving at the right must be balanced by the total external flux entering that interval:

$$Q[i] - Q[i+1] + N[i+1] = 0 \quad (i = 1, \dots, m-2) \tag{2.57}$$

Each of these $(m-2)$ balance equations can be written in terms of the unknown h (note:

$$\begin{aligned}
Q[i] - Q[i+1] + N_i[i+1] &= q_0[i] + q_l[i]h[i] + q_r[i]h[i] \\
h(x_b[i]) \approx h[i]: & \quad -q_0[i+1] - q_l[i+1]h[i] - q_r[i+1]h[i] \\
& \quad + N_0[i+1] + N_1[i+1]h[i]
\end{aligned} \tag{2.58}$$

which is equivalent to (note that we re-ordered the sequence considering $i = 2, \dots, m-1$):

$$-q_l[i]h[i] - q_r[i]h[i] + q_l[i-1]h[i] + q_r[i-1]h[i] + N_1[i]h[i] = -q_0[i-1] + q_0[i] - N_0[i] \tag{2.59}$$

2.6.2 The boundary conditions

$$\text{The boundary conditions: } \begin{cases} \alpha_L h[1] + \beta_L Q[1] + \gamma_L = 0 \\ \alpha_R h[m] + \beta_R Q[m-1] + \gamma_R = 0 \end{cases} \tag{2.60}$$

after substituting Equation 2.51 for Q , become

$$\begin{cases} \gamma_L = \alpha_L h[1] + \beta_L (q_0[1] + q_l[1]h[1] + q_r[1]h[2]) \\ \gamma_R = \alpha_R h[m] + \beta_R (q_0[m-1] + q_l[m-1]h[m-1] + q_r[m-1]h[m]) \end{cases} \tag{2.61}$$

which can be rewritten as:

$$\begin{cases} \gamma_L = \beta_L q_0[1] + (\alpha_L + \beta_L q_l[1])h[1] + \beta_L q_r[1]h[2] \\ \gamma_R = \beta_R q_0[m-1] + (\alpha_R + \beta_R q_r[m-1])h[m] + \beta_R q_l[m-1]h[m-1] \end{cases} \tag{2.62}$$

which can again be written in the following form:

$$\begin{cases} (\alpha_L + \beta_L q_l[1])h[1] + \beta_L q_r[1]h[2] = \gamma_L - \beta_L q_0[1] \\ (\alpha_R + \beta_R q_r[m-1])h[m] + \beta_R q_l[m-1]h[m-1] = \gamma_R - \beta_R q_0[m-1] \end{cases} \quad (2.63)$$

2.6.3 Total system of equations

The combination of Equations 2.59 and 2.63 results in a system of equations which can be represented in matrix form as: $\mathbf{A}\mathbf{h} = \mathbf{b}$

where \mathbf{A} is a matrix of the coefficients of the equations, \mathbf{h} is a vector of the state variable (unknown) and \mathbf{b} is the known right hand side vector. As can be easily seen from 2.59, the matrix \mathbf{A} is tridiagonal. This makes the computation of the solution of these equations very efficient (see also Appendix D).

2.7 Solution procedure of the general unsteady equation

The numerical technique that is described in this section can handle the following general unsteady equation:

$$f \frac{\partial h}{\partial t} = -\frac{\partial Q}{\partial x} + N \quad (2.64)$$

In this equation the f -term can be a function of x and of the state variable as $f(x, h(x))$. In case $f(x, h(x))$ is non-linear, it can be treated in a similar way as the internal flux. Knowing the solution procedure of the stationary case, the non-stationary case can be solved easily by considering each time step in the unsteady state case as a new steady state problem. The idea behind this approach is that for each time step the change in storage can be considered as a kind of external flux.

As a first step, the unsteady equation has to be discretized in time. For this, choose times t_0, t_1, \dots, t_n and define $h_n(x) = h(t_n, x)$. Choose $0 < \delta < 1$ and with $\delta' = 1 - \delta$, the time-finite difference discretization of Equation 2.64 is:

$$\begin{aligned} f \frac{h_{n+1}(x) - h_n(x)}{t_{n+1} - t_n} = \frac{\partial}{\partial x} \left\{ Q \left(\delta' t_n + \delta t_{n+1}, x, \delta' h_n + \delta h_{n+1}, \frac{\partial(\delta' h_n + \delta h_{n+1})}{\partial x} \right) \right\} \\ + N(\delta' t_n + \delta t_{n+1}, x, \delta' h_n + \delta h_{n+1}) \end{aligned} \quad (2.65)$$

In this, the parameter δ controls the implicitness. If $\delta = 1$ the numerical scheme is fully implicit and when it approaches zero, it means a fully explicit system, which will not be considered here.

Assume $h_n(x)$ known from the previous step. Then, after introducing the mid-time values:

$$\hat{h} = \delta' h_n + \delta h_{n+1} \quad (2.66)$$

$$\hat{t} = \delta' t_n + \delta t_{n+1} \quad (2.67)$$

Equation 2.65 can be written as:

$$0 = \frac{\partial}{\partial x} \left\{ Q \left(\hat{t}, x, h(\hat{t}, x), \frac{\partial h}{\partial x}(\hat{t}, x) \right) \right\} + N(\hat{t}, x, h(\hat{t}, x)) - f \frac{h(\hat{t}, x) - h(t_n, x)}{\hat{t} - t_n} \quad (2.68)$$

This equation can be rewritten as:

$$\hat{Q}\left(x, h(x), \frac{\partial h}{\partial x}(x)\right) = Q\left(\hat{t}, x, h(\hat{t}, x), \frac{\partial h}{\partial x}(\hat{t}, x)\right) \quad (2.69)$$

$$\hat{N}(x, h(x)) = N(\hat{t}, x, h(\hat{t}, x)) - f \frac{h(\hat{t}, x) - h(t_n, x)}{\hat{t} - t_n} \quad (2.70)$$

which is of the steady state form whose numerical solution has been discussed in the previous section. After finding the mid-time values, the end-time values can be found with:

$$h_{n+1} = \frac{\hat{h} - \delta' h_n}{\delta} \quad (2.71)$$

Application of this method for the dynamic hillslope equations is presented in Appendix E. Different components of the mass balance terms are shown in Figure 2.3 and the simulation procedure of the flow equation in the unsteady case is presented in Figure 2.4.

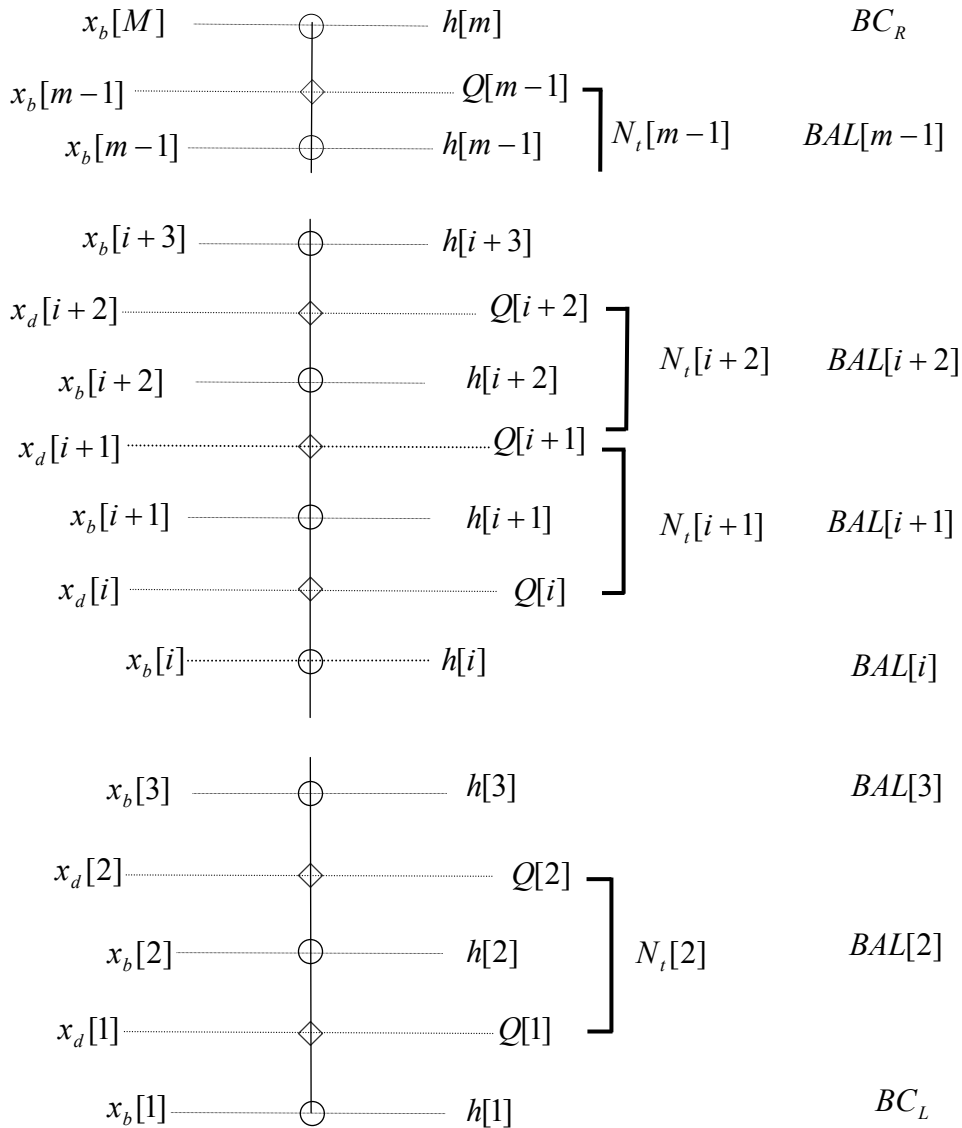


Figure 2.2: Spatial layout of the discretization (circle: base node, diamond: dual points, and BAL stands for balance).

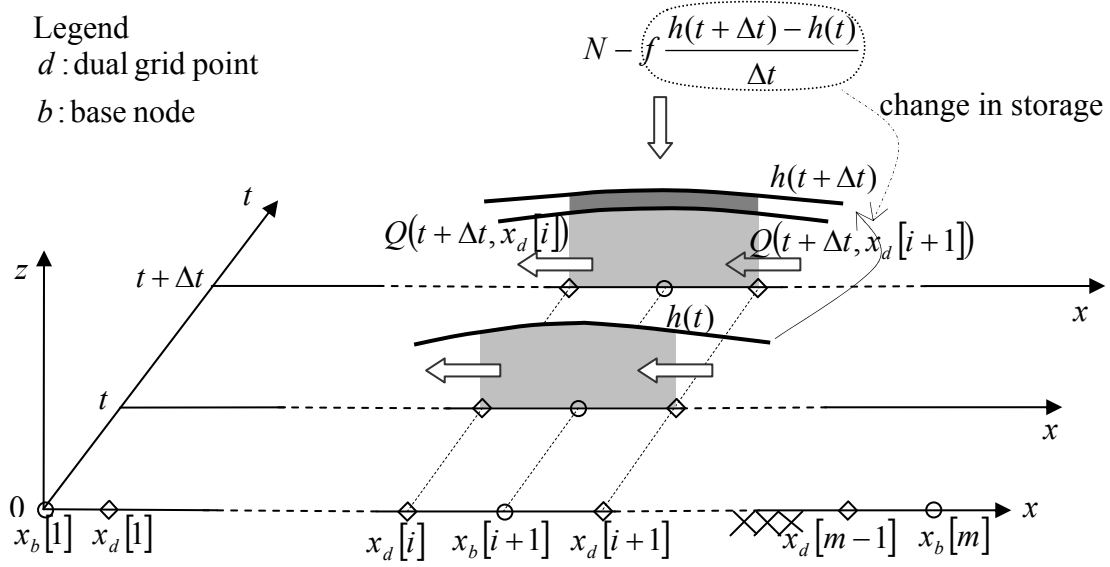
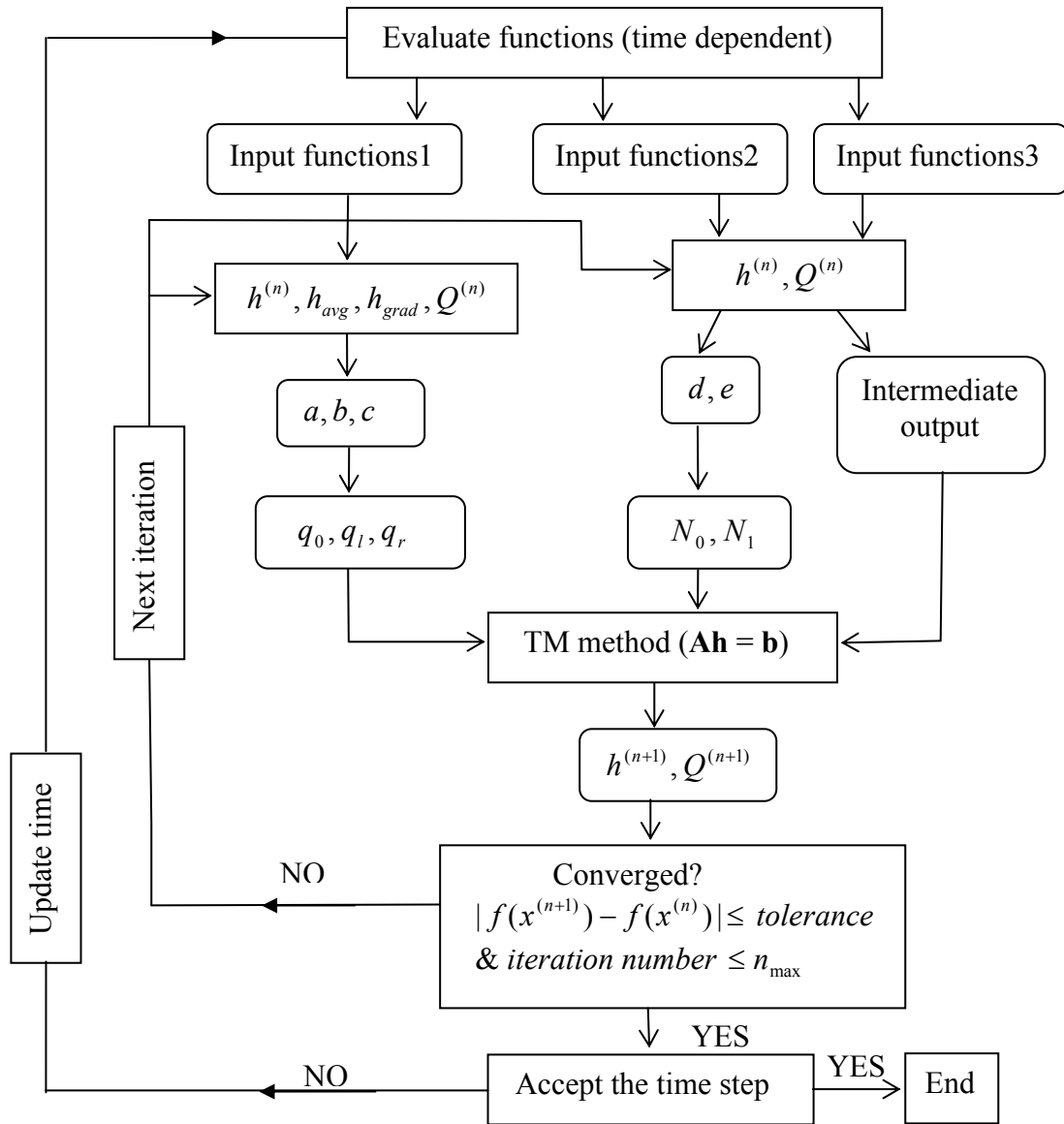


Figure 2.3: Schematic view of different components of the mass balance terms in the unsteady case.



- Input functions1 are Q_a , Q_b and Q_c .
- Input functions2 are N_d and N_e .
- Input functions3 are α_L , β_L , α_R , β_R , γ_L and γ_R .
- Intermediate output includes local variables of boundary conditions: α_L , β_L , α_R , β_R , γ_L and γ_R .
- Subscripts “avg” and “grad” stand for average and gradient of state variable h , respectively.
- “ n_{\max} ” and “TM” stand for maximum number of iterations and Tridiagonal Method, respectively.

Figure 2.4: Flow chart of solution of the system of linear equations in the unsteady case.

Chapter 3

**The role of the hillslope lower boundary condition on
groundwater response**

3.1 Introduction

For the management of hydrological systems it is useful to consider groundwater and surface water together, because these components are continuously interacting (Winter et al., 1998). Considering the interaction between stream and groundwater is also required for a better understanding of water flow processes in a hydrological system like a catchment. Traditionally, catchment models have been mainly applied to problems of surface water management, and similarly, groundwater models have been applied without treating surface water in detail (Nutzmann et al., 2006).

Several studies have been published on the importance of the stream-aquifer interaction in catchment hydrology (e.g., Mikhaelides and Wainwright, 2002; Triana et al., 2003). Mikhaelides and Wainwright (2002) studied the effects of hillslope-channel interaction on catchment runoff production. They presented a two-dimensional, physically-based, distributed catchment hydrological model. Triana et al. (2003) studied stream-aquifer interaction in river basin modeling. They proposed a methodology to represent stream-aquifer response at the regional scale. In their methodology they used an artificial neural network and a groundwater model.

Almost all of the existing models that consider stream-aquifer interaction, do not represent the hydrological processes at the hillslopes and streams in a unified way and they consist of modules for groundwater and surface water (e.g., Bates et al., 1996; El-Hames and Richards, 1998; Triana et al., 2003 and 2004). These models employ aquifer response as input into a stream model. This means that stream-aquifer interaction is modeled using separate numerical solutions for the stream and aquifer models. Mikhaelides and Wainwright (2002), however, conducted a study to unify the stream-aquifer interaction processes at the catchment scale. They used flow routing for both hillslope and stream and assumed Hortonian runoff generation. Unlike the study of Mikhaelides and Wainwright (2002), in this work we seek a way to combine hillslope and stream in one single model.

3.1.1 The downhill boundary condition and the backwater effect

The hillslope models modeled by differential equations in Chapter 1, need a lower boundary condition. Mathematically, the simplest solution is to prescribe a fixed head at the downhill end point (Dirichlet boundary condition). In this chapter, we will call such a model the “uncoupled” case. Physically, this is a less satisfying solution because at this point the hillslope is in contact with the open water, as illustrated by Figure 1.1. This figure also shows that contact occurs along a river, involving in this way several hillslopes. In this work, however, the choice was made to limit the modeling to one single hillslope and that part of the river with which it is in direct contact.

Due to the continuity of pressure, one may assume that the downhill open water level is equal to the downhill groundwater level. As the open water in general fluctuates, this coupling influences the hillslope and causes a feedback process that we call backwater effect in this

work. A model that includes this backwater effect will be called “coupled” in this chapter. We can distinguish the following backwater effects:

- when water flows from the hillslope into the open water at the outlet of the hillslope, the open water level rises, and the groundwater level in the hillslope is forced to follow that.
- when an external open water flow (from upstream) enters the open water part at the foot of the hillslope, the open water level rises faster than the groundwater levels uphill, and by that forces open water into the groundwater (= bank storage), which is to be released later.

This study limits itself to the first type of backwater effect. The backwater effect induced by the lower boundary condition will thus influence the hillslope process. The effect that this has on the outflow of the hillslope can, at least qualitatively, be described using Figures 3.1.a and 3.1.b. These figures present the coupled and uncoupled* cases, respectively.

- During period I, when groundwater table height rises (see Figure 3.1.a), the outflow of the hillslope will increase. In the coupled case, this increase of inflow will induce an increase of the stream water level and by that also an increase in lower boundary level in the hillslope. This in turn reduces the groundwater slopes in the downhill part of the hillslope and by Darcy’s law then also the outflow. In the coupled situation the groundwater outflow will be smaller compared to the same situation in Figure 3.1.b when the water level in the stream is fixed.
- In the other situation (period II), when the groundwater level drops down, the water level in the stream decreases, and as a result also the lower boundary condition of the hillslope will decrease. Hence the gradients in the hillslope will increase, resulting in an increase of the outflow in the case that both stream and groundwater fluctuate. During period II, less water flows into the stream in the uncoupled case compared to the coupled one.

This analysis raises the question: should one always use a coupled open water-hillslope model in order to properly model the hillslope? In this study we investigate the alternative of using a general lower boundary condition given by a discharge-head relationship (Cauchy boundary condition). So the key research question of this study is:

In modeling of hillslope-stream interaction can the stream system be replaced by a proper boundary condition, such that its natural characteristics are preserved?

The advantage of this approach lies in the fact that it could represent the dynamic behavior of one or many hillslopes with typical backwater effects without the requirement of an explicit open water model to couple groundwater and stream.

To solve the governing equations in the hillslope model and to test proposed numerical solution algorithm, we use the numerical scheme presented in Chapter 2. It will be shown that

* Uncoupled here means a case where the downhill boundary condition for the hillslope is kept constant, or mathematically equivalent with a constant open water level.

the numerical approach of that chapter can also handle very general (and non-linear) boundary conditions. The coupled and uncoupled cases will be compared and discussed.

3.2 Modeling setup

In this chapter, we use the extended Boussinesq equation for the hillslope (see Section 1.3.3). The reason for not choosing other models like the extended Boussinesq model based on the slanted Dupuit assumption or the curved Dupuit assumption (see Chapter 1) is that the effects of curved bedrock will not differ that much for the backwater problem discussed in this study.

The open water is modeled by a simple rectangular reservoir, as a general replacement of an open water flow system. We assume that the reservoir has a width B and a length equal to the width of the lower boundary of the hillslope (w). The volume in the reservoir can thus be calculated by:

$$S(t) = h_o(t) w B \quad (3.1)$$

where h_o is the water level measured with respect to the bottom of the reservoir.

The outflow of the reservoir is calculated using a typical open water relationship (see Figure 3.2):

$$Q_{out}(t) = \alpha_b h_o(t)^{\beta_b} \quad (3.2)$$

where α_b is a constant coefficient ($T^{-1}L^{3-\beta_b}$), β_b is dimensionless, and Q_{out} is in L^3T^{-1} .

Weirs (as suggested e.g. in Figure 3.1) and open water equilibrium cases are examples of this type of $Q_{out} - h_o$ relation. In some of the examples that follow, we use the values $\alpha_b = 1.296$ (in $d^{-1}m^{-0.5}$) and $\beta_b = 3.5$. This particular $Q_{out} - h_o$ is plotted in Figure 3.5.a. The values presented for α_b and β_b , are chosen in such a way that they give interesting results for the particular hillslopes and reservoir used in this study.

The mass balance equation of the reservoir is given by $\frac{\partial S}{\partial t} = Q_{in} - Q_{out}$, which will be solved here numerically using a simple explicit* scheme as:

$$S(t + \Delta t) = S(t) + \Delta t (Q_{in}(t) - Q_{out}(t)) \quad (3.3)$$

where S is storage in the reservoir, Q_{in} is inflow to the reservoir which equals the outflow of the hillslope.

3.2.1 Boundary conditions

Three different boundary conditions will be used in this study. In the uncoupled case (the case without feedback mechanism), a given head is used for the lower outflow point.

In the coupled hillslope-reservoir case, the boundary condition is a time-dependent head (time-dependent Dirichlet), given by $h(x_L, t) = h_o(t) - d_r$, where h_o is calculated stage in the reservoir and d_r is depth of the river.

* Due to the complex way of calculation for Q_{in} , an implicit scheme is rather difficult here.

The third type of boundary condition that will be used is a discharge-head relationship ($Q(x_L, t) - h(x_L, t)$ curve). Two different relations will be used: one derived from the analogue reservoir, and the other will be derived from the ‘observed’ $Q - h$ pairs obtained from the coupled model*.

3.2.2 Short discussion on the third type of boundary condition

The hillslope-reservoir coupling is an appropriate modeling approach, which is based on a feedback mechanism. However, it costs time to produce additional computer code and to do more calculations. Since the hypothesis in this study is that it is useful and computationally effective to replace a coupled mode with just a properly chosen boundary condition, we replace the reservoir by a general boundary condition in the hillslope model. This boundary condition describes the natural behavior of the reservoir through a discharge-head relationship. Using this type of boundary condition enables us to represent the hillslope-reservoir interaction process in a unified way, and to model these processes in a single computer program.

* These relations will be explained in 3.3.1 as examples of a mixed boundary condition.

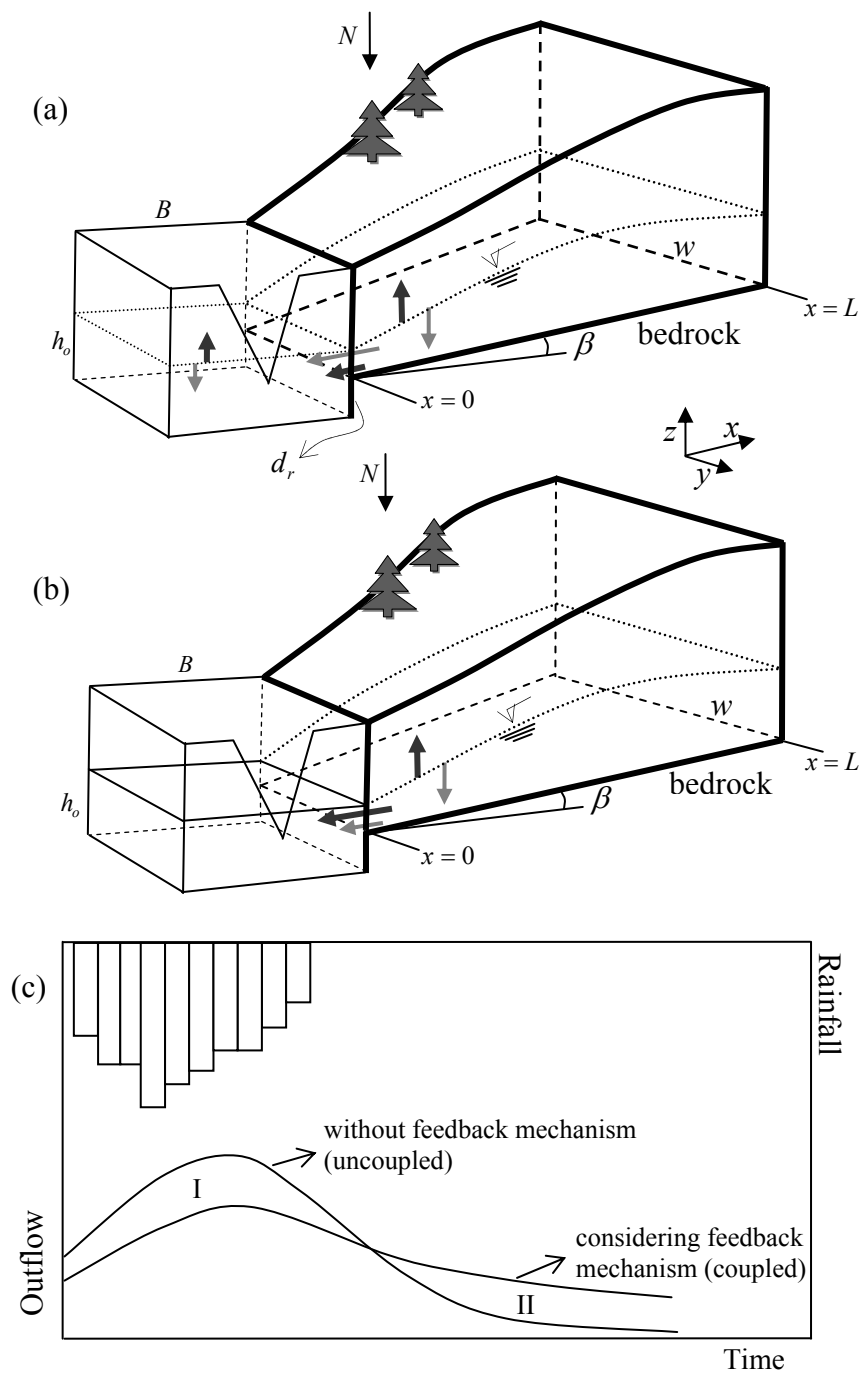


Figure 3.1: Definition of the coupled and uncoupled cases and their responses: (a) water level fluctuates in both reservoir and hillslope systems (coupled); (b) the reservoir has a fixed water level (uncoupled); and (c) rainfall (top), and groundwater outflow with and without feedback mechanism (bottom).

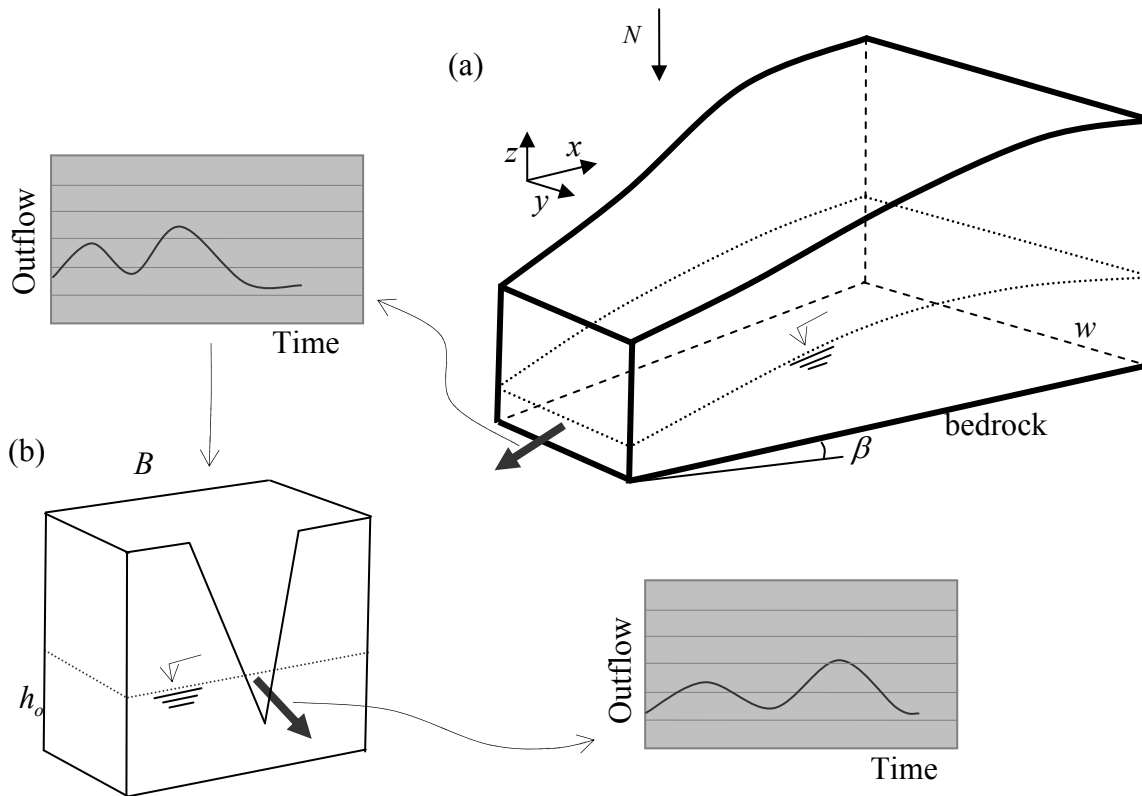


Figure 3.2: Schematic view of the systems involved in hillslope-stream interaction: (a) the hillslope system with relevant hydrograph; and (b) the reservoir system and hydrograph.

3.3 Numerical simulations

The numerical principles as discussed in Chapter 2 can be extended to also treat non-linear boundary conditions. To study the role of the hillslope lower boundary condition, we developed a numerical solution procedure to simulate the dynamics of groundwater head and flux in conjunction with the reservoir processes. In this context, we did three types of simulations based on the type of imposed lower boundary condition.

Numerical solution for the reservoir was carried out using Equation 3.1 through Equation 3.3. One challenge to couple open water and groundwater is the difference in their time scales. This problem arises due to their intrinsic differences in processes. The time step in the reservoir model is small because it is a faster process than the groundwater flow process. In this regard, to couple the reservoir and hillslope, we used a provision that in each time step of the extended Boussinesq equation there are several smaller time steps to compute the reservoir variables.

In the coupled hillslope-reservoir case, the hillslope and the reservoir models were simulated simultaneously. At the start of the simulation, the water level in the reservoir is calculated at each small time step and then the final result at the end of the longer time steps (the hillslope

time steps) is used in the extended Boussinesq model as the lower boundary condition. In other words, the calculated reservoir stage is used to adjust the head in the hillslope lower boundary once for each of the longer time steps. By running the extended Boussinesq model, the calculated outflow is exported to the reservoir model and this loop continues until the end of time period. Figure 3.3 presents a diagram of the numerical solution procedure in the coupled case.

The results of the coupled case (h and Q from both the hillslope and the reservoir) are used to build a discharge-head relationship, which can be expressed as $\gamma = \alpha h(x_L, t) + \beta Q(x_L, t)$ after linearization (as in Section 2.3) to be applied in the computer program. For a typical discharge-head curve, see Figure 1.15.a. The resulting model is called uncoupled with mixed boundary condition. It represents the role of the reservoir through a discharge-head boundary condition. For the concepts and differences of the coupled case and the uncoupled case (with mixed boundary condition) see Section 3.1.1. In the case where the resulting discharge-head relationship is non-linear it needs to be linearized. This can be done in several ways, two of which are similar to the linearization procedure for Q_{nl} explained in the previous chapter.

3.3.1 Examples of non-linear equations for the lower boundary condition

As mentioned before, we have two types of discharge-head relations as boundary conditions. When this relationship is obtained from the coupled model (using the head and discharge results of the hillslope) it exhibits a form as presented in Figure 3.5.c (dotted line). We approximated this relationship as $Q(x_L, t) = \alpha_b h(x_L, t)^{\beta_b}$, where α_b and β_b equal 7.08 and 1.85, respectively.

For the discharge-head relationship obtained from the reservoir, we applied Equation 3.2 as

$$Q(x_L, t) = \alpha_b (h(x_L, t) + d_r)^{\beta_b} \quad (3.4)$$

The results are presented in Figure 3.5.d (dotted line).

3.3.2 Taylor approximation

The boundary condition given by Equation 3.4 is by its analytical character one that can be efficiently linearized by a Taylor approach. Using the notation a_2, a_4 for its arguments (see Chapter 2), this equation becomes: $BC_L(a_2, a_4) = a_4 - \alpha_b (a_2 + d_r)^{\beta_b}$ (3.5)

Taylor approximation for Equation 3.5 gives:

$$\begin{aligned} \gamma_L(a_2, a_4) &= [a_4 - \alpha_b (a_2 + d_r)^{\beta_b}] - a_2 (-\beta_b \alpha_b (a_2 + d_r)^{\beta_b - 1}) - a_4(1) \\ &= -\alpha_b (a_2 + d_r)^{\beta_b} + a_2 \alpha_b \beta_b (a_2 + d_r)^{\beta_b - 1} \end{aligned} \quad (3.6)$$

$$\alpha_L(a_2, a_4) = -\alpha_b \beta_b (a_2 + d_r)^{\beta_b - 1} \quad (3.7)$$

$$\beta_L(a_2, a_4) = 1 \quad (3.8)$$

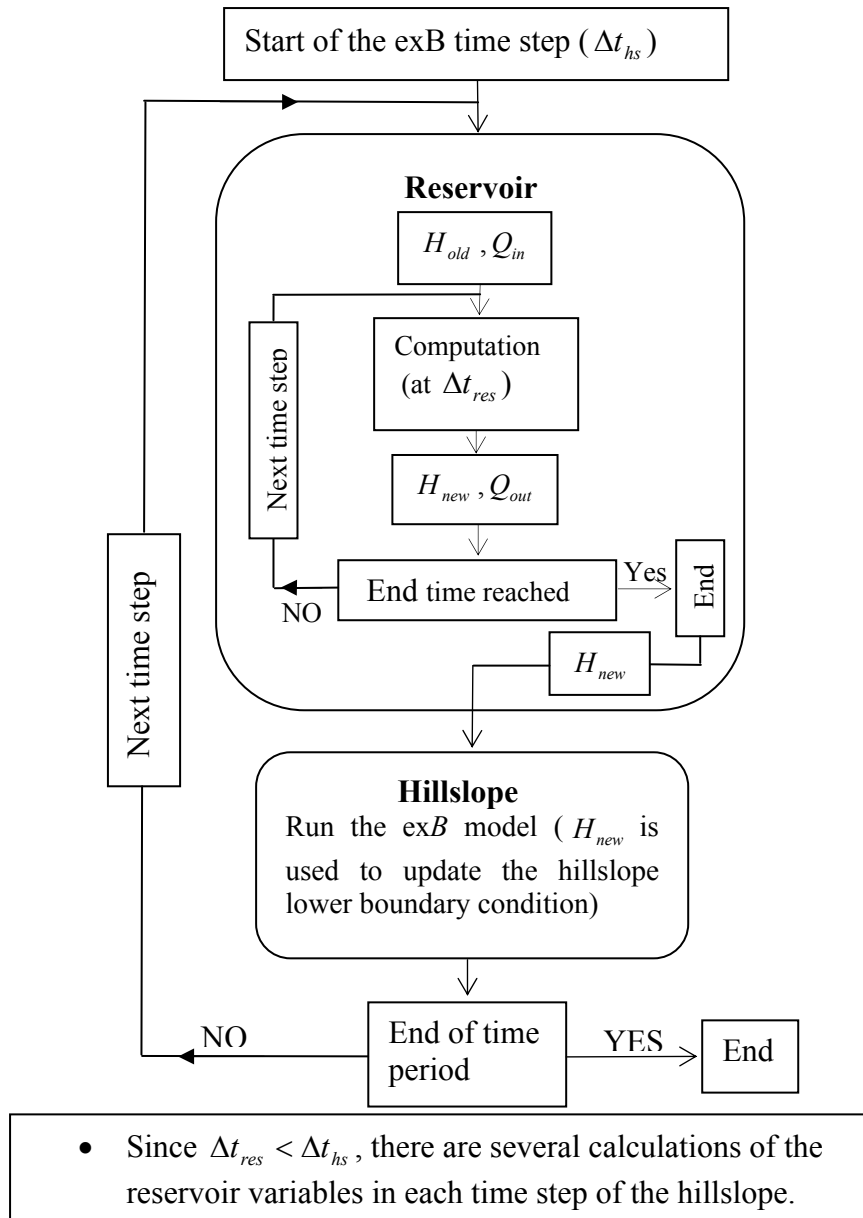


Figure 3.3: Diagram of solution procedure in coupled case (exB indicates extended Boussinesq).

3.3.3 Ad hoc method

This method (for explanation see Chapter 2) can be applied to all kinds of non-linear boundary conditions. Considering the principle of this method (see Section 2.4.2), for Equation 3.5 it results in:

$$\gamma_L(a_2, a_4) = 0 \quad (3.9)$$

$$\alpha_L(a_2, a_4) = -\alpha_b a_2^{-1} (a_2 + d_r)^{\beta_b} \quad (3.10)$$

$$\beta_L(a_2, a_4) = 1 \quad (3.11)$$

3.3.4 Piecewise linear boundary condition

Another type of boundary condition used in this chapter (see Section 3.4.3), is that where the $Q-h$ relation is given by a piecewise linear formula, as:

$$BC_L(a_2, a_4) = a_4 - a_2 \alpha[i] \quad \text{for } a_2[i-1] < a_2 < a_2[i]$$

For each of the intervals, the boundary condition as such is linear and the total linearization is given by the collection of the piecewise linearizations.

3.4 Results and discussion

We performed a series of computations over time and space in different cases. In this context, for the hillslope we used the extended Boussinesq equation with the Taylor approximation method. For all the cases, the same uniform width for the hillslope was applied.

In this section we will discuss the results of the models introduced in previous sections:

- 1- The uncoupled model with fixed boundary condition
- 2- The coupled model
- 3- The uncoupled model with the empirical $Q-h$ relation derived from model 2 as boundary condition
- 4- The uncoupled model with the reservoir $Q-h$ relation as boundary condition
- 5- A piecewise linear approximation of the model 4 above

For all the models the same meteorological forcing will be used: rainfall data was obtained from the Maastricht station in 2001 (KNMI). In a first run, only a small part (1 month) of these data will be used, with an artificial dry period added as in Figure 3.4 (top). Some runs using the whole year will be presented as well (see Figure 3.4 (bottom)).

Simulation results were compared for mass balance accuracy between the coupled and uncoupled cases, with different types of boundary conditions imposed at the hillslope lower boundary.

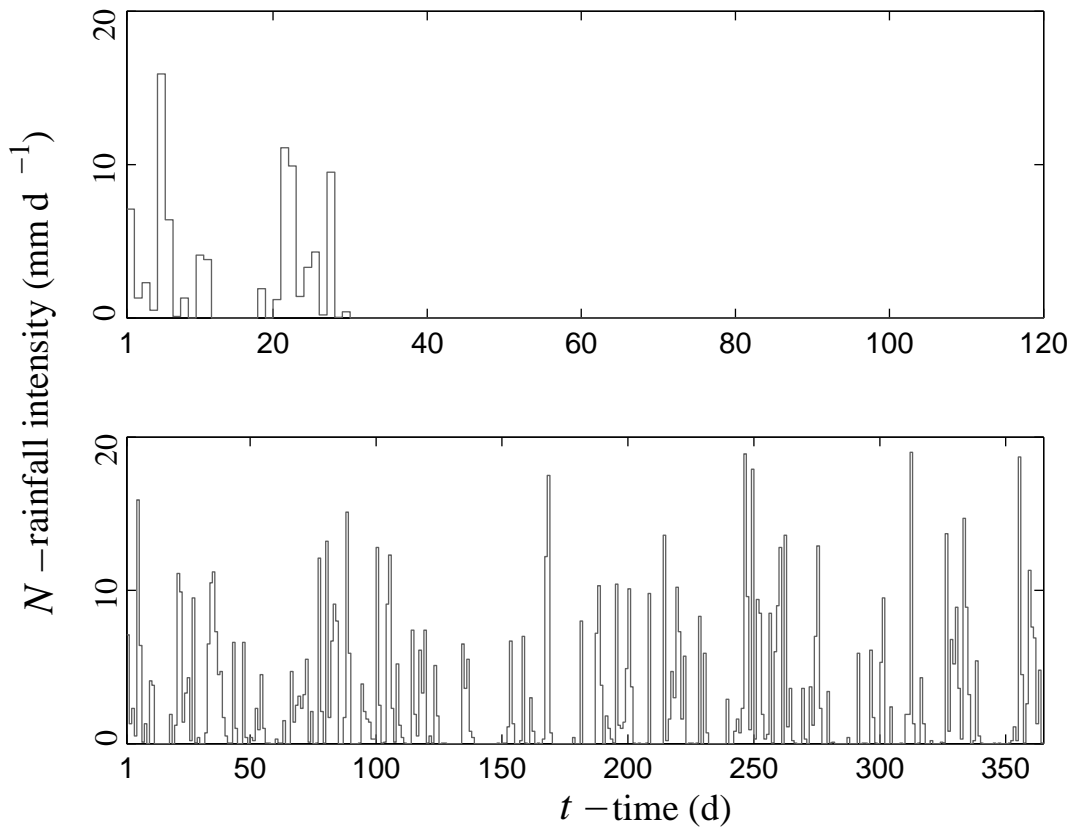


Figure 3.4: Rainfall intensity: (top) for 120 days; and (bottom) for 1 year.

3.4.1 Mass balance check

In the comparison of the different models, the focus will be on the outflow of the hillslope. For this reason, we have chosen to discuss the accuracy of the models by means of the mass balance for the total hillslope.

Tables 3.1 and 3.2 present the mass balance check for the models introduced above for 120 and 365 days, respectively. From these tables we may conclude that the computer code works equally well for all five models.

3.4.2 Comparison of the outflow hydrographs of model 1 and model 2

Figure 3.6.a shows the outflow results of the coupled (model 2) and uncoupled (model 1) cases for the hillslope. In this plot the peak of the hydrograph for the coupled case at early stage is lower than the peak for the uncoupled case. Due to the feedback mechanism in the coupled case, the outflow becomes larger in the tail. These results are consistent with what was to be expected from the discussion of Figure 3.1.c. This example shows that the feedback mechanism influences the response of the hillslope and that neglecting this mechanism will cause significant changes in the response of the hillslope. Hence, the backwater effect regulates the contribution of the hillslope outflow to the stream runoff. The backwater effect demonstrated in this chapter, although only presented for a few examples, can be thought of as

representative for many real hillslopes. However, there are also many cases where this backwater effect is negligible, e.g. if the river is very large compared to the hillslope.

Table 3.1: Mass balance check for the hillslope in 5 cases over 120 days using an hourly time step.

Case	Model 1	Model 2	Model 3	Model 4	Model 5
$\sum Inflow (m^3)$	426.35	426.35	426.35	426.35	426.35
$\sum outflow (m^3)$	433.74	389.80	399.91	389.94	389.97
$\sum Inflow - \sum Outflow$	-7.38	36.55	26.44	36.40	36.38
$S(initial) (m^3)$	161.35	161.21	161.35	161.35	161.35
$S(final) (m^3)$	152.27	196.02	186.06	196.01	195.99
$S(final) - S(initial)$	-9.08	34.80	24.70	34.65	34.63

Table 3.2: Mass balance check for the hillslope in 5 cases over 1 year using an hourly time step.

Case	Model 1	Model 2	Model 3	Model 4	Model 5
$\sum Inflow (m^3)$	4534.73	4534.73	4534.73	4534.73	4534.73
$\sum outflow (m^3)$	3732.29	3482.43	3479.72	3481.28	3483.18
$\sum Inflow - \sum Outflow$	802.44	1052.29	1055.00	1053.44	1051.54
$S(initial) (m^3)$	161.35	161.21	161.35	161.35	161.35
$S(final) (m^3)$	958.39	1208.02	1210.86	1209.30	1208.42
$S(final) - S(initial)$	797.04	1046.80	1049.51	1047.95	1047.06

3.4.3 Construction of the $Q - h$ boundary conditions

In this section we discuss the construction of mixed type of boundary conditions that should serve as a replacement of the stream coupling. Three different approaches are used:

1- An empirical $Q - h$ relationship

This relationship is established using the results of the coupled model by fitting a relation through the observed cloud of h 's and Q 's. Figure 3.5.c and 3.8.a represent the estimated

$Q-h$ curve (solid line) derived from head and discharge data of the hillslope (dotted line). Since the estimated $Q-h$ relationship was non-linear (because of $\beta_b \neq 1$), we applied the ad hoc method (as a choice) to linearize it.

2- $Q-h$ relation of the open water

To obtain this relationship, we used the results of Equation 3.4. Figure 3.5.d presents the $Q-h$ relationship in the reservoir (dotted line). In this example, the obtained relationship has been linearized using the Taylor approximation.

3- Approximate a $Q-h$ (as in #2 e.g.) by a piecewise linear one

As introduced in 3.3.4, approximation of the $Q-h$ curve (e.g., from the reservoir) as a collection of piecewise linearizations. Figure 3.5.f presents a discharge-head relationship obtained using the piecewise linearization method. We used the curve fitting tool in MATLAB. Based on a range of states h , the obtained curve has several linear pieces and each piece follows the relation $\beta Q(x_L) = \alpha h(x_L) + \gamma$. The coefficients of the obtained equations are used in the computer program to construct the mixed boundary condition for the hillslope.

3.4.4 Effect of the boundary condition

Figures 3.6.b, 3.6.c, 3.6.e, and 3.8.b present a comparison of the hillslope hydrological responses based on different types of boundary conditions. As shown in these figures, the outflow resulting from applying the mixed type of boundary condition is almost the same as the result of the coupled case. This slight difference indicates that the uncoupled case with mixed boundary condition is able to predict the response of the coupled hillslope-reservoir system. This implies that it is not necessary to explicitly account for the reservoir and couple it with the hillslope. In other words, using a mixed boundary condition provides a proper alternative to gain reasonable results in a computationally efficient manner. By comparison of the results of three methods that were applied for the approximation of the discharge-head relationship, we conclude that the linearization method does not affect the results of the uncoupled case with the mixed type of boundary condition.

As already mentioned, a $Q-h$ relationship can be derived from the hillslope or the reservoir. Hence, the source of this relationship can affect the hillslope response. In Figures 3.3.c and 3.3.d, we used the $Q-h$ relationship obtained from the hillslope and from the reservoir, respectively. As Figure 3.6.d shows, these two sources of boundary condition cause a little difference in outflow. This is due to difference between two discharge-head relationships (see Figure 3.5.e).

The slight difference in outflows suggests that the discharge-head relationship of the reservoir is applicable as the hillslope lower boundary condition. The benefit of using this $Q-h$ relationship is its simplicity, because we obtained this relationship from the coupled reservoir and hillslope. Simplicity means that we do not need additional model runs compared to the coupled system, as this relationship is known a priori.

3.4.5 Numerical instability and time step choice

Figure 3.7 shows the results of groundwater head and flux, which are calculated based on a daily and an hourly time step for the hillslope model. The reservoir computation time step is in seconds. As can be seen in the figures, there is a marked difference in outflow with different time step lengths. The coupled case with daily step shows numerical instability, but when we use an hourly step this is strongly improved (see Figures 3.7.a and 3.7.b). This difference is due to consistency between time step sizes of the hillslope (hour) and the reservoir (seconds). In the other test, when we apply a mixed boundary condition (the coupled case with a daily time step as shown in Figure 3.7.c) we do not encounter the numerical instability as in the coupled case (Figure 3.7.d). This result indicates that we can apply a daily time step for the uncoupled case (with mixed boundary), which has a fast execution time in comparison with the hourly calculation.

3.4.6 The length of temporal period

To observe the behavior of the coupled and uncoupled cases for a longer time period, we run the program for 1 year using rainfall data which was obtained from the Maastricht station in 2001 (KNMI). Figure 3.8.b shows a comparison of outflows based on the different boundary conditions. As can be seen, the outflow comparison shows a fast increase during the first stage (till day 100) and then it fluctuates around equilibrium. In general, the results of the coupled model and the uncoupled model (with mixed boundary condition) are approximately the same. These results are related to the particular choice of hillslope and reservoir used in this chapter, and then if these are changed, the results will be different.

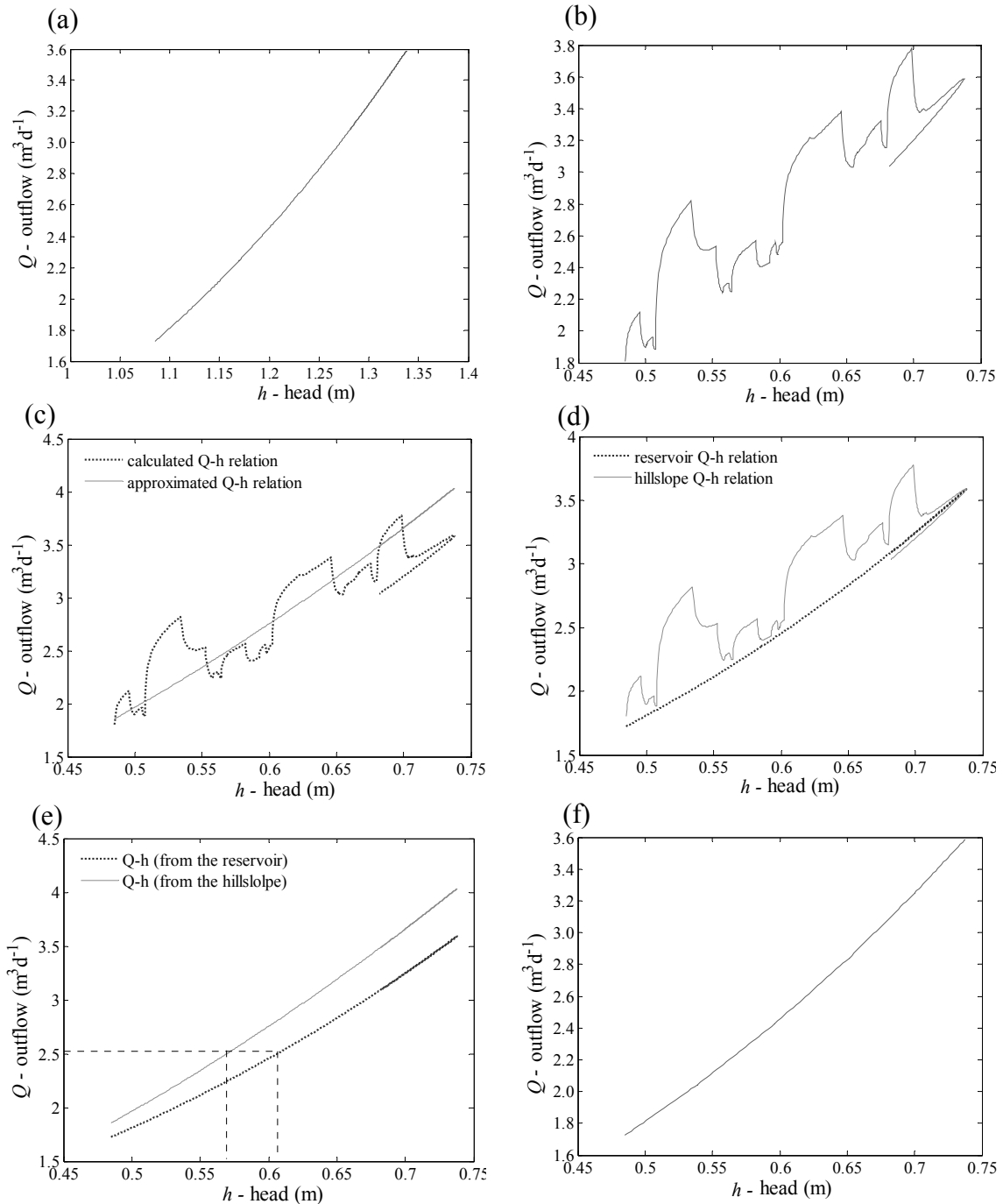


Figure 3.5: $Q-h$ relationships: (a) obtained by the reservoir equation ($Q = \alpha_b h_o^{3.5}$); (b) obtained by the coupled model; (c) A power-law $Q-h$ relationship (solid line) as approximation of the $Q-h$ relationship obtained from the hillslope (dotted line); (d) $Q_{out} - h_o$ relation (dotted line) obtained from the reservoir; (e) Comparison of $Q-h$ curves from the hillslope (solid line) and from the reservoir (dashed line); (f) $Q-h$ curve as approximation (using 5 linear pieces) of the $Q_{out} - h_o$ relationship of the reservoir.

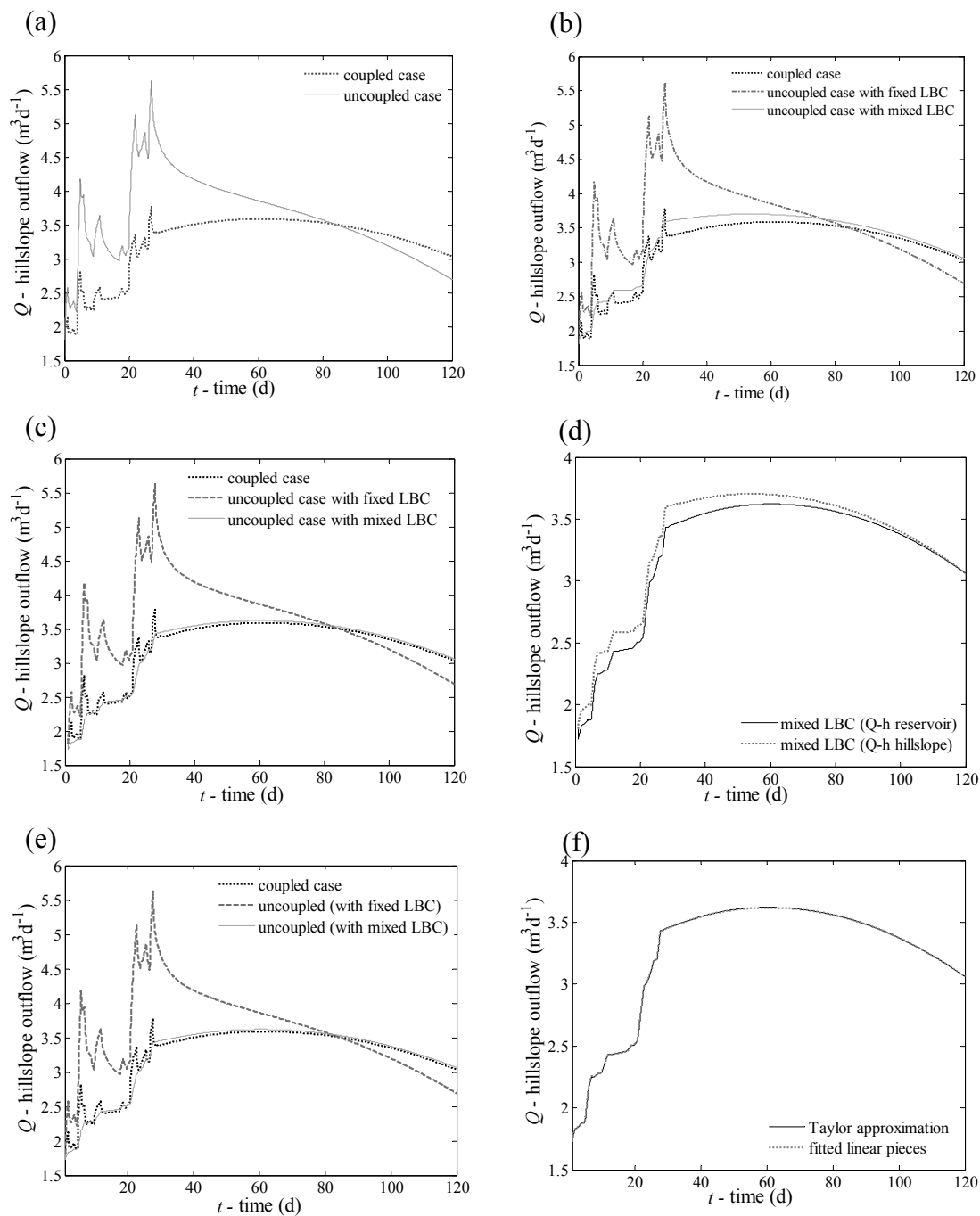
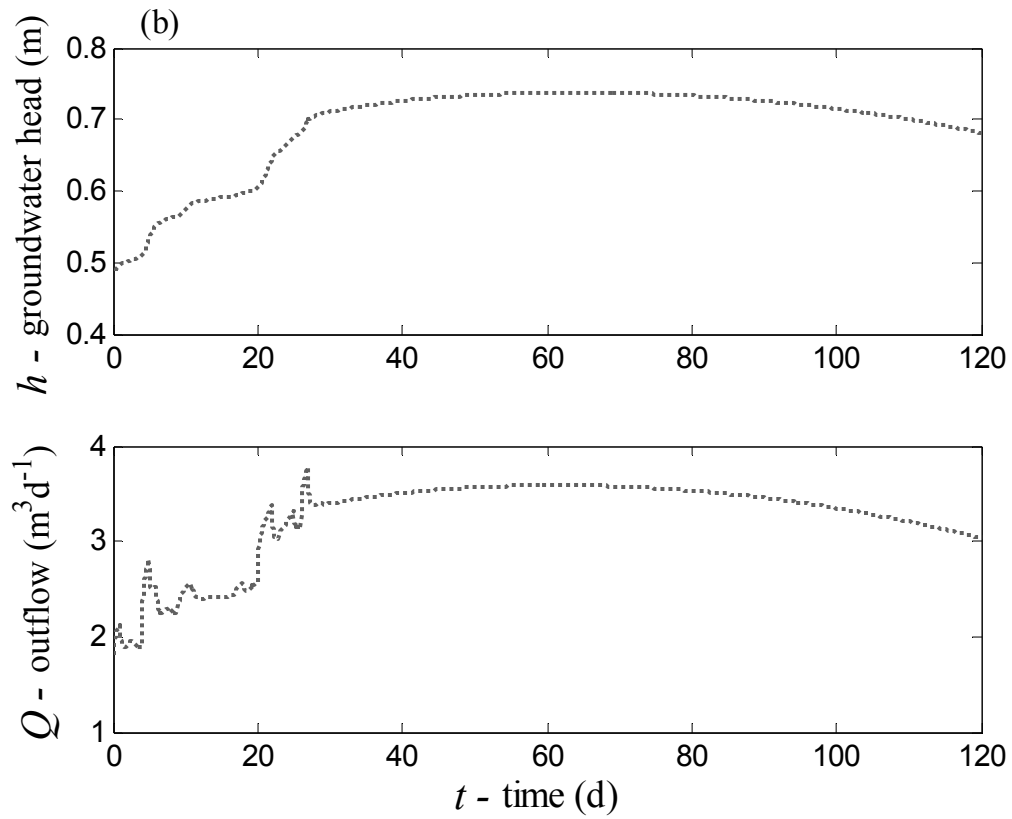
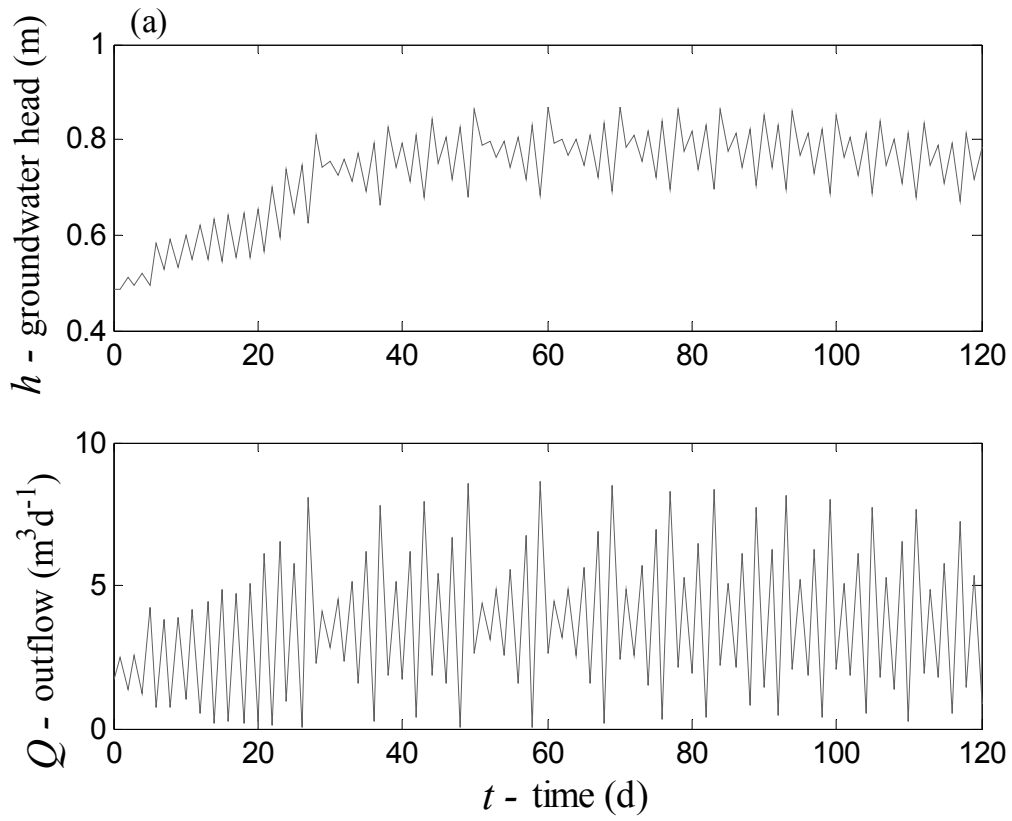


Figure 3.6: Comparison of the outflow results for different situations: (a) comparison between the uncoupled with fixed LBC (solid line) and coupled (dotted line) cases; (b) comparison between the uncoupled case with fixed LBC (dashed line), the coupled case (dotted line), and the uncoupled case with $Q-h$ relationship presented in Figure 3.5.c (solid line) as boundary condition (solid line); (c) comparison between the uncoupled case with fixed LBC (dashed line), coupled case (dotted line), and uncoupled case with $Q-h$ relationship presented in Figure 3.5.d (dotted line) as boundary condition (solid line); (d) comparison between the uncoupled case using the $Q-h$ relationship from the hillslope (dotted line) and from the reservoir (solid line); (e) comparison between the uncoupled case with fixed LBC (dashed line), coupled case (dotted line), and uncoupled case with mixed LBC presented in Figure 3.5.e (solid line); (f) comparison between the uncoupled cases using the $Q-h$ relationship from the reservoir with Taylor approximation (solid line) and fitted linear pieces (dotted line).



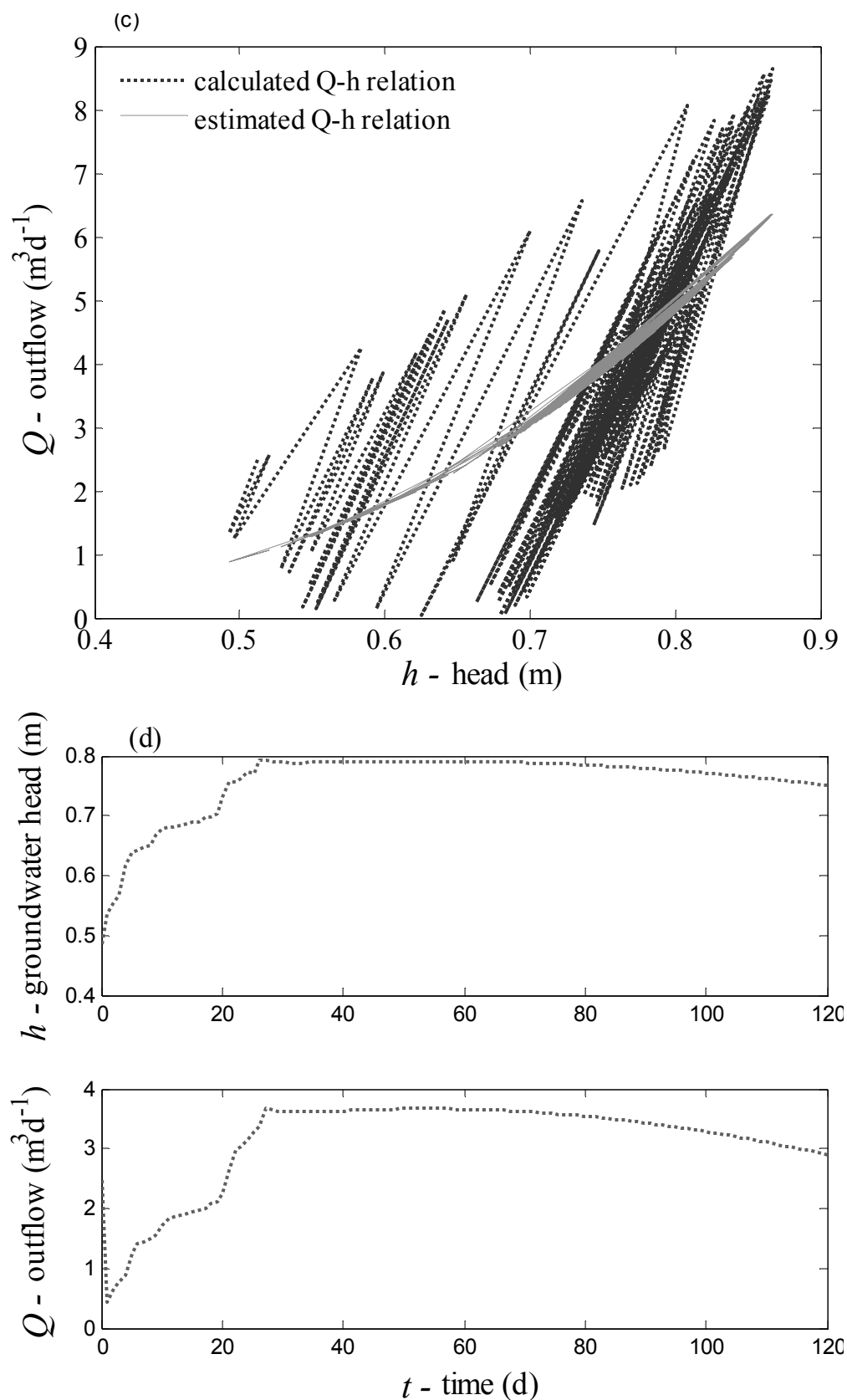


Figure 3.7: (continued from previous page) Time step choice and numerical instability: (a) daily calculation in coupled case; (b) hourly calculation in coupled case; (c) the $Q-h$ relationship obtained from the hillslope at daily basis; (d) daily calculation in uncoupled case with mixed boundary condition.

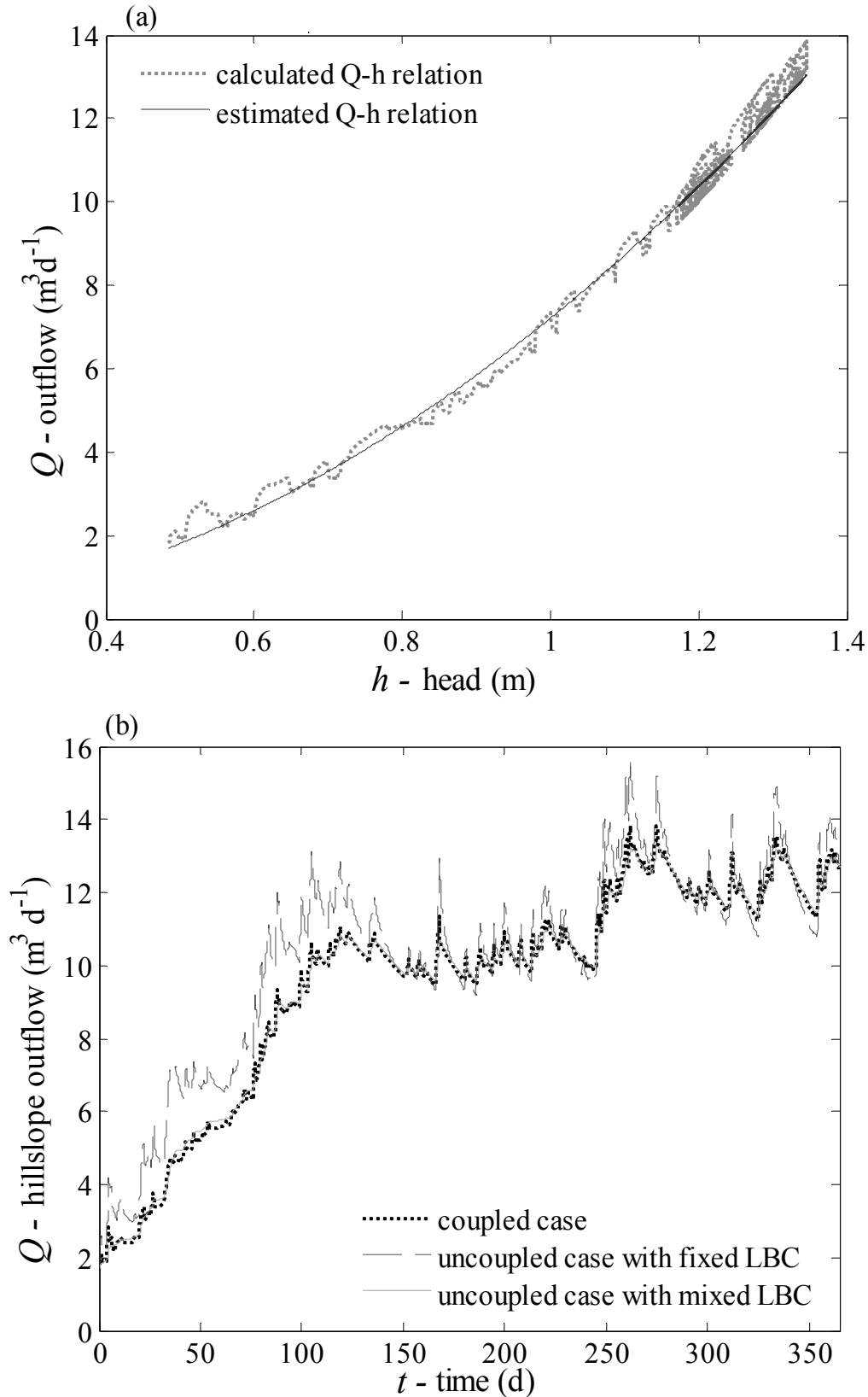


Figure 3.8: (a) $Q-h$ relationship from the hillslope (dotted line) and estimation of that (solid line) as boundary condition; (b) comparison of uncoupled case (with fixed boundary), coupled case, and uncoupled case (with mixed boundary shown as solid line in above figure).

3.5 Conclusions

This study presented a partly new approach to investigate hillslope-stream interaction. This approach accounts for the dynamic behavior of hillslope-stream interaction using the extended Boussinesq equation with a discharge-head relationship as boundary condition at the hillslope outlet.

Comparison of the results of the uncoupled case (with fixed boundary condition) and the coupled case show the important effect of the boundary condition on the hillslope response. Hence, different types of simulations were carried out in order to study the role of the hillslope lower boundary condition in the hillslope-stream interaction.

The results show that the application of the discharge-head relationship as the hillslope lower boundary condition creates a suitable alternative to the coupled hillslope-stream system. Hence, this application causes avoiding the explicit open water modeling by coupling the two systems of groundwater and stream. The method presented in this study describes a way of constructing a single integrated program instead of coupling separate systems.

Through the implementation of the proposed approach, we demonstrated the potential of our approach to accurately model the two systems in interaction. The approach that we presented in this study, unlike previous studies, provides an easy and efficient way to simulate the dynamics of catchment hydrological processes including hillslope-stream interaction.

Chapter 4

**The role of bedrock profile geometry on hillslope
hydrological response**

4.1 Introduction

Study of recharge-induced groundwater flow over a plane sloping bed has been the subject of continuing development (e.g., Childs, 1971; Verhoest and Troch, 2000) since the work of Dupuit (1863) and Boussinesq (1877), but at the scale of more recent applications in hillslope hydrology, a plane bedrock must be seen as a poor representation of a typical hillslope profile (Chapman and Ong, 2006). Several studies have shown that the topography of the bedrock surface is a key determinant of where subsurface flow is concentrated spatially across the hillslope (e.g., Brammer et al., 1995; Woods and Rowe, 1996).

Freer et al. (2002) and Hilberts et al. (2004) demonstrated that the bedrock topography has significant influence on subsurface hydrological response. Several studies have proposed the spatial pattern of the bedrock topographic index as a control on lateral subsurface stormflow patterns through the upslope contributing area concept (e.g., Peters et al., 1995; Tani, 1997; McDonnell et al., 1998; and Hutchinson and Moore, 2000). None of these studies, except Hilberts et al. (2004) and Chapman and Ong (2006), has attempted theoretically to tackle the role of non-constant bedrock slope on groundwater response.

Hilberts et al. (2004) studied the effect of bedrock profile on groundwater response by generalization of the hsB equation (Troch et al., 2003) for non-constant bedrock slope. They considered convex, concave and straight profile curvatures combined with convergent, divergent and parallel plan shapes to form a set of nine characteristic hillslopes. Chapman and Ong (2006) derived a new equation for shallow groundwater flow over a curved impermeable boundary. The latter was based on the Boussinesq equation for flow over continuous curvilinear bedrock. Neither of these studies considers mass balance conservation to parameterize the processes and to derive the flow equations, nor do they consider isolated dead storage zones which are located at the local minima of the bedrock profile. Hence, it remains a task to derive a new parameterization for groundwater flow processes over a complex bedrock profile.

The original hsB equation (Troch et al., 2003) is able to cope with a varying hillslope width function. We have generalized it to be able to simulate hydrological processes in a hillslope with complex bedrock geometry. For the generalization we have applied the curved Dupuit assumption. In order to solve the generalized hsB equation and to test the proposed numerical solution algorithm (Chapter 2) we have applied the algorithm to study the effect of bedrock geometry on hillslope groundwater response.

The main question we address in this chapter is how the geometry of the bedrock profile affects the hillslope hydrologic response. Examples of such geometries are presented in Figures 4.1 and 4.2. Special attention will be paid to the local geometrical bedrock complexity and the effect of so called dead storage zones. Dead storage zones are the convex parts of the bedrock profile. The other question is whether the simple but general and flexible algorithm of Chapter 2 is versatile enough to solve the more complex differential equations and of this chapter. In this respect, special attention will be paid to the numerical problems associated with very thin layers of water.

In the following section a brief summary (more detail can be found in Chapter 1) of the equations applicable to the complex geometry will be presented. The numerical solution setup of the equations will be presented in Section 4.3. In Section 4.4 problems associated with numerical solution are discussed. In Section 4.5 some results of the models are given. Finally, concluding remarks are presented in Section 4.6.

4.2 Governing equations

A brief description of the governing equations is presented in this section. Since we replaced S in original hsB equation by h and we called it extended Boussinesq (exB) equation (see Chapter 1), hereafter instead of the generalized hsB equation we use the generalized exB equation.

4.2.1 The differential equations

To model the complex geometries, we choose the geometrically most complex model of Chapter 1: the extended Boussinesq equation based on the curved Dupuit assumption (see 1.3.6)

$$f w(x) \frac{1}{\cos(\beta(x))} (1 - \kappa_B(x) h(x, t)) \frac{\partial h}{\partial t}(x, t) = - \frac{\partial}{\partial x} \left(\frac{K_s(x) w(x) \cos(\beta(x))}{\kappa_B(x)} \ln(1 - h(x, t) \kappa_B(x)) \right. \\ \left. \left(\cos(\beta(x)) \frac{\partial h}{\partial x}(x, t) + b'(x) - \sin(\beta(x)) \kappa_B(x) h(x, t) \right) \right) + N(t) w(x) \quad (4.1)$$

where $\beta(x)$ is the variable slope angle of bedrock, κ_B is the bedrock profile curvature, K_s is the saturated hydraulic conductivity, w is the hillslope width function, N is the rate of external flux (recharge), b' is the derivative of bedrock elevation (b) measured vertically, f is the effective soil porosity ($f = \theta_s - \theta_r$), and h is the groundwater table.

We will also discuss stationary cases, given by:

$$- \frac{\partial}{\partial x} \left(\frac{K_s(x) w(x) \cos(\beta(x))}{\kappa_B(x)} \ln(1 - h(x) \kappa_B(x)) \left(\cos(\beta(x)) \frac{\partial h}{\partial x}(x) + b'(x) - \sin(\beta(x)) \kappa_B(x) h(x) \right) \right) \\ + N(x) w(x) = 0 \quad (4.2)$$

4.2.2 Bedrock geometry

The bedrock geometry of actual hillslopes is highly complex. The most common geometrical form of hillslope profile is an upslope convex profile due to erosion and a downslope concave profile due to deposition, but it is impossible to derive one single general parameterization (Chapman and Ong, 2006). It is however clear that this complex bedrock geometry does influence the hillslope hydrological response (see e.g. Brammer et al. (1995)). To study this, we use in this chapter a few artificial bedrock profiles, plots of which can be seen in Figures 4.1.a, 4.1.b and 4.1.c. Note that unlike other studies (e.g., Hilberts et al., 2004), these profiles have both concave and convex parts.

The convex parts play a special role. If gravity drainage would be the only water (re)moving mechanism, water would be trapped in these depressions during long dry periods. For that reason, these convex parts are also called dead storage zones. To study the role of these zones (also in dynamic situations), the third bedrock profile (see Figure 4.1.c) was constructed by taking the concave envelope of the second profile.

4.2.3 Initial and boundary conditions

For all the models of this chapter, we will use a simple head boundary condition at the hillslope outlet ($h = 0.5m$ above the bedrock), and the bedrock and the hillslope divides are treated as no-flux boundaries. The reason for not choosing other types of boundary conditions (as presented in the previous chapter) is that (at least qualitatively) the backwater effect will not differ that much for the curved bedrock discussed in this chapter. If an initial condition is needed, we use a stationary solution with the same boundary condition and an average rainfall intensity.

4.2.4 Parameters

The parameters that are used for the simulation in this chapter correspond to a sandy soil (Hilberts et al., 2007): $K_s = 5 \text{ m d}^{-1}$, $f = 0.354$ ($f = \theta_s - \theta_r$). The hillslope has a horizontal length of 100 m and a uniform width of 50 m. For dynamic calculations, as in the previous chapter, the daily rainfall from the Maastricht station in January 2001 (KNMI) is used.

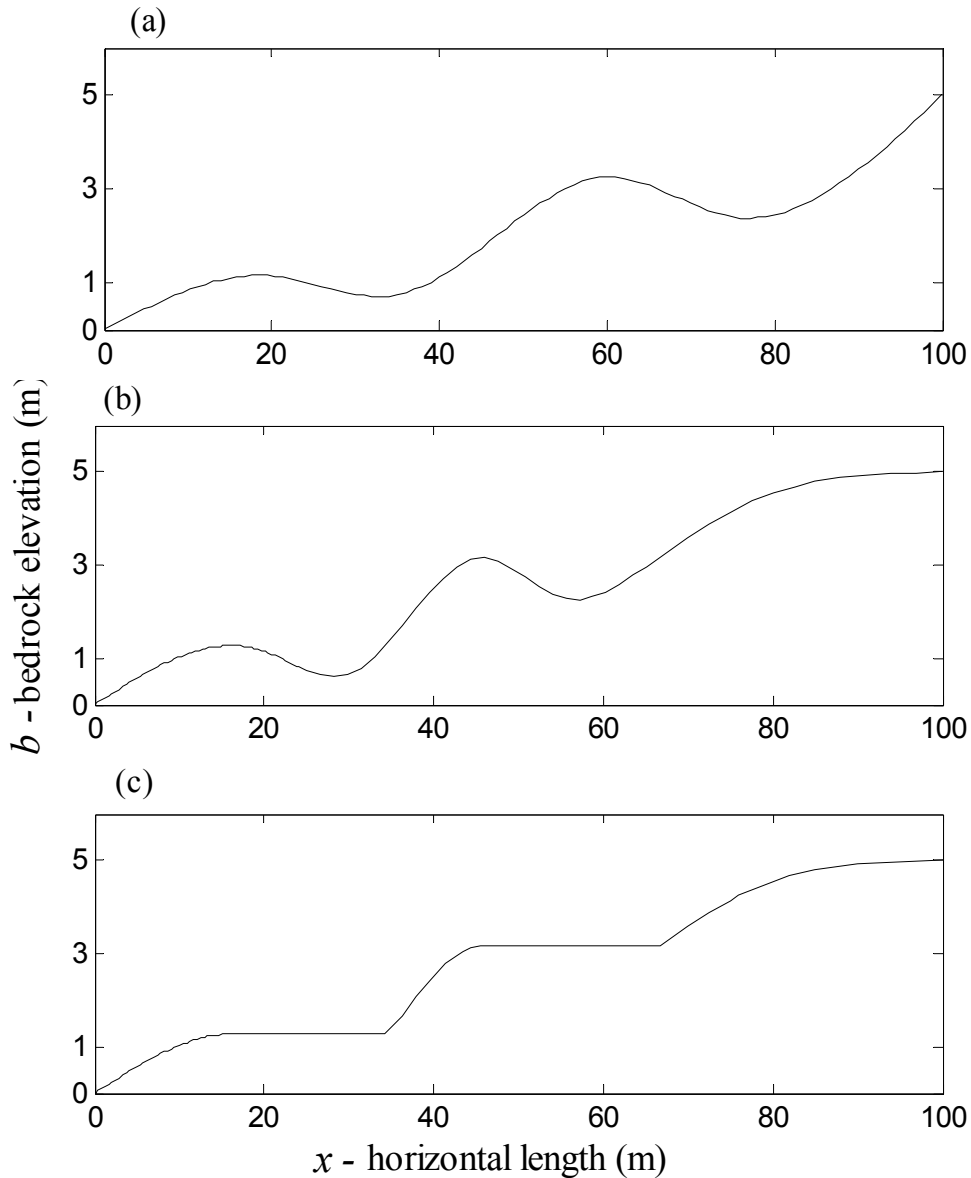


Figure 4.1: Examples of bedrock profiles: (a) curved with concave and convex parts and steep at the divide; (b) curved with concave and convex parts and gentle upslope; and (c) profile like (b) without local minima.

4.3 Numerical simulation setup

As described in Chapter 2, space is discretized by a dual grid approach. The grid points can be chosen non-equidistant in space (see e.g. Section 4.4). The exB Equations 4.1 and 4.2 are solved using the numerical solution algorithm proposed in Chapter 2. Since the linearization method is not an issue, we applied the ad hoc method to linearize the non-linear generalized exB equation.

The differential Equations 4.1 and 4.2 require the existence of first and second order derivatives of the bedrock function. For this reason, the bedrock profiles of Figures 4.1.a, 4.1.b and 4.1.c were constructed by specifying a finite number of points and using a cubic spline interpolation technique (Burden and Faires, 1997).

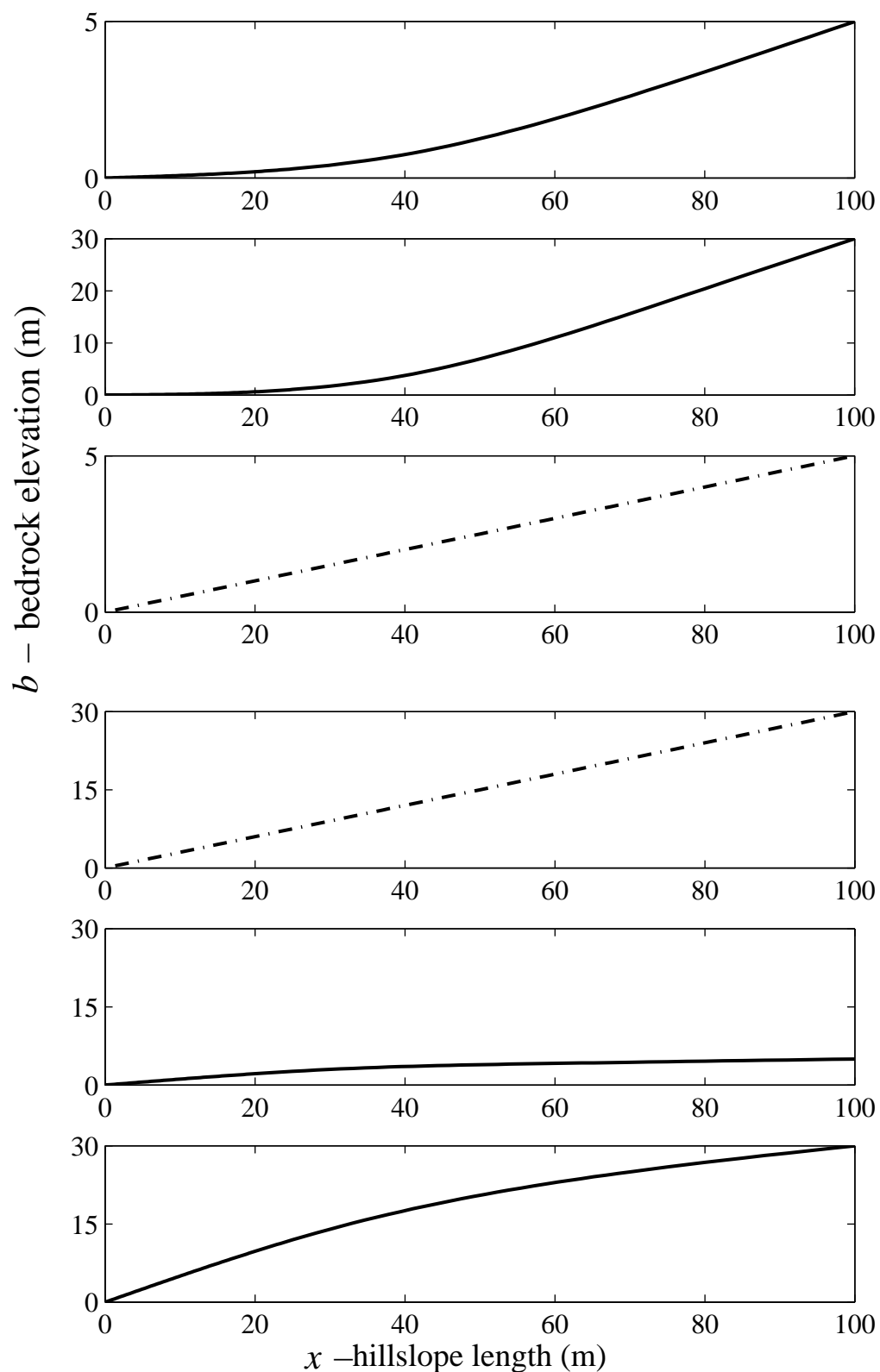


Figure 4.2: Different bedrock profiles: convex (two figures at the top with 5% and 30% average slope angles), straight (two figures in the middle with 5% and 30% average slope angles) and concave (two figures at the bottom with 5% and 30% average slope angles).

4.4 Problems associated with numerical solution

In the numerical simulations made for this chapter, instabilities occurred mainly at places where the bedrock has steep slopes. These numerical instabilities usually resulted in negative groundwater heads, large flux values and oscillatory behavior during the iterations. They occurred both during the steady and unsteady calculations.

To tackle these problems, the following approaches were used:

- The first bedrocks tested for the calculations of this chapter had a rather steep slope at the upper boundary where a divide was modeled by a no-flux boundary condition (see top figures of Figure 4.3 and 4.4). There the numerical problems of the steep slope were even amplified by the fact that the water layer is likely to be very thin. This increases the danger of negative heads during the iterations. Changing the slope near the divide to very gentle (in many cases physically more realistic) clearly improved the stability, as can be seen from Figure 4.4. In this figure, both subfigures (top and middle) produce the same flux (bottom).
- One of the problems causing numerical instabilities is that during the iterative procedure very small heads are approximated by (very small) negative ones. Transformation methods as discussed in Chapter 2 are one way to solve this problem: by taking the square or the exponent one is assured of positiveness. As discussed in Chapter 2, the numerical approach adopted in this thesis is capable of handling these complex non-linearities. Figure 4.5 show different approximations employing these transformations.
- Spatial resolution of the numerical grid is a factor that influences the numerical stability. Since this spatial resolution is not necessarily uniform, this resolution can be changed locally. In general, choosing a higher spatial resolution with a smaller tolerance parameter (for more information the reader is referred to Chapter 2) does produce more accurate results. These approaches were not successful here. Increasing the number of grid points increases the number of h values and by that in very sensitive regions the danger of oscillations. It even proved to be the case that decreasing the number of grid points at a very steep part of the slope improved the numerical stability (see top figure of Figure 4.3). Changing the tolerance parameter as discussed in Chapter 2 could be another solution. Making this parameter smaller does not improve the accuracy of the results in this case, as shown in the bottom figure of Figure 4.3. However, this improvement is not sufficient to make all the heads positive. A decrease of the tolerance parameter also results in significantly longer runtimes. Whenever we need to model a bedrock profile with a steep slope at the divide, we use a low spatial resolution (locally at the hillslope divide). Due to the steep slope and the nearby presence of the boundary condition this influences only a small fraction of the hillslope. Since the tolerance parameter proved to have only a limited influence on numerical stability, we use the larger one for sake of faster convergence.

4.5 Results and discussion

We have performed a number of computations in order to study the hydrological response in time and space of a hillslope with an impermeable curved bedrock. These models differ in rainfall intensities and bedrock profiles:

- 1- The stationary exB equation based on the curved Dupuit assumption for curved bedrock (see Figures 4.3 to 4.8).
- 2- The non-stationary exB equation based on the curved Dupuit assumption:
 - 2-a- for a curved bedrock (see Figures 4.8, 4.9, and 4.10).
 - 2-b- for a non-dead storage zone bedrock (see Figures 4.8, 4.9, and 4.10).
 - 2-c- for a convex bedrock with an average slope of 5% (see Figures 4.13, 4.14).
 - 2-d- for a convex bedrock with an average slope of 30% (see Figures 4.13, 4.14).
 - 2-e- for a concave bedrock with an average slope of 5% (see Figures 4.13, 4.14).
 - 2-f- for a concave bedrock with an average slope of 30% (see Figures 4.13, 4.14).
- 3- The original non-stationary exB equation (see Equation 1.17)
 - 3-a- for a straight bedrock with an average slope of 5% (see Figures 4.8, 4.9, 4.10, 4.14).
 - 3-b- for a straight bedrock with an average slope of 30% (see Figures 4.14).

4.5.1 Influence of rainfall intensity on groundwater flux

Stationary calculations for a curved bedrock profile (model 1 as identified in the previous section), were carried out for four rainfall intensities of 1, 2, 5, and 10 mmd^{-1} . Figure 4.6 shows the results. For low rainfall intensities, the groundwater table is clearly influenced by the geometry and follows in general the concave envelope. For high rainfall intensities however the results are hardly influenced by the bedrock profile. These findings are consistent with the results obtained by Chapman and Ong (2006), who found that at low rainfall intensity (recharge) the groundwater head is influenced by the bedrock topography. They are also in agreement with the findings obtained by Tromp-van Meerveld and McDonnell (2006), in that the bedrock topography might not be the only dominant control on subsurface flow, as was suggested earlier from the analysis of only a few storms by McDonnell et al. (1996) and Freer et al. (1997, 2002).

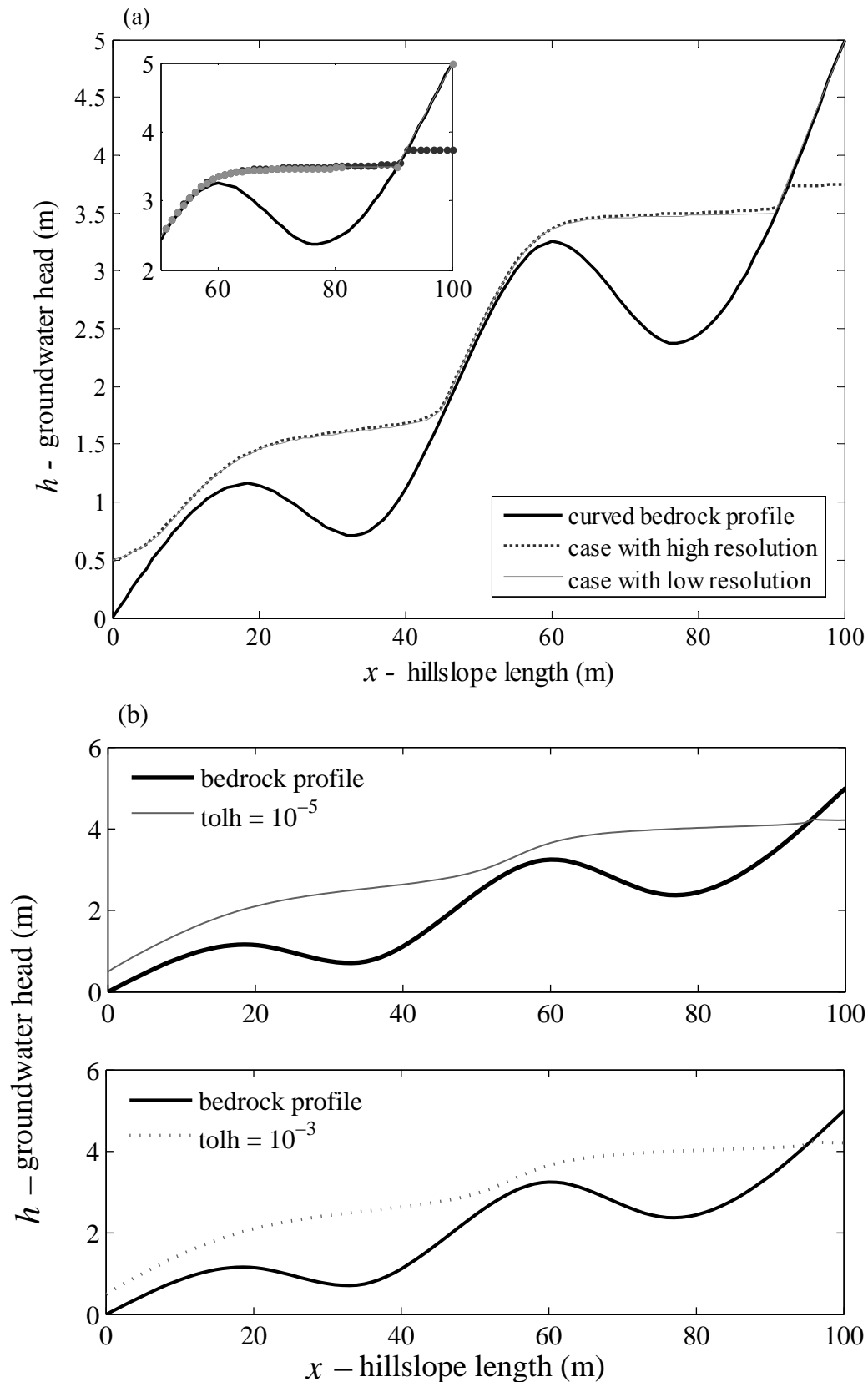


Figure 4.3: The effect of spatial resolution (top: steep slope near hillslope divide and occurrence of numerical problem close to the divide) and tolerance parameter (bottom) on the numerical simulation results (in bottom figure, both subfigures present the same results based on different tolerance parameters).

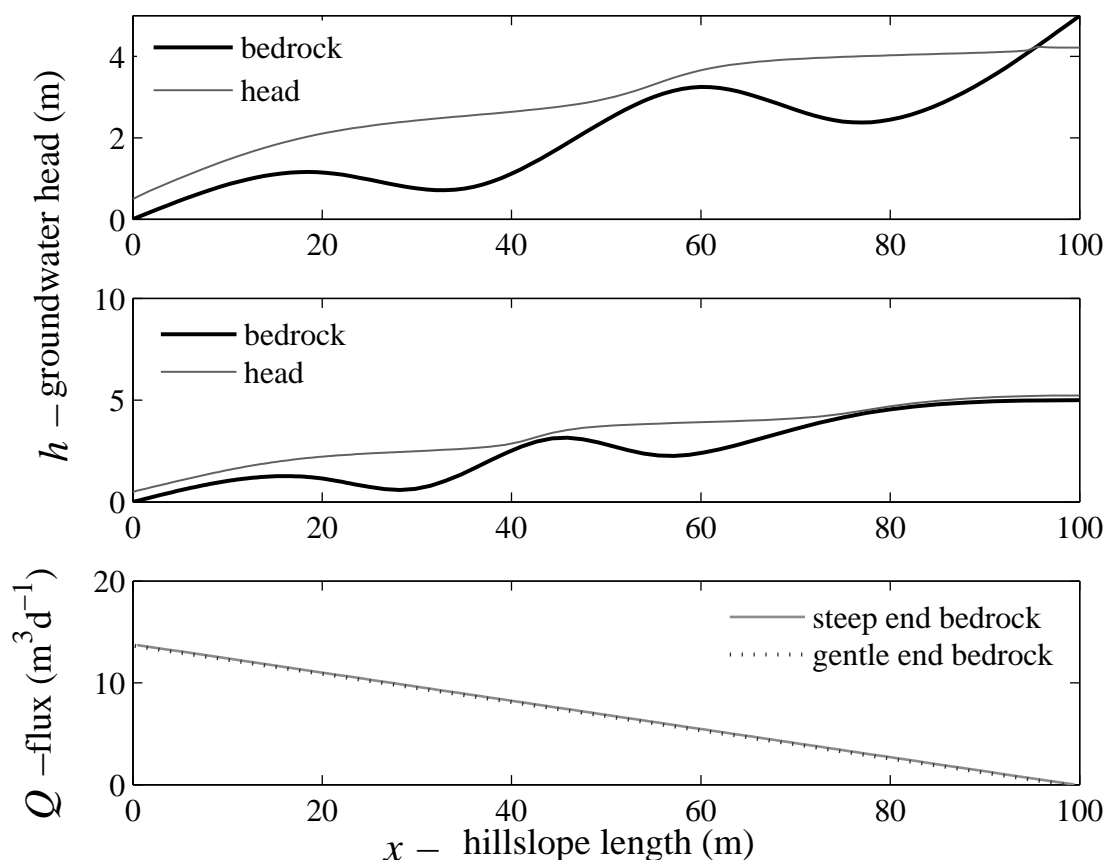


Figure 4.4: Groundwater head over a sharp and smooth bedrock profile (top and middle), and groundwater flux along hillslope (bottom).

4.5.2 Influence of different types of bedrock profiles

Models 2 (2-a, 2-b) and 3-a were used to compare different bedrock profiles in non-stationary situations. Figures 4.8.a and 4.9 show the spatial variations of groundwater head and discharge at the end of a one-month time period (for rainfall, see Figure 4.7 (top)). The groundwater heads on the curved bedrock (model 2-a) are clearly higher than those of models 2-b and 3-a. This means that curvature causes an accumulation of water and an increase of groundwater head.

The results also differ in terms of fluxes in space (see Figure 4.9). As the fluxes depend both on the head and gradient of the head (see Equation 1.16), Figure 4.8.b was created to show both components, at the end of the one month time period. This figure demonstrates that the differences in flux can be more due to differences in head than due to differences in the head gradients. As can be seen in the figure, the difference between the maximum and minimum head is more than that of the corresponding gradients. Another point is that the differences between the graphs of the head in the three cases are larger than those between the gradient

graphs. Hence, we can conclude that in this context the role of head is more important than that of head gradient.

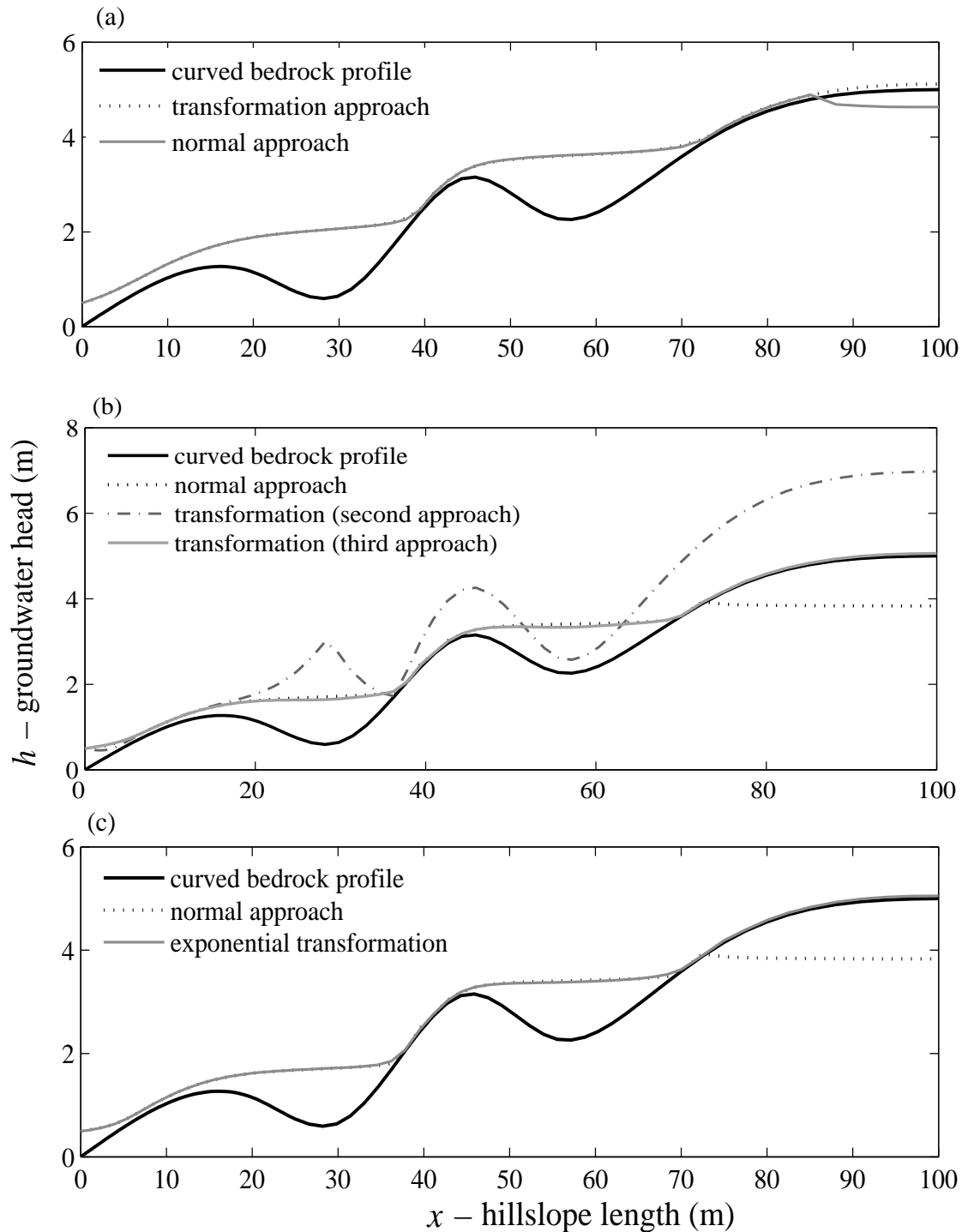


Figure 4.5: The effect of a transformation to improve the simulation results near the hillslope divide (a) square form transformation and first linearization approach (see Chapter 2); (b) square form transformation with two different linearization approaches; (c) exponential form of transformation.

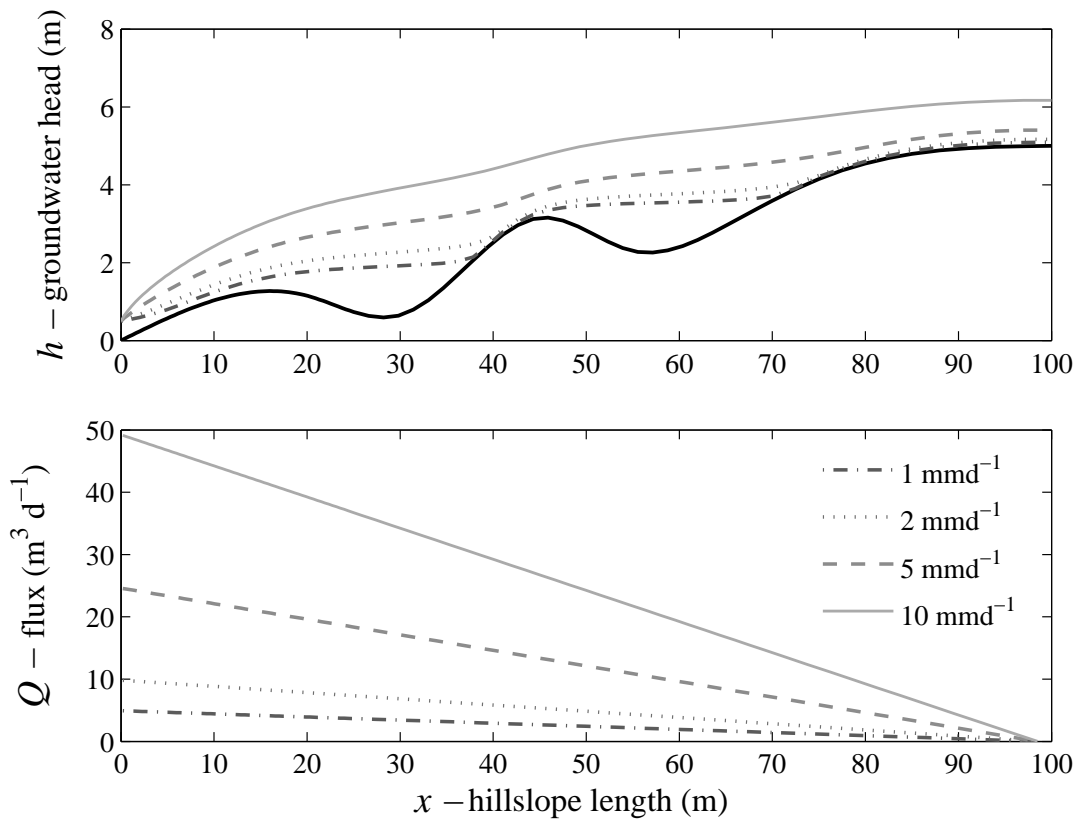


Figure 4.6: Influence of rainfall intensity on groundwater head and flux on curved bedrock.

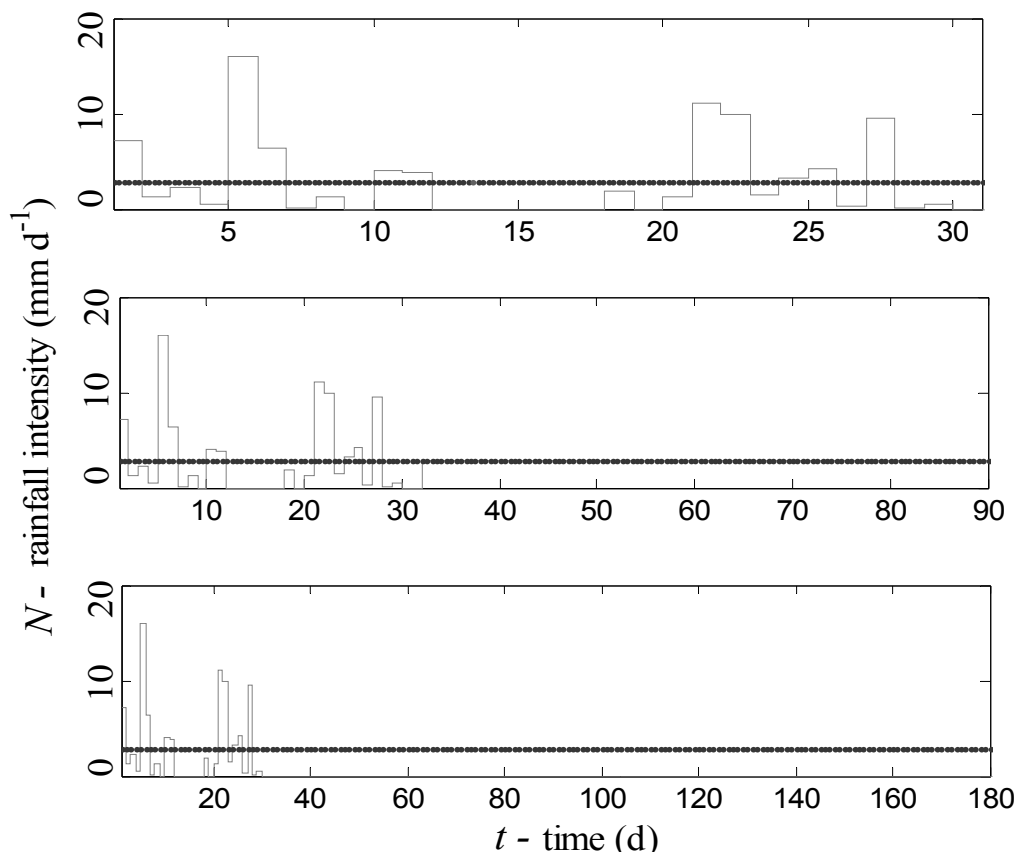


Figure 4.7: Rainfall intensity in one month (top), artificially extended until 3 months (middle) using average of first month and extended until 6 months (bottom) using zero rainfall after first month.

4.5.3 Bedrock profile and groundwater flux

Figure 4.10 presents the temporal variation of the groundwater fluxes (of models 2-a, 2-b, and 3-a) at four specific locations ($x=0$, $x=16\text{m}$, $x=45\text{m}$, and $x=75\text{m}$) along the hillslope. In these figures we can distinguish three types of behavior:

- 1) At the outlet during the rainfall period there is hardly any difference in outflow from hillslopes with different bedrock profiles. This shows that these models perform equally well as rainfall-runoff generators for wet periods.
- 2) At the outlet during the dry period (starting from day 30 onwards), significant differences are observed. This shows that if one wants to use these models for low flow or drought studies, the bedrock geometry does play a role.
- 3) At uphill locations (especially in the two middle figures) the three cases show a clearly different behavior.

The construction of the initial condition is important for a proper understanding of the conclusions above. All initial conditions were constructed starting from the same water level downhill and the same constant rainfall intensity (the mean of the first month was chosen). Although the physical parameters according to which these initial conditions were determined were the same, they resulted in very different initial storages for the different hillslopes. Figure 4.12 was made to illustrate these differences by ways of mass balances.

If we integrate at a certain position on the hillslope the fluxes over time, then (for a long interval) that integral should equal the total amount of rainfall that has fallen upstream of that point minus the changes in storage in that part of the hillslope. To check the conservation of mass and also to verify a proper functioning of the code, we tested the mass balance for the hillslope with different bedrock types. As can be seen for instance in Figure 4.12, the fact that the total outflow is smaller for the case with non-dead storage zone profile can be explained by the lower initial storage compared to the two other cases. The other conclusion that can be drawn from this figure is that the drainage is fast for the case with a straight slope, while it takes more time in curved and non-dead storage zone profiles.

To check the differences of the hillslope response over different bedrock profiles, the recession limbs of the hydrographs were analyzed by fitting pure exponential decays to subparts of the discharge at the outlet (see Figure 4.11). As can be seen in this figure, the outflow over straight bedrock will drain more quickly compared to the two other cases.

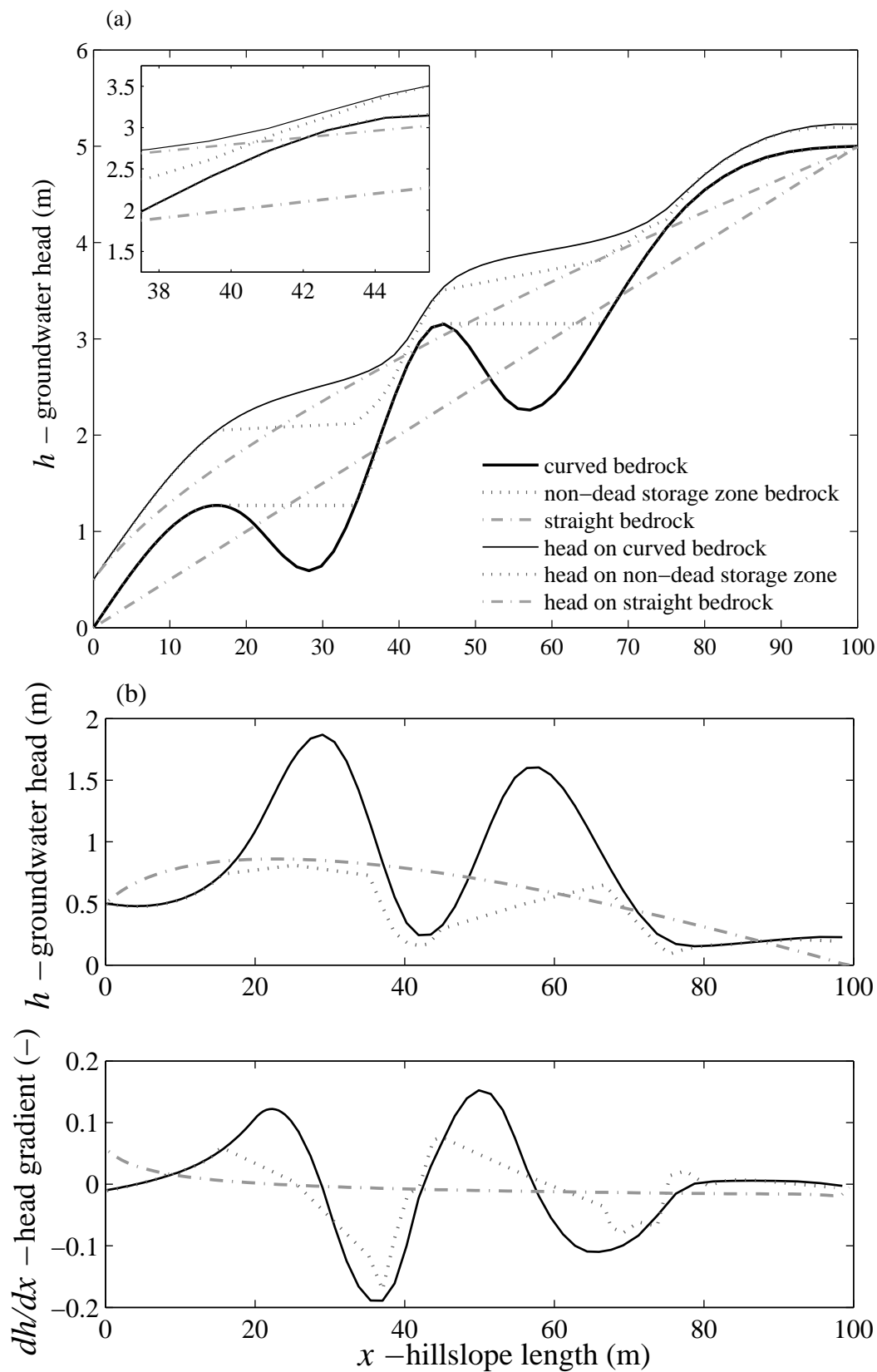


Figure 4.8: Comparison of groundwater head (a) over 3 types of bedrock profiles in space along the hillslope (dash-dotted line for straight, solid line for curved and dotted line for non-dead storage zone). Figure (b) shows differences in head and head gradient in the abovementioned cases.

4.5.4 Influence of bedrock profile convexity and concavity

To study the role of the local bedrock variations, the same generalized exB equation was used to model a few monotone concave and convex profiles (models 2-c, 2-d, 2-e and 2-f). Figure 4.13 illustrate the results thus obtained. The results of groundwater head and flux hardly varies in time for bedrock profile with 5% average slope angle in both convex and concave curvatures. Figures 4.13 and 4.14 compare the results obtained for the convex, the straight (models 3-a, 3-b) and the concave bedrock profiles.

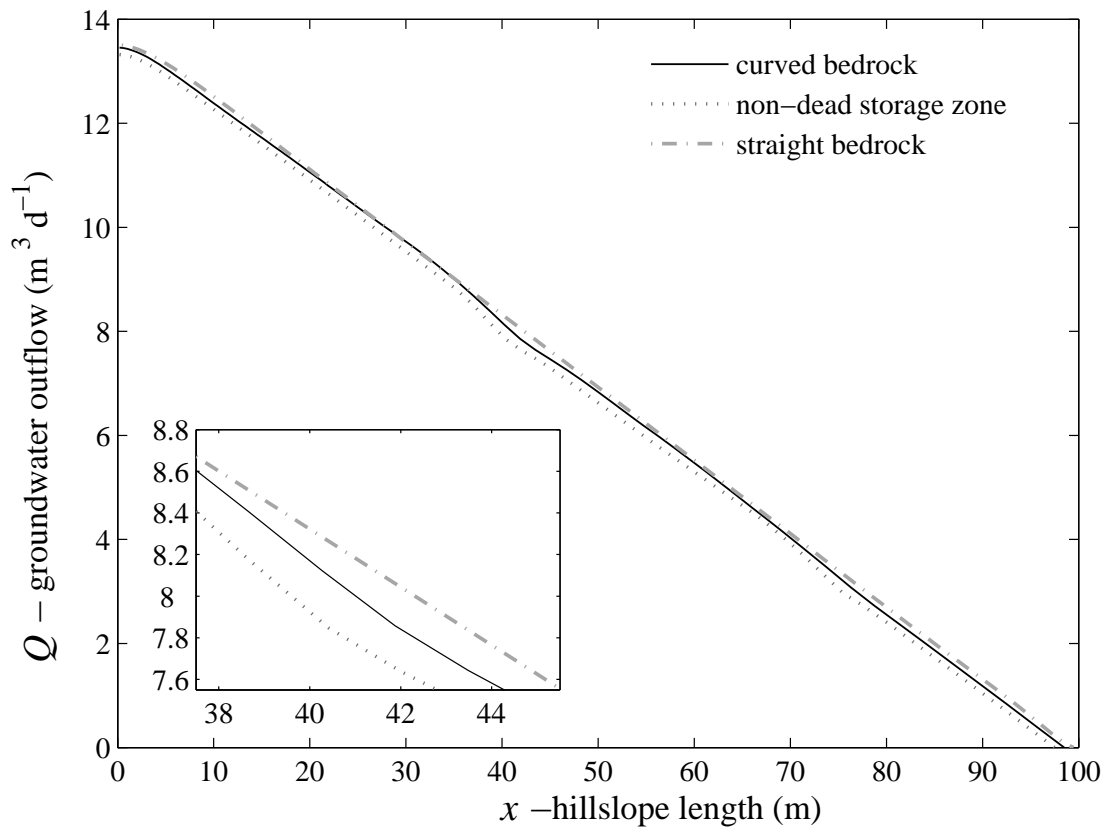


Figure 4.9: Comparison of groundwater flux over 3 types of bedrock profiles in space along the hillslope (dash-dotted line for straight, solid line for curved and dotted line for non-dead storage zone).

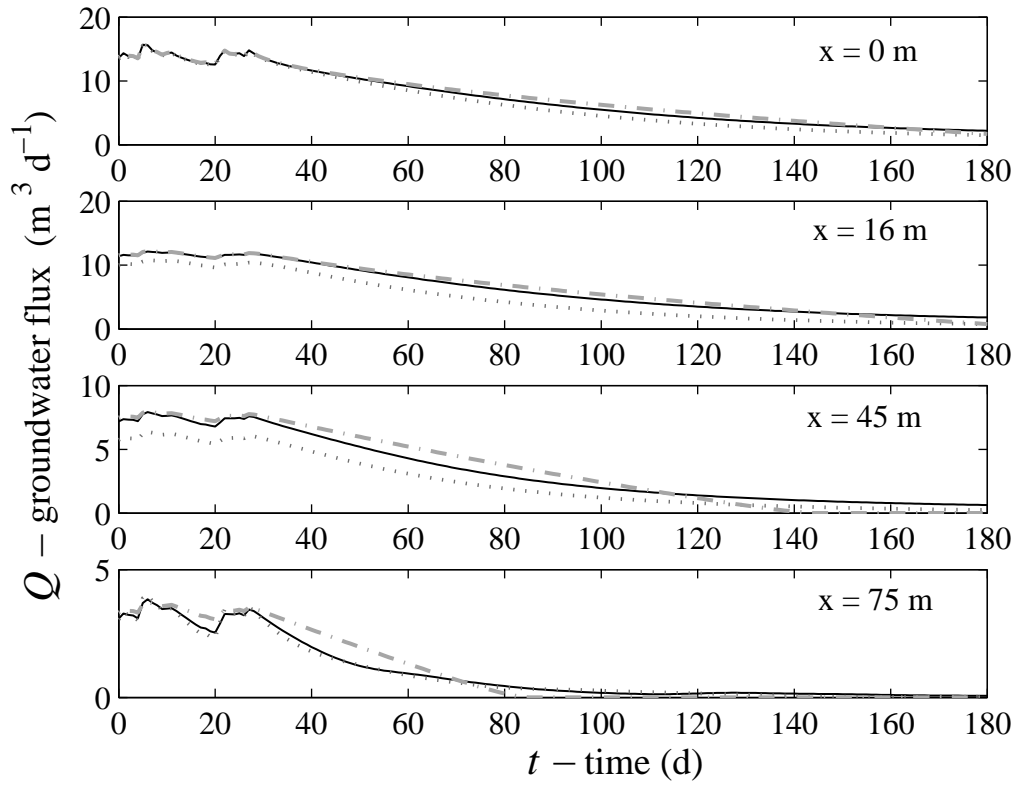


Figure 4.10: Temporal variation of groundwater flux at different locations for 3 types of bedrock profiles (dash-dotted line for straight, solid line for curved and dotted line for non-dead storage zone).

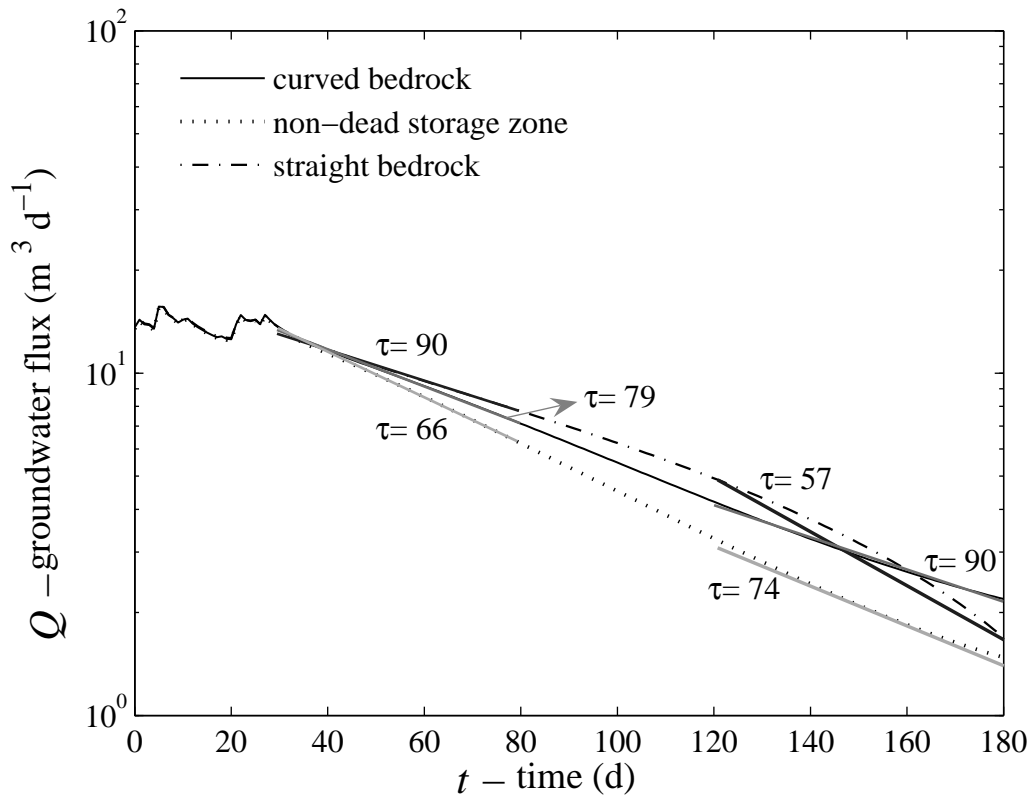


Figure 4.11: Recession analysis (at the hillslope outlet). We fitted three exponential decay functions ($\exp(-t/\tau)$) on two different parts of the recession limb, where τ is the recession time in days.

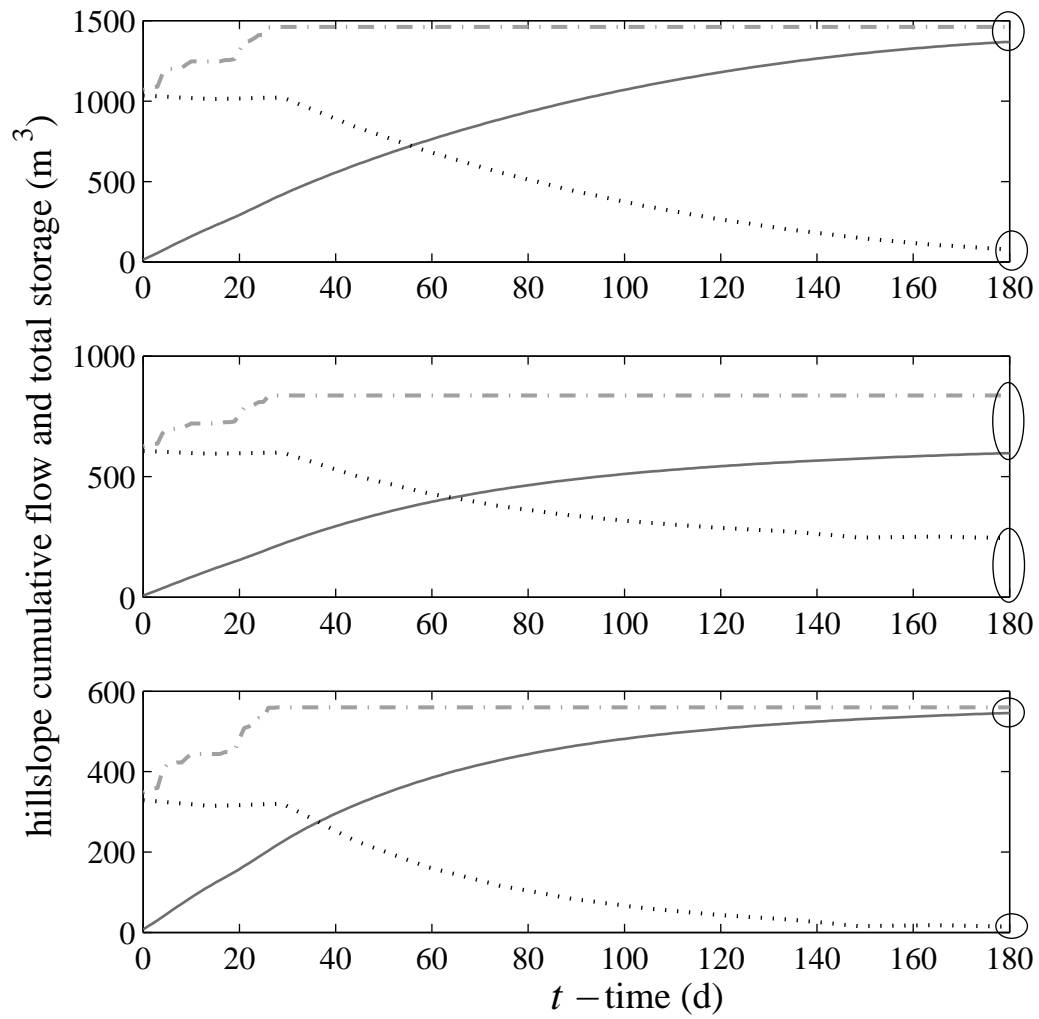


Figure 4.12: Mass balance check: (top) for whole hillslope with straight bedrock; for area upstream of $x=45\text{m}$ in two cases: with curved bedrock (middle) and with non-dead storage zone (bottom). Cumulative inflow initiated by initial storage value (dash-dotted line), cumulative outflow (solid line) and total storage (dotted line) are in balance (ellipses in each figure show the same value).

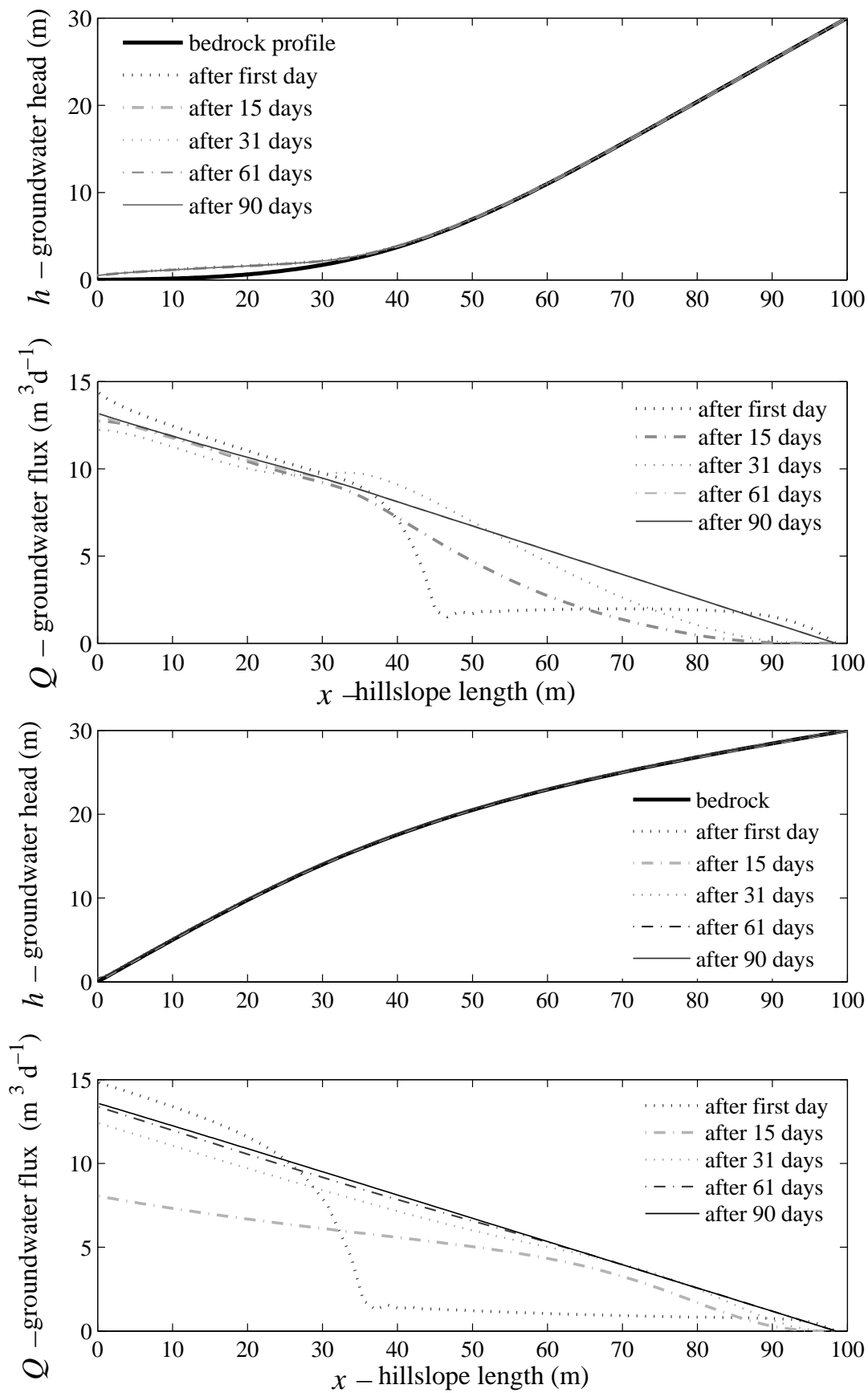


Figure 4.13: Groundwater head and flux over 30% convex (top) and 30% concave bedrock profiles.

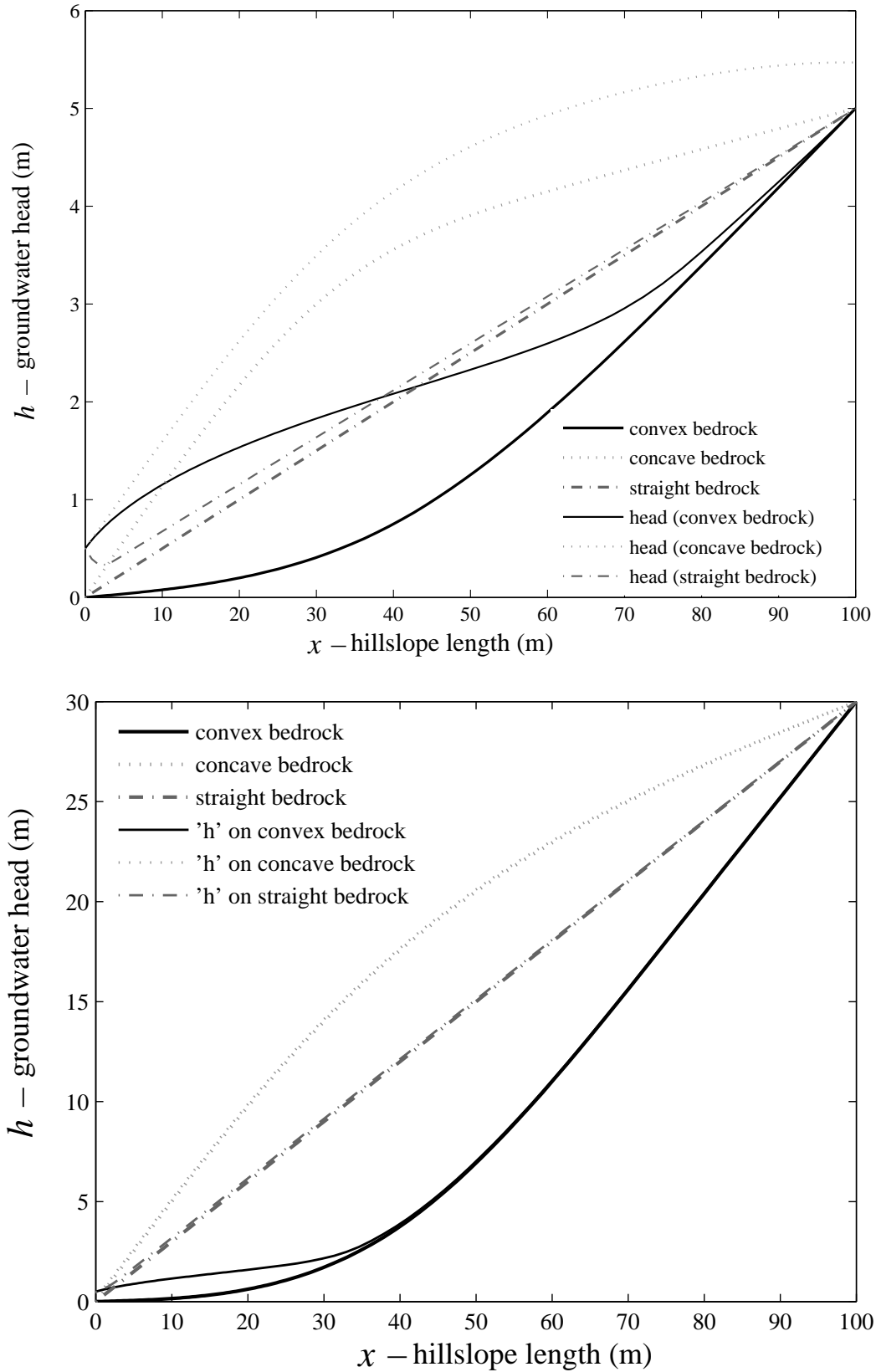


Figure 4.14: Comparison of groundwater head after 90 days (steady state) over straight (dashed line), convex (solid line) and concave (dotted line) bedrock profiles (with average slope angle 5% (top) and 30% (bottom)).

4.6 Conclusions

In this chapter, we have presented a generalized form of the exB equation for groundwater over a curved bedrock profile. The model accounts for the effects of bedrock geometry on hillslope hydrological response using the curved Dupuit assumption. Furthermore, we tested the applicability of the generalized equation to investigate the effects of bedrock profiles with and without dead-storage zone. We have conducted a set of comparisons based on rainfall intensity and geometrical characteristics of the bedrock profile.

The results show that the generalized exB equation is capable of handling saturated groundwater flow processes over complex bedrock profiles including curved bedrock and bedrock profiles including non-dead storage zones. This capability leads to more reliable results. Additionally, the obtained results indicate that the proposed numerical solution approach can handle all these simulations, which cover a wide range of conditions.

Through the comparison of the results based on different bedrock profiles, we demonstrated that for wet and dry situations, the response of the hillslope is different. Regarding the hillslope outflow, the difference in bedrock profile geometry does not play an important role.

Local minima and maxima in the curved bedrock profile influence the groundwater head for small rainfall intensities. The groundwater flux over a curved bedrock and over a profile with non-dead storage zone shows almost the same behavior, which demonstrates that local minima have a minimum effect on the hydrological response when they are filled with water.

In addition to considering the mass balance principle, our numerical models provide a theoretical framework to test the effect of complex bedrock profiles on the hillslope hydrological response.

Chapter 5

**Lumping the hillslope hydrological model through a
quasi-steady state approach**

5.1 Introduction

Physically-based distributed models are not universally accepted as providing the only way to better prediction in hydrology; indeed, not all prediction problems in hydrology require the complexity of a physically-based distributed model, but they do require a sound physical basis to be scientifically credible (O'Connell and Todini, 1996). Considering the role of subsurface runoff in hillslope hydrology, obtaining a simple representation of this process, with a sound physical basis, would be useful for hydrological studies.

The outflow from an aquifer can be computed using either a theoretical or a conceptual approach (Basha and Maalouf, 2005). The theoretical approach applies a physically-based model (e.g., the Boussinesq equation), whereas the conceptual approach is based on storage-discharge relationship, which is a spatially lumped model. This lumped model is based on the assumption that at every time step steady state is instantaneously reached. This assumption results in:

- 1) At every time, the groundwater table has an equilibrium shape;
- 2) At every time the state of the hillslope is uniquely determined by the total volume stored, which will be denoted by S ;
- 3) The downhill outflow is uniquely determined by the total volume stored, as this volume corresponds to one unique groundwater table from which one can calculate the gradient at the lower end point and from that calculate the outflow by Darcy's law. From this follows that the downhill outflow can be written a function of the storage: $Q = Q_{ss}(S)$ where $Q_{ss}(S)$ is the hillslope response resulting from the steady state approach. This functional relation will be different for each hillslope.

This approach is called Quasi-Steady State (QSS) or the method of successive steady states (Polubarinova-Kochina, 1962). Technically the method consists of applying the storage-discharge relationship derived from steady-state conditions to non-steady state situations (Basha and Maalouf, 2005).

A number of investigators have studied the approximation of groundwater response using the QSS approach (e.g., Koussis, 1992; Verhoest and Troch, 2000; Basha and Maalouf, 2005; and Akylas et al., 2006). These studies used an analytical solution of the 1D linearized Boussinesq equation at steady state with specific boundary conditions, and then obtain a quasi-steady model using the thus obtained storage-outflow relationship. Application of the QSS to real field situations can e.g. be found in Moore and Thompson (1996), Sloan (2000), Seibert et al. (2003), Basha and Maalouf (2005), and Xiangjun et al. (2006). Three of these except Sloan (2000) and Seibert et al. (2003), demonstrated that the QSS approach gives a good approximation of the groundwater response in the studied case. Also in other fields the QSS approach is used: the SIMGRO model for instance applies the QSS approach to compute the soil water dynamics in the root zone and shallow subsoil (van Walsum et al., 2006).

The advantage of the QSS approximation is that it reduces the dimension of system, going from a two dimensional system (space and time) to a one dimensional (only time) and thus increases the speed of numerical simulations dramatically. By eliminating space, QSS avoids

the time-consuming calculation of spatial fluctuations and by that also avoids numerical problems such as discussed in Chapter 4. The numerical price that we have to pay for this is that we have to calculate the volume-discharge relation. Although this can be done in advance and should be done only once, it requires many steady state calculations. As finding steady state solutions is at the very heart of our proposed numerical solution approach (see Chapter 2), it is easy to implement the QSS approach for our purpose.

This chapter is organized as follows. In the next section, the setup and governing equations are presented. The solution procedure of the QSS approach is discussed in Section 5.3. Results of the simulation methods and their discussion are presented in Section 5.4. In this section a comparison is presented of outflow profiles computed using the QSS approach with other profiles resulting from dynamic simulations. Section 5.5 provides concluding remarks.

5.2 Setup

In this chapter different types of models will be used:

- 1) The full dynamic models that are only used for comparison with the QSS model. For this we use two cases of uncoupled models (a hillslope with either a straight or a curved bedrock profile, see Figures 5.2.a and 5.2.b and a coupled hillslope-reservoir model (a hillslope with a straight bedrock profile).

The upper boundary condition (see Figure 1.1) at $x = L$ is a no-flux boundary as usual

$$\left(\frac{\partial h}{\partial t}(L, t) = 0\right).$$

For the lower boundary condition at $x = 0$ either a fixed head is assumed (in case of an uncoupled model) as $h(0, t) = h$ or a head determined by a downhill reservoir water level (as seen in Chapter 3) as $h(0, t) = h(t)$. For the initial condition at $t = 0$ a constant head is assumed ($h(x, 0) = h_0$ for $x \in [0, L]$).

- 2) The steady state models (the steady state versions of the models mentioned above) that will be used to derive volume-discharge relations.
- 3) The QSS models which are the main topic of this chapter.

Different types of hillslope model setups were used to study the performance of the QSS approximation. These models are based on bedrock profiles (either straight or curved) which have either a uniform or a convergent plan shapes (see Figures 4.1.b, 4.2 (in middle with 5% slope), and a profile which has the same geometry as Figure 5.4.b used by Hilberts, 2006). For each of these different models, a volume-discharge relation will be derived that will be compared with the full solution.

To model the hillslope in this chapter, we use the extended Boussinesq equation (see Section 1.3.3) and the extended Boussinesq equation based on the curved Dupuit assumption (see Section 1.3.6). For the steady state versions of these equations, we use Equations 2.11 and 2.17, respectively (see Chapter 2). The solution procedure of the QSS approximation will be explained in the next section.

In all simulations the hillslope is assumed to have a spatially uniform rainfall, saturated hydraulic conductivity (5 m d^{-1}), and effective drainable porosity (0.354). For all the models the same rainfall data were used: those obtained from the Maastricht station in 2001 (KNMI).

5.3 Solution procedure of QSS approximation

5.3.1 Steady state storage-discharge relation

To derive the storage-discharge relation, first a wide range of rainfall intensities is selected as input. For each of these rainfall intensities a steady state is calculated. From this steady state, one calculates the total storage in the hillslope. These storages are then combined with the downhill outflow into a so called $S - Q$ table. Figure 5.1 gives an overview of this procedure.

In the coupled case, first the water level of the reservoir that corresponds with inflow is calculated. Then this level is imposed as the hillslope lower boundary condition. The $Q_{ss}(S)$ will be approximated by this $S - Q$ table using linear interpolation.

5.3.2 QSS approximation

The steady-state storage-discharge relationship can then be used in a lumped (for the whole hillslope) water balance equation, which is written using an explicit finite difference scheme:

$$S(t + \Delta t) = S(t) + \Delta t(I(t) - Q_{ss}(S(t))) \quad (5.1)$$

$$I(t) = N(t)A \quad (5.2)$$

where t is time, S is the hillslope total storage, $I(t)$ is the spatially integrated volume of inflow, N is the rate of inflow, Δt is the time increment, A is the hillslope area. An explicit scheme was chosen because an implicit would be difficult due to the nonlinearity of the $Q_{ss}(S(t))$ function.

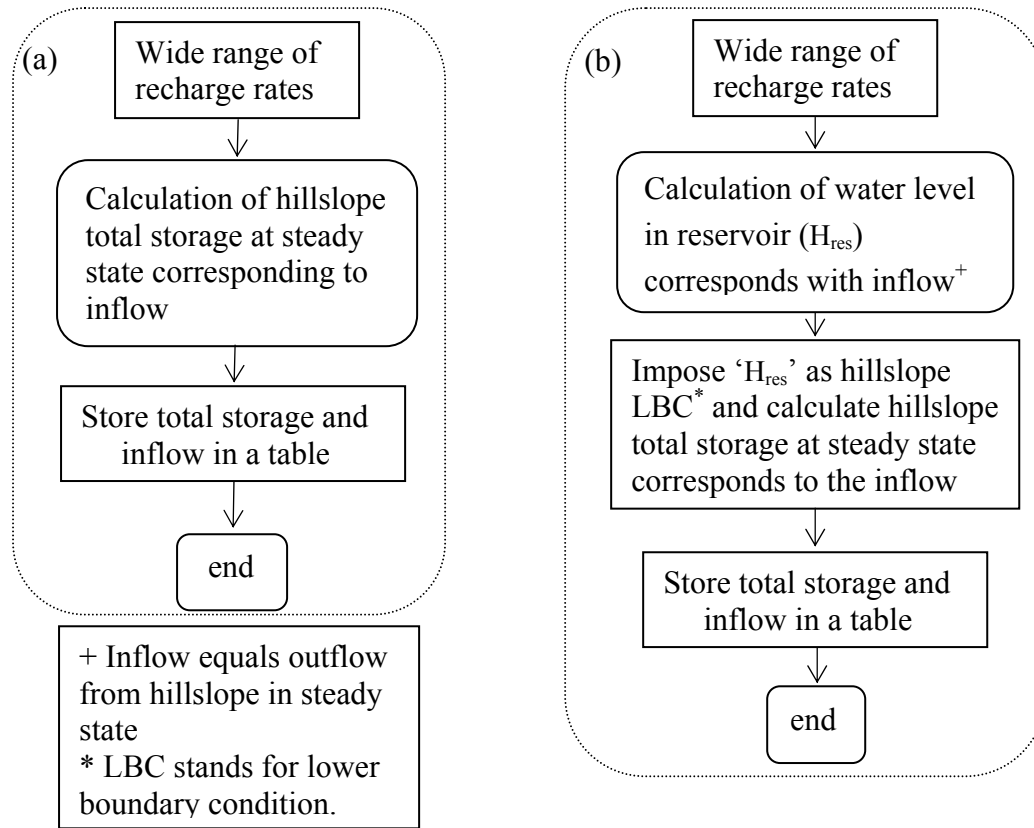


Figure 5.1: Diagram of solution procedure in QSS approach: (a) uncoupled case (hillslope); and (b) coupled case (hillslope-reservoir).

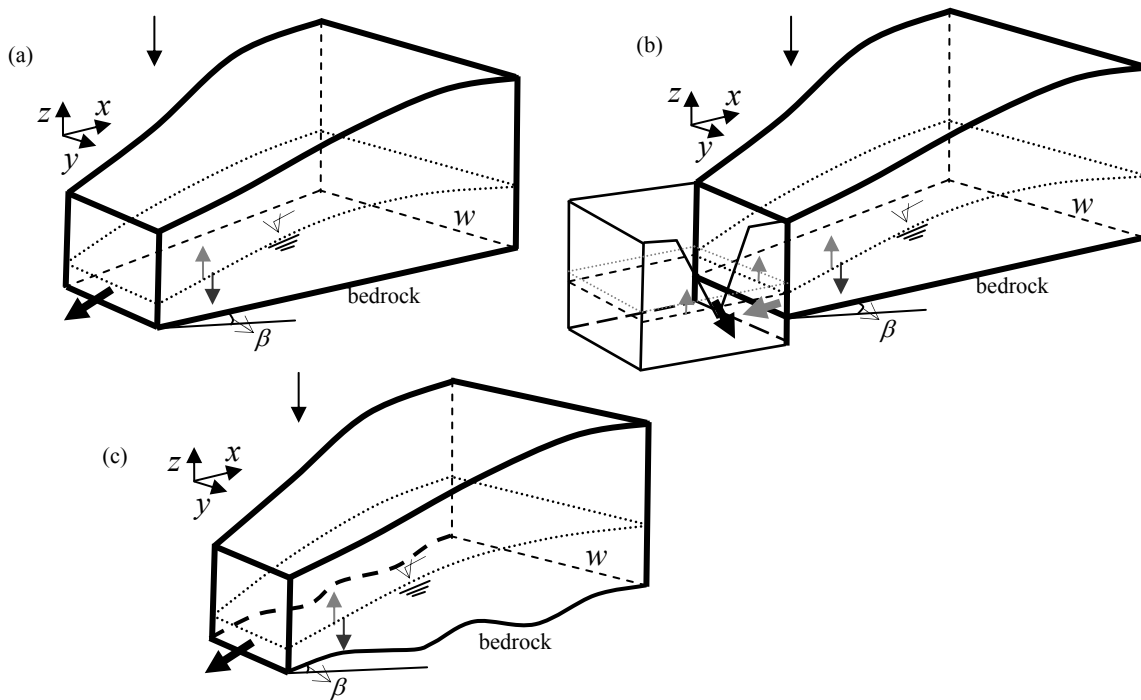


Figure 5.2: Schematic view of examples of hillslopes to test the QSS approximation approach: (a) straight bedrock; (b) coupled with reservoir; and (c) curved bedrock.

5.4 Results and discussion

In this section we will discuss the results of the models introduced in the previous sections:

- 1- The uncoupled hillslope model with straight bedrock and uniform plan shape.
- 2- The coupled hillslope-reservoir (for a hillslope with straight bedrock and uniform plan shape).
- 3- The uncoupled hillslope model with curved bedrock and uniform plan shape.
- 4- The uncoupled hillslope model with straight bedrock and convergent plan shape.
- 5- The coupled hillslope-reservoir (for a hillslope with straight bedrock and convergent plan shape).

For more information about the relevant equations for each case, see Sections 1.3.3 (models 1 and 4), 3.2 (models 2 and 5), and 1.3.6, respectively.

5.4.1 Storage-outflow ($S - Q$) relationship

Plots of the $S - Q$ tables (see e.g. Figure 5.3) reveal that this relationship can be either linear or non-linear. For most applications only a small range of this curve is actually used, which is shown in more detail in the enlarged subfigure.

In the hillslope-reservoir coupled case (with straight bedrock), the $S - Q$ curve differs only a little from the $S - Q$ curve of the uncoupled case with straight bedrock (see Figure 5.3). Comparison of the $S - Q$ curves in Figure 5.3 shows that the shape of the hillslope (as determined by the width function) affects the $S - Q$ relationship. As shown in this figure, the $S - Q$ curves for both models 4 and 5 reveal a different non-linear relationship compared to the others. These curves are for convergent hillslopes with straight bedrock in the uncoupled and coupled cases, respectively.

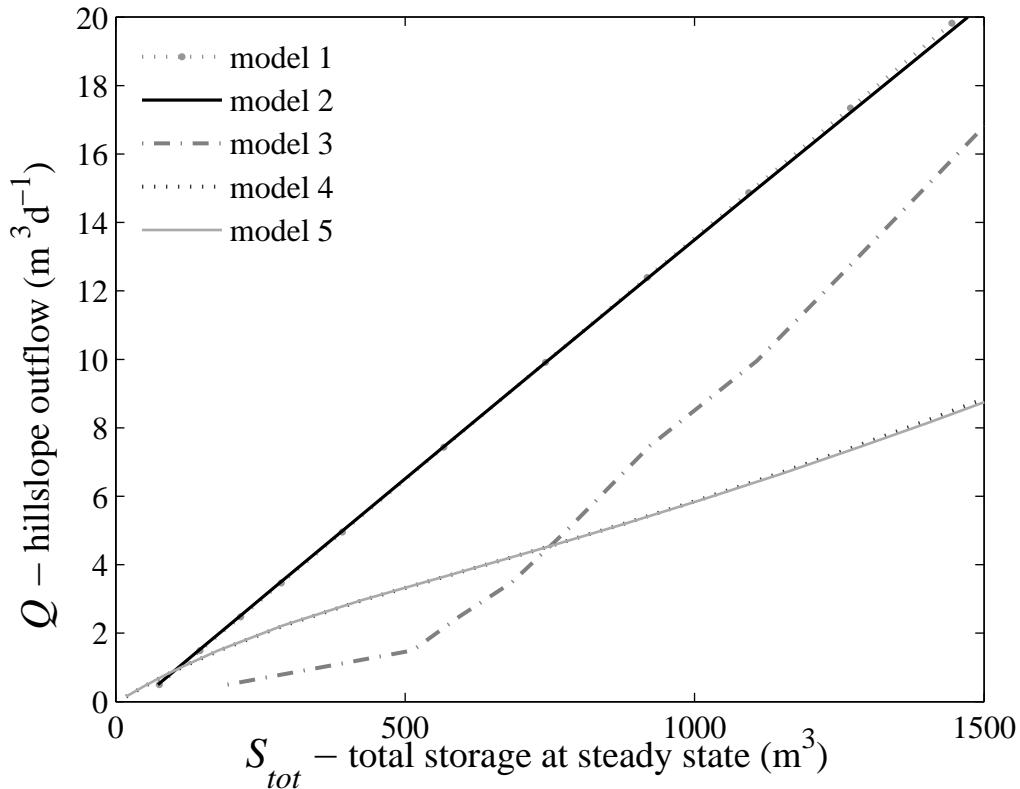


Figure 5.3: Relation between the hillslope total storage and outflow in different cases (models 1 to 5).

5.4.2 QSS approximation in different cases

The hillslope hydrological response was approximated using the QSS approach for the three cases mentioned in Section 5.4. Each simulation (from models 1 through 5) was run for 1 year, and the results were compared to the results of the dynamic simulations for those cases.

Figures 5.4, 5.5, and 5.6 present the results of the comparison between the dynamic simulation and the QSS approximation for models 1 through 3, respectively. In the coupled case, the outflow comparison shows a fast increase at first stage (until day 100) where there is large difference. Then it fluctuates around equilibrium where the difference is smaller in magnitude (see Figure 5.5). In general, the results highlight that after day 150, the dynamic model and the QSS approximation show approximately the same character in terms of their fluctuations.

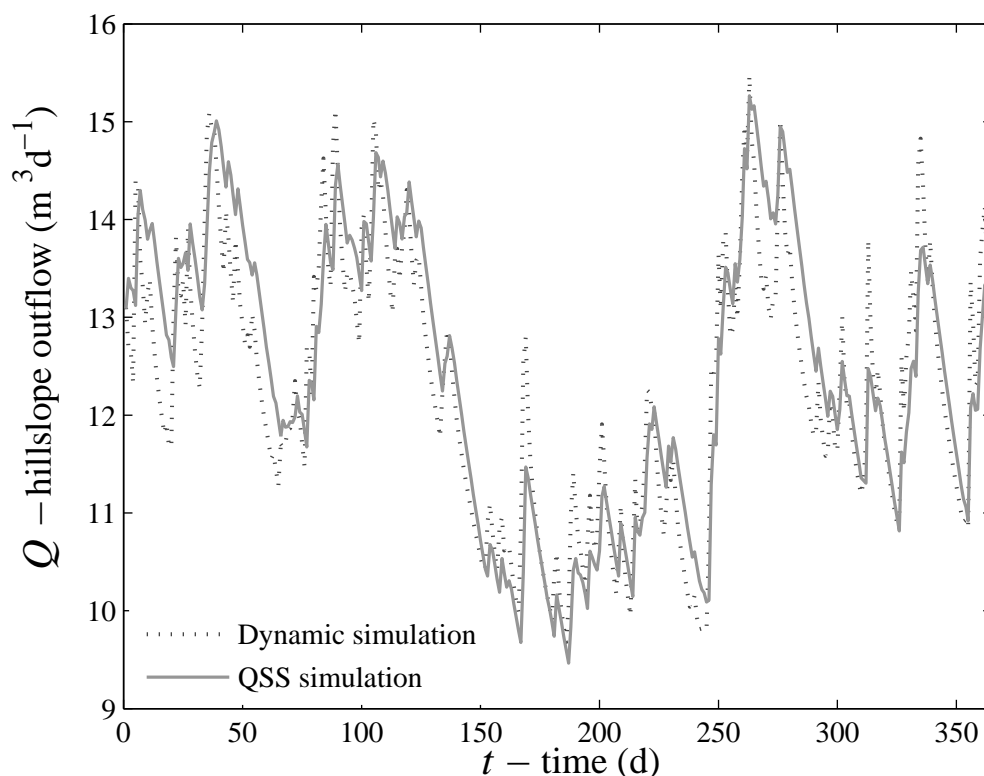


Figure 5.4: Comparison of the hillslope outflow of the dynamic model and the QSS approximation in case of a straight bedrock.

In all these figures, both outflow curves follow the same general trend and they have the same magnitude of fluctuation, but they clearly differ in the recession limbs of the hydrographs. The difference with the full dynamic case changes from the uphill end towards the outlet. This is due to the fact that the full dynamic simulation can react also locally to changes in inflow, while the QSS is a spatially lumped approach and can only have a global dynamic reaction. It should be noted that as our numerical solution scheme preserves mass balance (see also Section 5.4.4), at the end the same amount of discharge should leave the aquifer. Hence, where the full dynamic case first produces higher fluxes than the QSS approach, for instance near a peak, afterwards this order has to reverse to keep the balance.

Differences between the results of the dynamic simulation and the QSS approximation for three cases are presented in Figure 5.7. The Y-axis in this figure, shows the percentage of days (in a year), plotted in bars. It is calculated for the whole year as the percentage of days where the difference falls into a certain class. In this figure, one can see that QSS overestimates the outflow in the coupled case (straight bedrock) and uncoupled case (curved bedrock). This is not seen in the uncoupled case with straight bedrock. The range of fluctuation in the coupled case is due to the fact that dynamic case shows larger fluctuations, and the QSS approximation has difficulty to follow it.

Average differences in these cases are presented in Table 5.1, showing that both models give on average approximately the same results. Figures 5.10, 5.11 and 5.12 present the results of a comparison between the dynamic simulation and the QSS approximation for models 4 and 5, respectively.

Table 5.1: Average difference between outflows (obtained from the dynamic simulation and the QSS approximation for a hillslope with uniform and convergent plan forms in three cases) in m^3d^{-1} .

case \ form of hillslope	straight bedrock	coupled & straight bedrock	curved bedrock
uniform	$-0.139 \cdot 10^3$	$-0.716 \cdot 10^3$	$-0.242 \cdot 10^3$
convergent	$-0.068 \cdot 10^3$	$-0.085 \cdot 10^3$	-----

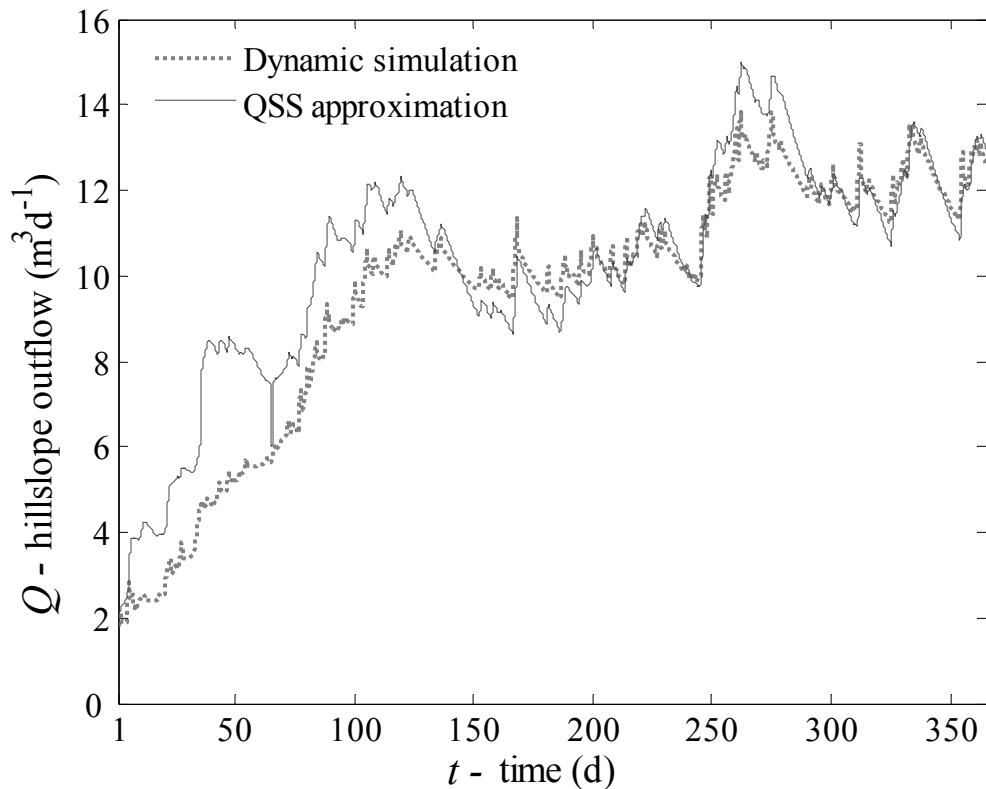


Figure 5.5: Comparison of the hillslope outflow of the dynamic model and the QSS approximation in case of a coupled hillslope-reservoir.

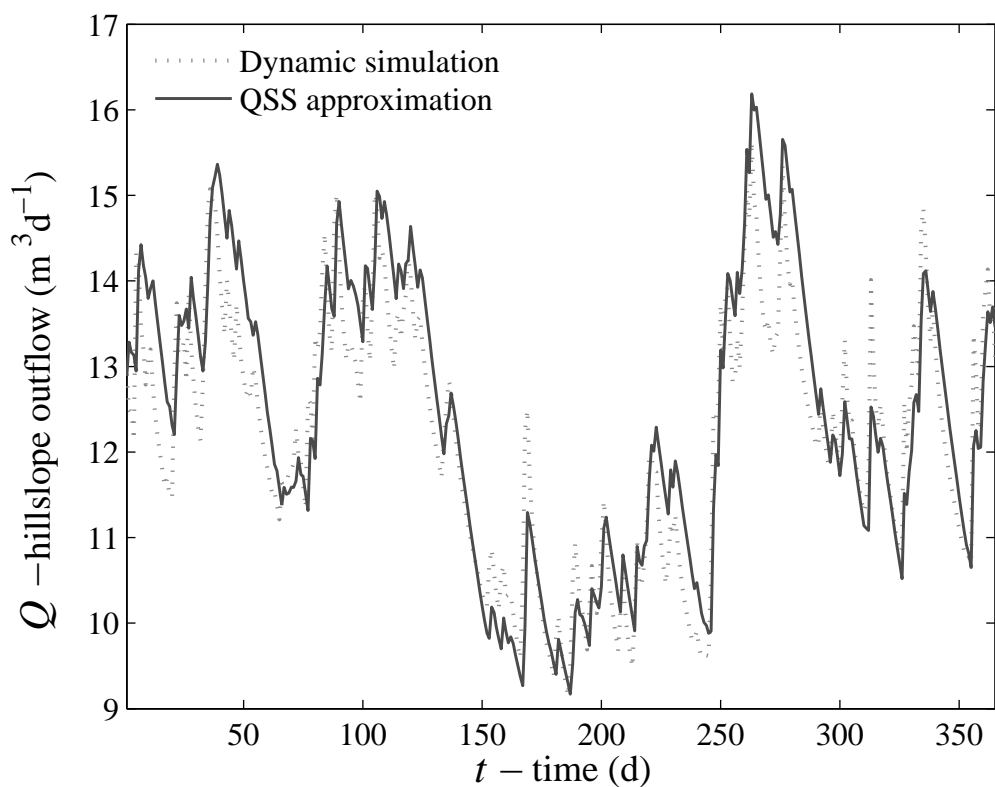


Figure 5.6: Comparison of the hillslope outflow of the dynamic model and the QSS approximation in case of a curved bedrock.

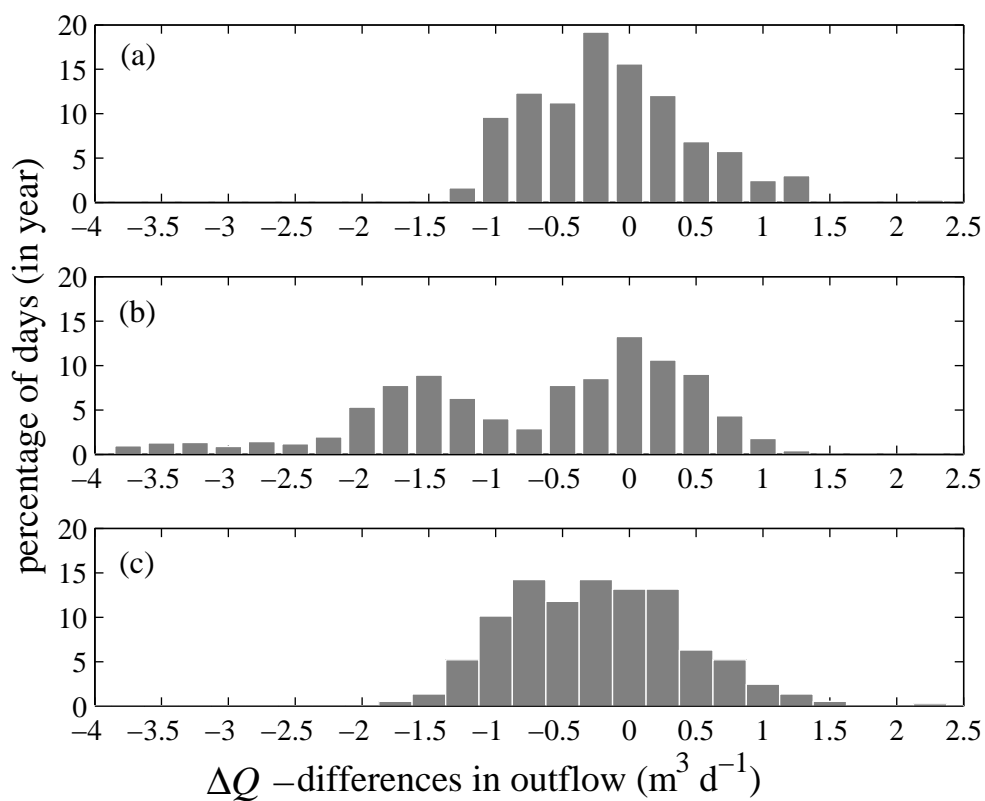


Figure 5.7: Distribution of difference between outflow of the dynamic and QSS simulations in percentage of days: (a) straight bedrock; (b) coupled hillslope-reservoir; and (c) curved bedrock.

5.4.3 Effect of time step

The proper choice of numerical time step for the QSS model should be discussed. One reason for this is that the QSS approximation assumes instantaneous equilibrium and that numerically this instantaneous is translated as “within one calculation step”. The other reason is that an explicit scheme was used in the solution procedure (see also the discussion in Chapter 3). To study this, simulations were carried out for time steps of 1 day and 12 hours.

QSS with a small time step shows a little better approximation than that with a 1 day time increment, which can be seen especially around peaks (see Figure 5.8). However, the limited magnitude of the differences in general (as can be seen in the figure), does not justify any preference. For that reason a time step of one day was used throughout the remainder of this chapter.

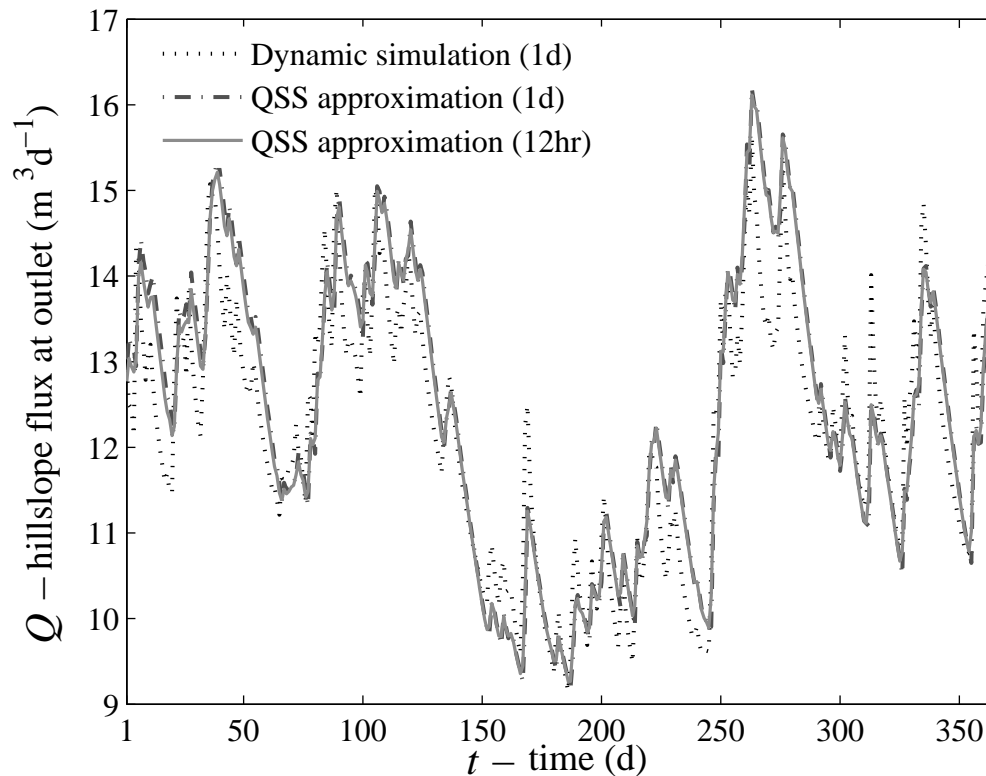


Figure 5.8: Comparison of the hillslope outflow of the dynamic model and the QSS approximation in case of a curved bedrock for different time steps.

5.4.4 The mass balance check

The QSS model is based upon a storage and consequently on the mass balance concept. As balance among input and output is a crucial issue in the proposed numerical solution algorithm (Chapter 2), the mass balance of each model was checked to test the accuracy of the model. The mass balance is calculated based on the cumulative amount of inflow and outflow of fluid entering and leaving the hillslope. Two ways to check the balance were considered:

$$S(t) - S(0) = \int_0^t dt Q_{in}(t) - \int_0^t dt Q_{out}(t) \quad (5.3)$$

where $S(t) - S(0)$ is the change in water storage in the hillslope, $\int Q_{in}(t)$ is the cumulative inflow into the hillslope and $\int Q_{out}(t)$ is the cumulative outflow from the hillslope.

The difference between cumulative inflow and cumulative outflow over a curved bedrock in time is shown in Figure 5.9. Table 5.2 reports the summary of the mass balance check in case of a hillslope with uniform plan shape over a curved bedrock. Comparison of the difference between cumulative inflow and cumulative outflow in the dynamic model and the QSS approximation reveals that this difference is consistent with the average difference mentioned in Table 5.1. This difference is due to the change in storage in the dynamic simulation. The results presented in Table 5.2 show that the computer program works properly. This implies the accuracy of the applied numerical simulation algorithm.

Table 5.2: Mass balance check for the hillslope over curved bedrock for different time steps for the QSS simulation.

Case	QSS approximation ($\Delta t = 1$ d)	QSS approximation ($\Delta t = 12$ hr)
$\sum Inflow - \sum Outflow$ (m^3)	19.05	31.1
$S(final) - S(initial)$ (m^3)	19.05	31.1
$\Delta h = \frac{(\sum Inflow - \sum Outflow)}{Af}$ (mm)	10.8	17.6
$\Delta h = h(t_{end}) - h(t_1)$ (mm)	10.8	17.6

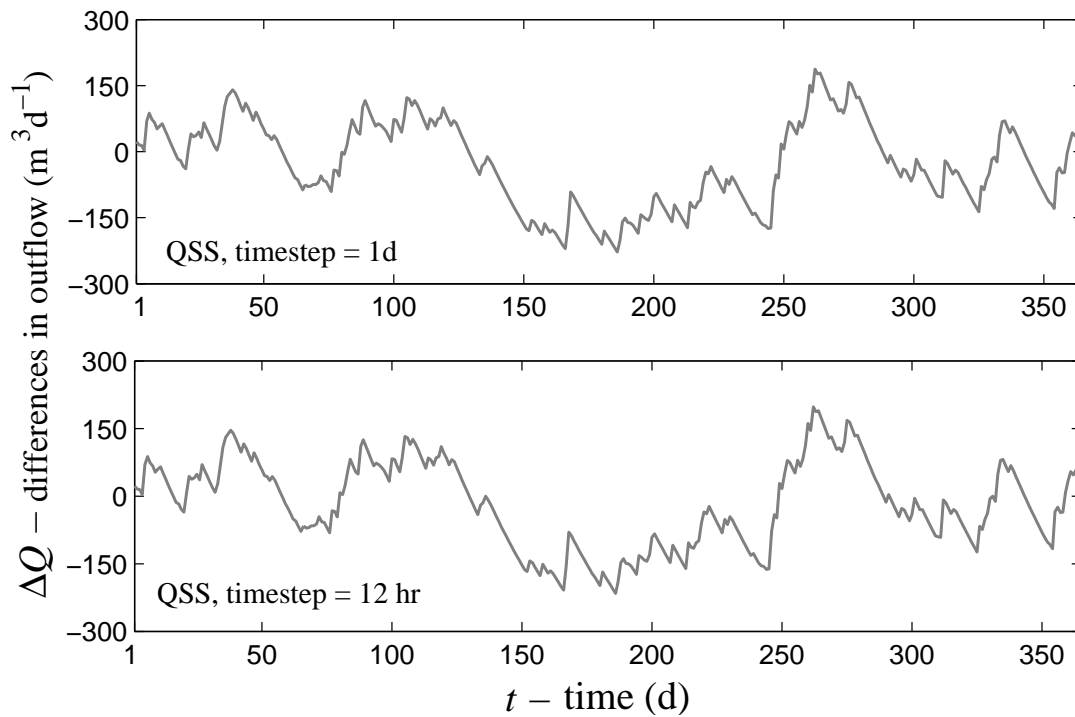


Figure 5.9: Difference of the hillslope cumulative inflow and cumulative outflow over a curved bedrock for different time steps.

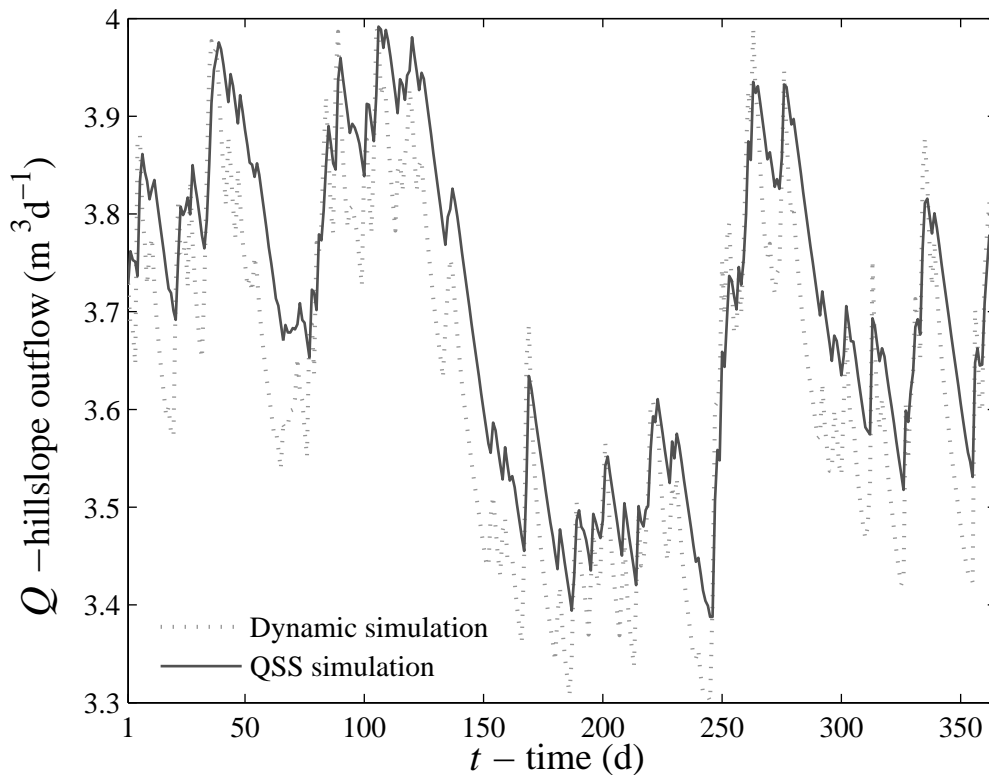


Figure 5.10: Comparison of the hillslope outflow of the dynamic model and the QSS approximation in case of a hillslope with convergent form and straight bedrock.

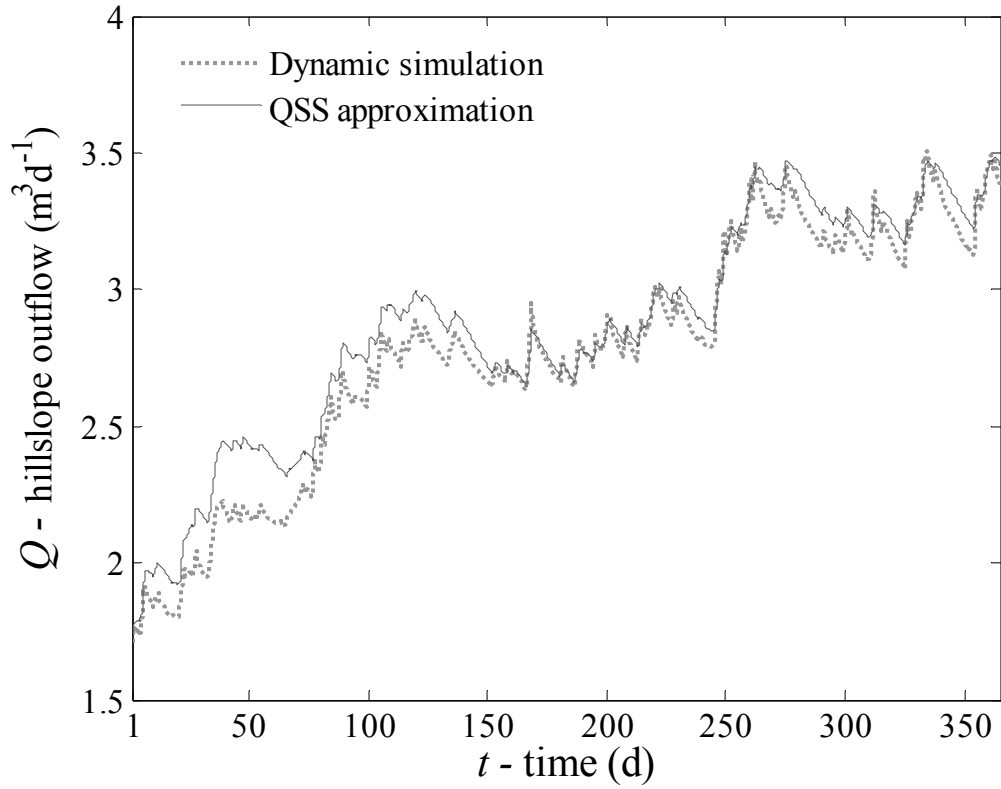


Figure 5.11: Comparison of the hillslope outflow of the dynamic model and the QSS approximation in the coupled case for a hillslope with convergent form.

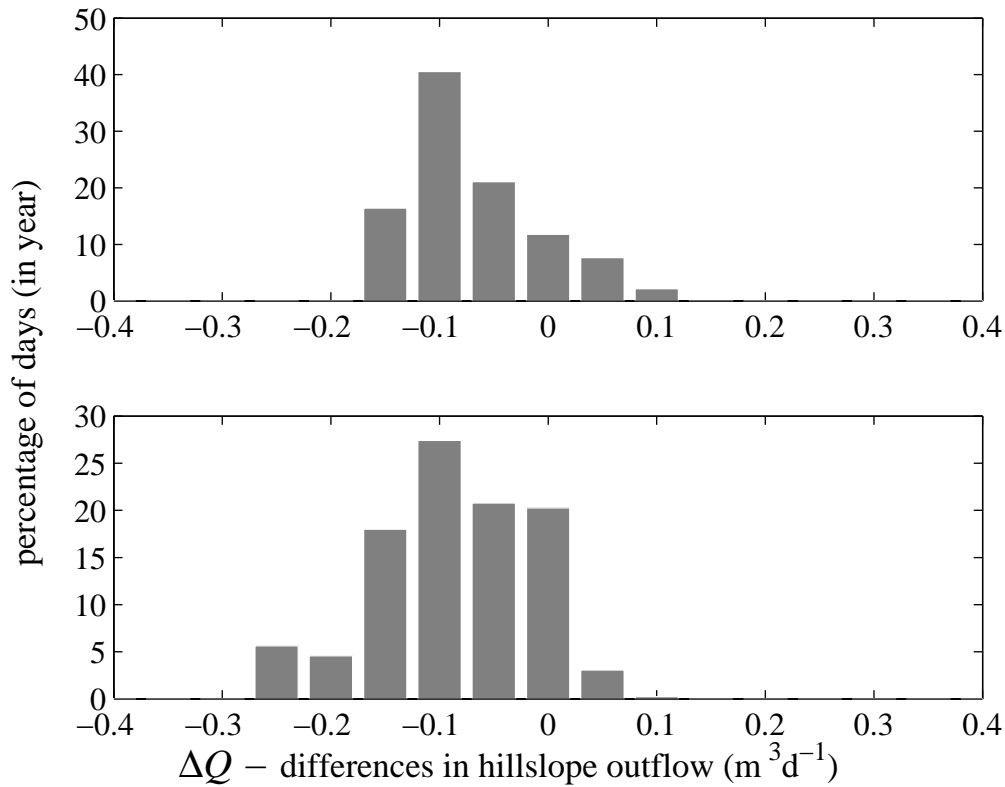


Figure 5.12: Distribution of difference between outflow of the dynamic and QSS simulations in percentage of days: (a) straight bedrock; (b) coupled hillslope-reservoir.

5.4.5 Further test of QSS approximation

The conclusions above were based on a particular rainfall series. To check whether these conclusions also hold for other series, the rainfall of the Maastricht station for 2002 (KNMI) was used. Comparison of Figure 5.13 to Figure 5.4 and Figure 5.14 to Figure 5.6, shows that, at least qualitatively, the behavior of the QSS is the same.

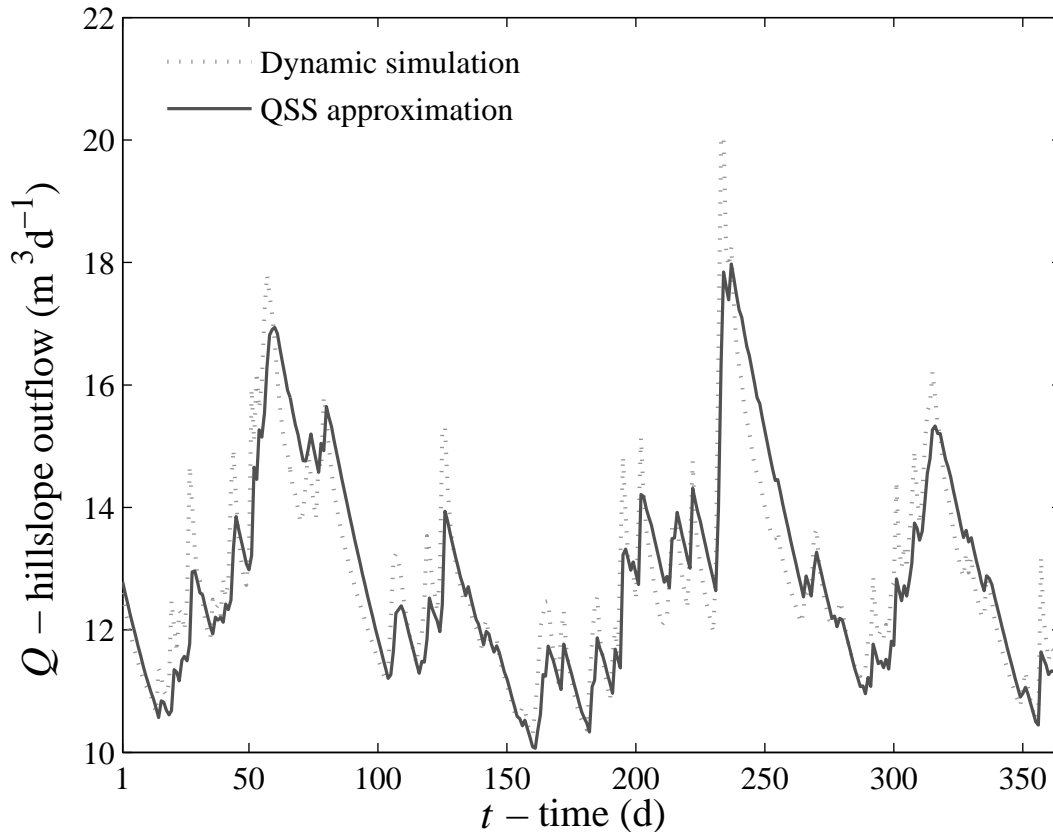


Figure 5.13: Comparison of the hillslope outflow of the dynamic model and the QSS approximation in case of a straight bedrock (in year 2002).

5.5 Conclusions

The quasi-steady state (QSS) method proves to be a simple and computationally efficient method to simulate the groundwater dynamics. The method consists of lumping the whole hillslope and using the stationary storage-discharge relationship.

To test this idea we have conducted a set of comparisons between a dynamic simulation model and the QSS approach based on different plan forms, different types of bedrock profiles and coupled and uncoupled cases. As can be seen from the results, the QSS methodology is in general able to reproduce the right variation in output. Generally, this indicates capability of the QSS approach to approximate the hillslope response. The limitations of the QSS approach are that in general it underestimates the discharge peaks. Additionally, the obtained results for

the mass balance check indicate that the proposed numerical simulation approach can handle these simulations under different conditions.

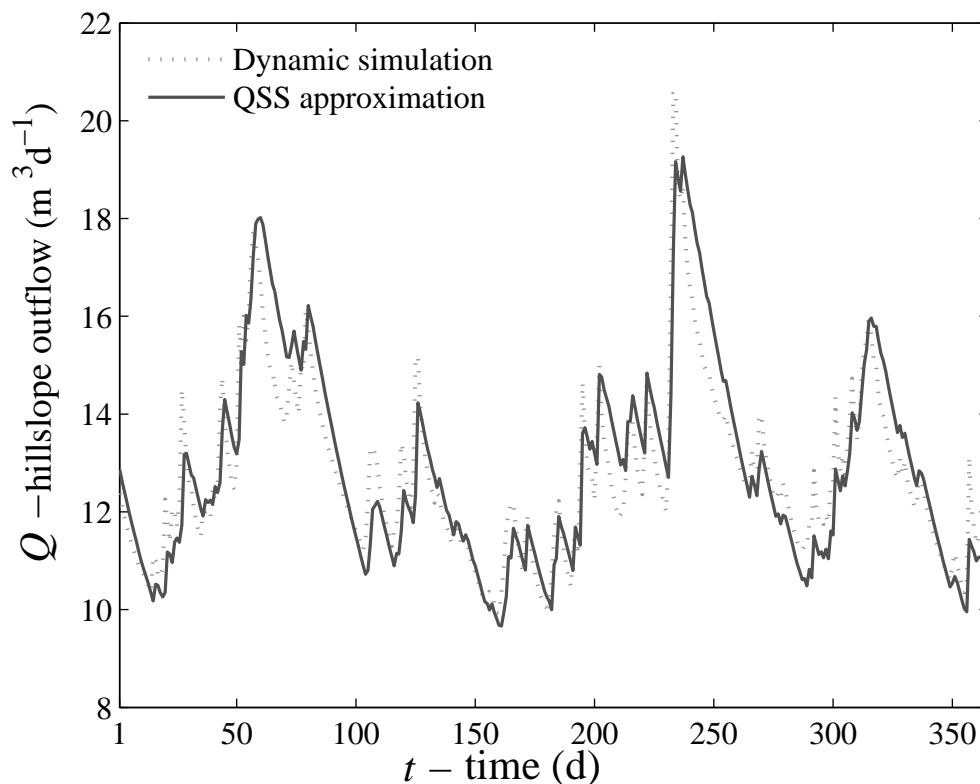


Figure 5.14: Comparison of the hillslope outflow of the dynamic model and the QSS approximation in case of a curved bedrock (in year 2002).

The fast execution time of the QSS approximation approach is a powerful aspect of this approach. Due to dependence of the results of the QSS approach on the specific parameters of the selected cases, it cannot be concluded in general that the QSS approach performs better than the dynamic simulation. Because of its simplicity (regarding both model structure and computation time) it is nevertheless worthy to apply. In all cases presented in this chapter, QSS performed rather well.

Chapter 6

Summary and conclusions

6.1 Overview

This final chapter summarizes the previous chapters and focuses on the important conclusions. The last section contains some ideas for future research. The general objective of this research was to investigate simple but physically realistic alternative parameterizations of the hydrological processes at the hillslope scale. All these models only consider saturated flow. In this research, special attention was paid to geometrically complex bedrock profiles and different types of downhill boundary conditions.

Chapter 1 presents several models for the hydrological response at the hillslope scale. As three-dimensional groundwater models are too complex to be an efficient hillslope model, Chapter 1 presents various one-dimensional approximations, varying in the underlying assumptions. These equations range from the most simple (Dupuit equation) to the most complex (extended Boussinesq equation based on the generally curved bedrock Dupuit assumption). They were generalized step by step to incorporate the complexity of bedrock geometry in models of the hillslope hydrological response. All these models have their own geometrical-physical assumptions, resulting in mathematical differential equations that differ in complexity.

In **Chapter 2** a general and flexible numerical solution algorithm is presented that enables the handling of all the hillslope models of Chapter 1. This technique is especially flexible in terms of the choice of linearization method. Another important aspect of the proposed technique is that fluxes are calculated explicitly in the code, allowing precise mass balance checks. The technique concentrates on the spatial redistribution aspects of the equations. It does so by first solving the stationary case, and based on this solution technique handles the transient one. The flexibility of the proposed numerical technique makes a uniform and fair comparison between models possible in the following chapters.

Chapter 3 investigates the downhill boundary condition. Physically this boundary will be defined by an interaction with an open water stream, resulting in possible backwater effects. As the use of a coupled hillslope-open water model is considered too complex in general, this is replaced by a discharge-head relationship. The extended Boussinesq equation and a simple open water formulation are used to study this alternative.

Comparison of the results for the uncoupled case (with fixed boundary condition) and the coupled case shows the importance of the backwater effect. Comparison of the results of the uncoupled case (with mixed boundary condition) and the coupled case shows that the open water system can be replaced by a discharge-head relation. This approach provides a simple and efficient way to simulate catchment hydrological processes.

Chapter 4 investigates the role of geometrical complexity of the bedrock. It does so by using the extended Boussinesq equation of Chapter 1 for different types of bedrock profiles: curved,

non-dead storage zone, concave, and convex. The results are compared to a straight bedrock profile.

The numerical techniques of Chapter 2 proved to be powerful and flexible enough to obtain accurate results even in these difficult cases. By comparing the results of curved, non-dead storage zone, and straight profiles, it was demonstrated that the outflow characteristics in general and the recession characteristics in particular depend on their bedrock profiles.

It was also found that local minima and maxima in the curved bedrock profile influence the groundwater head for small rainfall intensities. The groundwater flux over curved bedrock and non-dead storage zone shows almost the same results, which demonstrates that local minima have a minimal effect on the hydrological response at least after they are filled.

In general there is no difference between the Taylor approximation and the ad hoc method. However, the problems regarding the positiveness of the head could only be solved by a general linearization technique.

In **Chapter 5**, the replacement of the full dynamics by a simpler approach called Quasi-Steady State (QSS) is investigated. The method consists of lumping the whole hillslope and using the stationary storage-discharge relationship. The QSS approximation was tested through comparison with dynamic simulations over one year based on different plan forms (uniform, convergent), bedrock profiles (straight, curved) and coupled and uncoupled situations.

The results show that the QSS approximation generates almost the same results as the dynamic model. Generally, this indicates the capability of the QSS approach to approximate the hillslope response. The fast execution time of the QSS approximation is a strong aspect of this approach.

In summary, we hope that the hillslope hydrological models that have been presented in this thesis will contribute to rainfall-runoff modeling at the catchment scale.

6.2 Ideas for future research

The numerical technique presented in Chapter 2 was shown to be useful in investigating many interesting hillslope models (Chapter 3, Chapter 4, and Chapter 5). Without changes the same technique may also be used to investigate even more complex models, which may be interesting for hillslope hydrological research. We present here two such models.

6.2.1 Two-dimensional equations

All the models presented in this thesis are one-dimensional in space and neglect the variation of groundwater head and the corresponding fluxes in the y -direction. A two-dimensional could lead to a better understanding of hillslope hydrological processes. We will argue here that the numerics of Chapter 2 can be easily adapted to also solve this type of model.

Let us assume that the bedrock slope in the y -direction can be neglected. The two-dimensional differential equation generalizing the one-dimensional form of Equation 1.17 is given by:

$$f \frac{1}{\cos(\beta_x)} \frac{\partial h}{\partial t}(x, y, t) = -\frac{\partial}{\partial x} \left(-K_s(x, y) h(x, y, t) \left(\cos^2(\beta_x) \frac{\partial h}{\partial x}(x, y, t) + \sin(\beta_x) \right) \right) - \underbrace{\frac{\partial}{\partial y} \left(-K_s(x, y) h(x, y, t) \frac{\partial h}{\partial y}(x, y, t) \right)}_{=L_f} + N(x, y, t) \quad (6.1)$$

For fixed y this equation can be considered as a one-dimensional equation of the same form as Equation 1.17 where the last two terms should now be interpreted as “external flux”. This flux, after discretization in the y -direction, in y_k (the k^{th} node in the y -direction) takes the form

$$N_k(x, h, t) = \frac{\partial}{\partial y} \left(K_s(x, y_k) h(x, y_k, t) \frac{\partial h}{\partial y}(x, y_k, t) \right) + N(x, y_k, t) \quad (6.2)$$

which can be numerically approximated by:

$$N_k(x, h, t) = -K_s(x, y_k) \left[\frac{1}{2} \left(\frac{h(x, y_k, t) - h(x, y_{k-1}, t)}{d((x, y_k), (x, y_{k-1}))} \right) \left(\frac{h(x, y_k, t) + h(x, y_{k-1}, t)}{2} \right) + \frac{1}{2} \left(\frac{h(x, y_{k+1}, t) - h(x, y_k, t)}{d((x, y_{k+1}), (x, y_k))} \right) \left(\frac{h(x, y_{k+1}, t) + h(x, y_k, t)}{2} \right) \right] + N(x, y_k, t) \quad (6.3)$$

where d stands for distance. The fact that this term depends on h , and due to the presence of $h^2(x, y_k, t)$ even in a non-linear way, forms no obstacle to applying the techniques of Chapter 2, where this form of dependency is treated in Equations 2.3 and 2.22.

The system of equations (Equation 6.1), with $h_k(x, t) = h(x, y_k, t)$ as unknowns, can be solved by solving iteratively the following equations for y_k :

$$f \frac{1}{\cos(\beta_x)} \frac{\partial h}{\partial t}(x, y_k, t) = -\frac{\partial}{\partial x} \left(-K_s(x, y_k) h(x, y_k, t) \left(\cos^2(\beta_x) \frac{\partial h}{\partial x}(x, y_k, t) + \sin(\beta_x) \right) \right) + N_k(x, h(x, y_{k-1}, t), h(x, y_k, t), h(x, y_{k+1}, t), t) \quad (6.4)$$

where the left and right h -values are as given in the previous iteration.

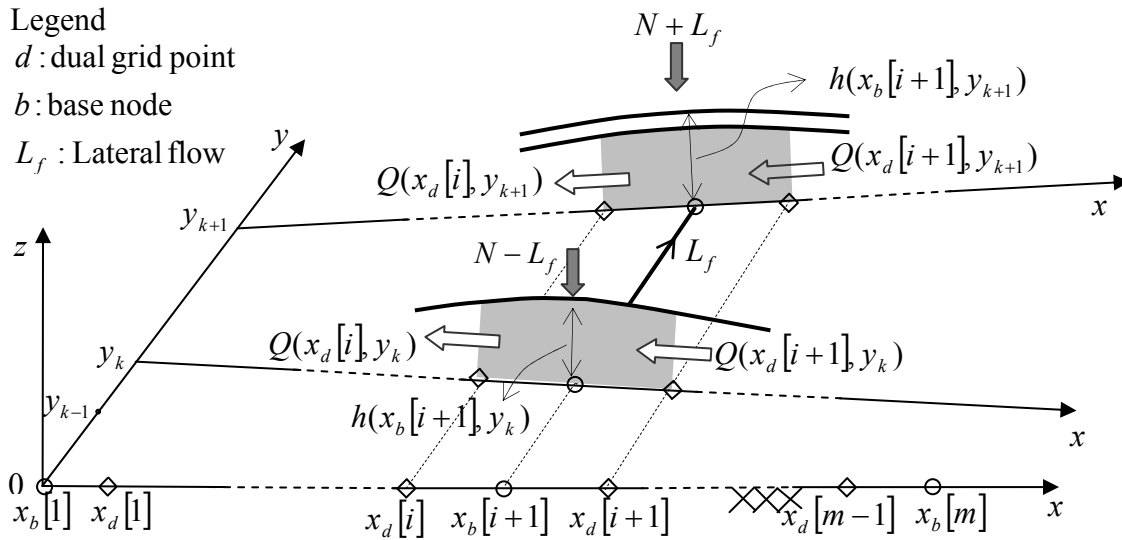


Figure 6.1: Schematic view of the spatial discretization in a two-dimensional network.

6.2.2 Further generalization of the curved Dupuit assumption

In all the models presented in Chapter 1 it was assumed that the h -values were constant over a straight line (see Section 1.3). This assumption however can easily be relaxed to h being constant over curved lines, as suggested by Figure 6.2. These lines should locally be orthogonal to the streamlines. Figure 6.2 is made based on the intuitive idea that streamlines near the bedrock follow the bedrock shape, and closer to the soil surface these streamlines become more parallel to that surface.

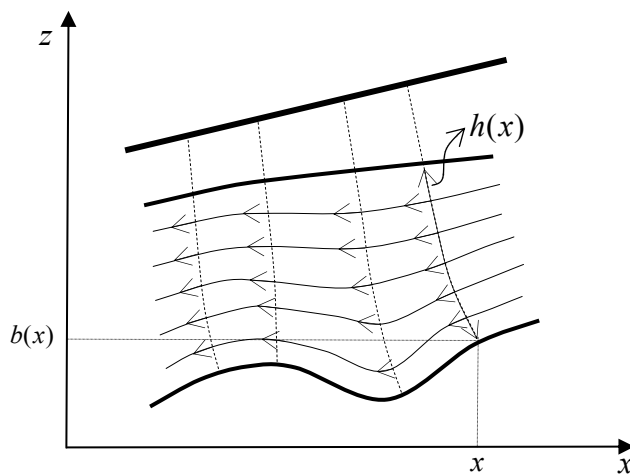


Figure 6.2: Schematic view of a possible generalization of the curved Dupuit assumption.

Appendix A: Linearization of the hillslope steady state equations

A.1 Taylor approximation

A.1.1 The Boussinesq equation

For the Boussinesq equation (see 2.2.1.2) one can derive:

$$Q_{nl}(a_1, a_2, a_3) = -K_s(a_1) a_2 (\cos^2(\beta) a_3 + \sin(\beta)) \quad (\text{A.1})$$

$$\frac{\partial Q_{nl}}{\partial a_2}(a_1, a_2, a_3) = -K_s(a_1) (\cos^2(\beta) a_3 + \sin(\beta)) \quad (\text{A.2})$$

$$\frac{\partial Q_{nl}}{\partial a_3}(a_1, a_2, a_3) = -K_s(a_1) a_2 \cos^2(\beta) \quad (\text{A.3})$$

And thus: $Q_a(a_1, a_2, a_3) = K_s(a_1) a_2 \cos^2(\beta) a_3 \quad (\text{A.4})$

$$Q_b(a_1, a_2, a_3) = -K_s(a_1) (\cos^2(\beta) a_3 + \sin(\beta)) \quad (\text{A.5})$$

$$Q_c(a_1, a_2, a_3) = -K_s(a_1) a_2 \cos^2(\beta) \quad (\text{A.6})$$

A.1.2 The extended Boussinesq equation

In a similar manner as for the previous equation, for the extended Boussinesq equation (see 2.2.1.3) we have:

$$Q_{nl}(a_1, a_2, a_3) = -K_s(a_1) w(a_1) a_2 (\cos^2(\beta) a_3 + \sin(\beta)) \quad (\text{A.7})$$

$$\frac{\partial Q_{nl}}{\partial a_2}(a_1, a_2, a_3) = -K_s(a_1) w(a_1) (\cos^2(\beta) a_3 + \sin(\beta)) \quad (\text{A.8})$$

$$\frac{\partial Q_{nl}}{\partial a_3}(a_1, a_2, a_3) = -K_s(a_1) w(a_1) a_2 \cos^2(\beta) \quad (\text{A.9})$$

and thus:

$$Q_a(a_1, a_2, a_3) = K_s(a_1) w(a_1) a_2 \cos^2(\beta) a_3 \quad (\text{A.10})$$

Since $Q_b(a_1, a_2, a_3) = \frac{\partial Q_{nl}}{\partial a_2}(a_1, a_2, a_3)$ and $Q_c(a_1, a_2, a_3) = \frac{\partial Q_{nl}}{\partial a_3}(a_1, a_2, a_3)$, $Q_b(a_1, a_2, a_3)$

and $Q_c(a_1, a_2, a_3)$ take the forms of the Equations A.8 and A.9, respectively.

A.1.3 The extended Boussinesq equation based on the slanted Dupuit

Like the previous example, for the extended Boussinesq equation based on the slanted Dupuit assumption (see 2.2.1.4) we have:

$$Q_{nl}(a_1, a_2, a_3) = \frac{-K_s(a_1) w(a_1) \cos(\beta(a_1)) a_2}{\cos(\beta(a_1) - \omega)} ((\cos(\omega) a_3) + b'(a_1)) \quad (\text{A.11})$$

$$\frac{\partial Q_{nl}}{\partial a_2}(a_1, a_2, a_3) = \frac{-K_s(a_1) w(a_1) \cos(\beta(a_1))}{\cos(\beta(a_1) - \omega)} ((\cos(\omega) a_3) + b'(a_1)) \quad (\text{A.12})$$

$$\frac{\partial Q_{nl}}{\partial a_3}(a_1, a_2, a_3) = \frac{-K_s(a_1) w(a_1) a_2 \cos(\beta(a_1))}{\cos(\beta(a_1) - \omega)} \cos(\omega) \quad (\text{A.13})$$

and thus:

$$Q_a(a_1, a_2, a_3) = \frac{K_s(a_1) w(a_1) a_2 \cos(\beta(a_1))}{\cos(\beta(a_1) - \omega)} (\cos(\omega) a_3) \quad (\text{A.14})$$

Since $Q_b(a_1, a_2, a_3) = \frac{\partial Q_{nl}}{\partial a_2}(a_1, a_2, a_3)$ and $Q_c(a_1, a_2, a_3) = \frac{\partial Q_{nl}}{\partial a_3}(a_1, a_2, a_3)$, $Q_b(a_1, a_2, a_3)$

and $Q_c(a_1, a_2, a_3)$ take the forms of the Equations A.12 and A.13, respectively.

A.1.4 The extended Boussinesq equation based on the curved Dupuit

To linearize the extended Boussinesq equation based on the curved Dupuit assumption (see 2.2.1.5) we have:

$$Q_{nl}(a_1, a_2, a_3) = \frac{K_s(a_1) w(a_1) \cos(\beta(a_1))}{\kappa_B(a_1)} \ln(1 - a_2 \kappa_B(a_1)) \cdot (\cos(\beta(a_1)) a_3 + b'(a_1) - \sin(\beta(a_1)) \kappa_B(a_1) a_2) \quad (\text{A.15})$$

$$\frac{\partial Q_{nl}}{\partial a_2}(a_1, a_2, a_3) = \frac{K_s(a_1) w(a_1) \cos(\beta(x))}{\kappa_B(a_1)} \left[(\ln(1 - a_2 \kappa_B(a_1)) (-\sin(\beta(a_1)) \kappa_B(a_1))) + \left(\frac{-\kappa_B(a_1)}{1 - a_2 \kappa_B(a_1)} \right) (\cos(\beta(a_1)) a_3 + b'(a_1) - \sin(\beta(a_1)) \kappa_B(a_1) a_2) \right] \quad (\text{A.16})$$

$$\frac{\partial Q_{nl}}{\partial a_3}(a_1, a_2, a_3) = \frac{K_s(a_1) w(a_1) \cos(\beta(x))}{\kappa_B(a_1)} (\cos(\beta(a_1)) \ln(1 - a_2 \kappa_B(a_1))) \quad (\text{A.17})$$

and thus:

$$Q_a(a_1, a_2, a_3) = \frac{K_s(a_1) w(a_1) \cos(\beta(x))}{\kappa_B(a_1)} \left[(\ln(1 - a_2 \kappa_B(a_1)) b'(a_1)) + \left(\frac{\kappa_B(a_1)}{1 - a_2 \kappa_B(a_1)} \right) (\cos(\beta(a_1)) a_3 + b'(a_1) - \sin(\beta(a_1)) \kappa_B(a_1) a_2) \right] \quad (\text{A.18})$$

Since $Q_b(a_1, a_2, a_3) = \frac{\partial Q_{nl}}{\partial a_2}(a_1, a_2, a_3)$ and $Q_c(a_1, a_2, a_3) = \frac{\partial Q_{nl}}{\partial a_3}(a_1, a_2, a_3)$, $Q_b(a_1, a_2, a_3)$ and

$Q_c(a_1, a_2, a_3)$ take the forms of the Equations A.16 and A.17, respectively.

A.2 Ad hoc method

A.2.1 The Boussinesq equation

For the Boussinesq equation (see 2.2.1.2), the ad hoc method results in:

$$Q_a(a_1, a_2, a_3) = -K_s(a_1) a_2 \sin(\beta) \quad (\text{A.19})$$

$$Q_b(a_1, a_2, a_3) = 0 \quad (\text{A.20})$$

$$Q_c(a_1, a_2, a_3) = -K_s(a_1) a_2 \cos^2(\beta) \quad (\text{A.21})$$

A.2.2 The extended Boussinesq equation

In a similar manner as for the previous equation, for the extended Boussinesq equation (see 2.2.1.3) we have:

$$Q_a(a_1, a_2, a_3) = -K_s(a_1) w(a_1) a_2 \sin(\beta) \quad (\text{A.22})$$

$$Q_b(a_1, a_2, a_3) = 0 \quad (\text{A.23})$$

$$Q_c(a_1, a_2, a_3) = -K_s(a_1) w(a_1) a_2 \cos^2(\beta) \quad (\text{A.24})$$

A.2.3 The extended Boussinesq equation based on the slanted Dupuit assumption

The ad hoc method for this equation (see 2.2.1.4) results in:

$$Q_a(a_1, a_2, a_3) = \frac{-K_s(a_1) w(a_1) a_2 \cos(\beta(a_1))}{\cos(\beta(a_1) - \omega)} b'(a_1) \quad (\text{A.25})$$

$$Q_b(a_1, a_2, a_3) = 0 \quad (\text{A.26})$$

$$Q_c(a_1, a_2, a_3) = \frac{-K_s(a_1) w(a_1) a_2 \cos(\beta(a_1))}{\cos(\beta(a_1) - \omega)} \cos(\omega) \quad (\text{A.27})$$

A.2.4 The extended Boussinesq equation based on the curved Dupuit assumption

In a similar manner as for the previous example, the ad hoc method for this equation (see 2.2.1.5) leads to:

$$Q_a(a_1, a_2, a_3) = \frac{K_s(a_1) w(a_1) \cos(\beta(a_1))}{\kappa_B(a_1)} (\ln(1 - a_2 \kappa_B(a_1)) (b'(a_1) - \sin(\beta(a_1)) \kappa_B(a_1) a_2)) \quad (\text{A.28})$$

$$Q_b(a_1, a_2, a_3) = 0 \quad (\text{A.29})$$

$$Q_c(a_1, a_2, a_3) = \frac{K_s(a_1) w(a_1) \cos(\beta(a_1))}{\kappa_B(a_1)} (\cos(\beta(a_1)) \ln(1 - a_2 \kappa_B(a_1))) \quad (\text{A.30})$$

Appendix B: Other linearization methods

Transforming h to η^2 and substitution in Equation 2.25 results in:

$$Q^{(n+1)}(x) = Q_a\left(x, h^{(n)}(x), \frac{\partial h^{(n)}}{\partial x}(x)\right) + Q_b\left(x, h^{(n)}(x), \frac{\partial h^{(n)}}{\partial x}(x)\right) (\eta^{(n+1)}(x))^2 + Q_c\left(x, h^{(n)}(x), \frac{\partial h^{(n)}}{\partial x}(x)\right) \left(2\eta^{(n)}(x) \frac{\partial \eta^{(n+1)}}{\partial x}(x)\right) \quad (\text{B.1})$$

if we assume that $\eta = \eta^{(n)} + (\eta - \eta^{(n)})$, then we have

$$\eta^2 = (\eta^{(n)})^2 + 2(\eta - \eta^{(n)})\eta^{(n)} + (\eta - \eta^{(n)})^2 \quad (\text{B.2})$$

Due to small value of the third term, neglecting this term results in

$$\eta^2 = 2\eta^{(n)}\eta - (\eta^{(n)})^2 \quad (\text{B.3})$$

Substitution of this equation in the second term of Equation B.1 leads to

$$\begin{aligned}
 Q^{(n+1)}(x) = & \left\{ Q_a \left(x, h^{(n)}(x), \frac{\partial h^{(n)}}{\partial x}(x) \right) - Q_b \left(x, h^{(n)}(x), \frac{\partial h^{(n)}}{\partial x}(x) \right) (\eta^{(n)})^2 \right\} \\
 & + Q_b \left(x, h^{(n)}(x), \frac{\partial h^{(n)}}{\partial x}(x) \right) (2\eta^{(n)} \eta^{(n+1)}) + Q_c \left(x, h^{(n)}(x), \frac{\partial h^{(n)}}{\partial x}(x) \right) \left(2\eta^{(n)}(x) \frac{\partial \eta^{(n+1)}}{\partial x}(x) \right)
 \end{aligned} \tag{B.4}$$

In case this approach leads to a numerical problem, it can be avoided as follows. In the first approach we adopted $\frac{\partial \eta^2}{\partial x} = 2\eta^{(n)}(x) \frac{\partial \eta^{(n+1)}}{\partial x}(x)$, whereas it can be written as

$\frac{\partial \eta^2}{\partial x} = \eta^{(n)}(x) \frac{\partial \eta^{(n+1)}}{\partial x}(x) + \eta^{(n+1)}(x) \frac{\partial \eta^{(n)}}{\partial x}(x)$. Using this equation, Equation B.1 becomes:

$$\begin{aligned}
 Q^{(n+1)}(x) = & Q_a \left(x, h^{(n)}(x), \frac{\partial h^{(n)}}{\partial x}(x) \right) + Q_b \left(x, h^{(n)}(x), \frac{\partial h^{(n)}}{\partial x}(x) \right) (\eta^{(n+1)}(x))^2 + \\
 & Q_c \left(x, h^{(n)}(x), \frac{\partial h^{(n)}}{\partial x}(x) \right) \left(\eta^{(n)}(x) \frac{\partial \eta^{(n+1)}}{\partial x}(x) + \eta^{(n+1)}(x) \frac{\partial \eta^{(n)}}{\partial x}(x) \right)
 \end{aligned} \tag{B.5}$$

which can be rewritten as

$$\begin{aligned}
 Q^{(n+1)}(x) = & \left\{ Q_a \left(x, h^{(n)}(x), \frac{\partial h^{(n)}}{\partial x}(x) \right) - Q_b \left(x, h^{(n)}(x), \frac{\partial h^{(n)}}{\partial x}(x) \right) (\eta^{(n)})^2 \right\} \\
 & + \left\{ Q_b \left(x, h^{(n)}(x), \frac{\partial h^{(n)}}{\partial x}(x) \right) 2\eta^{(n)} + Q_c \left(x, h^{(n)}(x), \frac{\partial h^{(n)}}{\partial x}(x) \right) \left(\frac{\partial \eta^{(n)}}{\partial x}(x) \right) \right\} \eta^{(n+1)} \\
 & + Q_c \left(x, h^{(n)}(x), \frac{\partial h^{(n)}}{\partial x}(x) \right) \eta^{(n)}(x) \frac{\partial \eta^{(n+1)}}{\partial x}(x)
 \end{aligned} \tag{B.6}$$

As a third approach the $\frac{\partial \eta^2}{\partial x}$ term can be defined as

$$\frac{\partial \eta^2}{\partial x} = (\alpha) \eta^{(n)}(x) \frac{\partial \eta^{(n+1)}}{\partial x}(x) + (2 - \alpha) \eta^{(n+1)}(x) \frac{\partial \eta^{(n)}}{\partial x}(x) \tag{B.7}$$

Compared to the previous approach, in this case the coefficients of the Q_c -terms are as follows:

$$\begin{aligned}
 Q^{(n+1)}(x) = & \left\{ Q_a \left(x, h^{(n)}(x), \frac{\partial h^{(n)}}{\partial x}(x) \right) - Q_b \left(x, h^{(n)}(x), \frac{\partial h^{(n)}}{\partial x}(x) \right) (\eta^{(n)})^2 \right\} \\
 & + \left\{ Q_b \left(x, h^{(n)}(x), \frac{\partial h^{(n)}}{\partial x}(x) \right) 2\eta^{(n)} + (2 - \alpha) Q_c \left(x, h^{(n)}(x), \frac{\partial h^{(n)}}{\partial x}(x) \right) \left(\frac{\partial \eta^{(n)}}{\partial x}(x) \right) \right\} \eta^{(n+1)} \\
 & + \alpha Q_c \left(x, h^{(n)}(x), \frac{\partial h^{(n)}}{\partial x}(x) \right) \eta^{(n)}(x) \frac{\partial \eta^{(n+1)}}{\partial x}(x)
 \end{aligned} \tag{B.8}$$

The other type of transformation ($h = e^\eta$) leads to an alternative form of the Equation 2.25 as follows

$$\begin{aligned}
 Q^{(n+1)}(x) = & Q_a \left(x, h^{(n)}(x), \frac{\partial h^{(n)}}{\partial x}(x) \right) + Q_b \left(x, h^{(n)}(x), \frac{\partial h^{(n)}}{\partial x}(x) \right) \left(e^{\eta^{(n+1)}(x)} \right) + \\
 & Q_c \left(x, h^{(n)}(x), \frac{\partial h^{(n)}}{\partial x}(x) \right) \left(e^{\eta^{(n)}(x)} \frac{\partial \eta^{(n+1)}}{\partial x}(x) \right)
 \end{aligned} \tag{B.9}$$

Using the Taylor approximation for the $e^{\eta^{(n+1)}(x)}$ term results in

$$e^\eta = e^{\eta^{(n)}} + e^{\eta^{(n)}} (\eta - \eta^{(n)}) \tag{B.10}$$

Substitution of this equation in Equation B.9 gives

$$\begin{aligned}
 Q^{(n+1)}(x) = & Q_a \left(x, h^{(n)}(x), \frac{\partial h^{(n)}}{\partial x}(x) \right) + Q_b \left(x, h^{(n)}(x), \frac{\partial h^{(n)}}{\partial x}(x) \right) \left(e^{\eta^{(n)}(x)} \right) \\
 & - Q_b \left(x, h^{(n)}(x), \frac{\partial h^{(n)}}{\partial x}(x) \right) \left(\ln \left(e^{\eta^{(n)}} \right) e^{\eta^{(n)}(x)} \right) + Q_b \left(x, h^{(n)}(x), \frac{\partial h^{(n)}}{\partial x}(x) \right) \left(e^{\eta^{(n)}(x)} \right) \eta \\
 & + Q_c \left(x, h^{(n)}(x), \frac{\partial h^{(n)}}{\partial x}(x) \right) \left(e^{\eta^{(n)}(x)} \right) \frac{\partial \eta^{(n+1)}}{\partial x}(x)
 \end{aligned} \tag{B.11}$$

The terms Q_a , Q_b and Q_c that are involved in the construction of Q_{nl} are defined using Equations B.4, B.6, B.8, and B.11, respectively, for the first, second, third (state transformation in square form) and fourth approach (state transformation in exponential form). For a discussion of the results of using this type of linearization, the reader is referred to Chapter 4.

Appendix C: A remark on the local density of grids

The density of grid points does affect the quality of the numerical approximation. In general, one can say that a higher local density improves the results at that position. Figure C.1 illustrates a more subtle effect. Here the difference in resolution between two neighboring regions causes numerical irregularities near the transition.

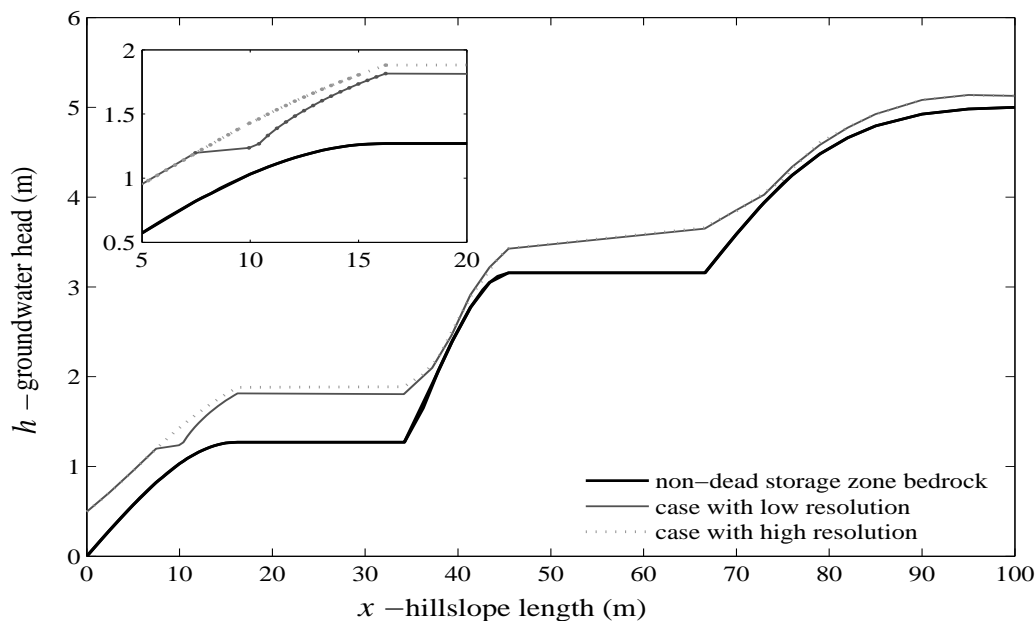


Figure C.1: The effect of the local density of the grid on the quality of the numerical approximation.

Appendix D: Tridiagonal matrix method

To implement the tridiagonal matrix method, three vectors of main, lower and upper diagonals are used. Hence, elements to construct \mathbf{A} and \mathbf{b} are given by (also see Figure D.1):

1- For the first row that represents the left hand side boundary condition:

$$\begin{aligned} A_{md}[1] &= (\alpha_L + \beta_L q_l[1]) \\ A_{ud}[1] &= \beta_L q_r[1] \\ b[1] &= \gamma_L - \beta_L q_0[1] \end{aligned} \quad (D.1)$$

2- For internal points ($i = 2, \dots, m-1$):

$$\begin{aligned} A_{md}[i] &= q_l[i] - q_r[i-1] - N_1[i] \\ A_{ld}[i-1] &= -q_l[i-1] \\ A_{ud}[i] &= q_r[i] \\ b[i] &= q_0[i-1] - q_0[i] + N_0[i] \end{aligned} \quad (D.2)$$

3- For the last row that represents the right hand side boundary condition:

$$\begin{aligned} A_{md}[m] &= (\alpha_R + \beta_R q_r[m-1]) \\ A_{ld}[m-1] &= \beta_R q_l[m-1] \\ b[m] &= \gamma_R - \beta_R q_0[m-1] \end{aligned} \quad (D.3)$$

where subscripts md , ld and ud indicate main diagonal, lower diagonal and upper diagonal, respectively.

Another step in this procedure is construction of \mathbf{M} , \mathbf{L} , \mathbf{U} and \mathbf{Z} vectors based on the Crout factorization algorithm (Burden and Faires, 1997) as follows:

1- For the first row: $M_d[1] = A_{md}[1]$

$$\begin{aligned} U_d[1] &= A_{ud}[1] / M_d[1] \\ b[1] &= \gamma_L - \beta_L q_0[1] \\ Z[1] &= b[1] / M_d[1] \end{aligned} \quad (D.4)$$

2- For internal points ($i = 2, \dots, m-1$):

$$\begin{aligned} M_d[i] &= A_{md}[i] - [L_d[i-1]U_d[i-1]] \\ U_d[i] &= A_{ud}[i] / M_d[i] \\ L_d[i-1] &= A_{ld}[i-1] \\ b[i] &= q_0[i-1] - q_0[i] + N_0[i] \\ Z[i] &= (1/M_d[i])(b[i] - L_d[i-1]Z[i-1]) \end{aligned} \quad (D.5)$$

3- For the last row:

$$\begin{aligned} L_d[m-1] &= A_{ld}[m-1] \\ M_d[m] &= A_{md}[m] - (L_d[m-1]U_d[m-1]) \\ b[m] &= \gamma_R - \beta_R q_0[m-1] \end{aligned}$$

$$Z[m] = (1/M_d[m])(b[m] - L[m-1]Z[m-1]) \quad (D.6)$$

Finally \mathbf{h} is calculated by:

$$1\text{- for last row: } h^{(n+1)}[m] = Z[m] \quad (D.7)$$

$$2\text{- for } i = m-1, \dots, 1: h^{(n+1)}[i] = Z[i] - (U_d[i] h^{(n+1)}[i+1]) \quad (D.8)$$

$$\mathbf{A} = \begin{bmatrix} A_{md}[1,1] & A_{ud}[1,2] & 0 & \dots & 0 & 0 & 0 \\ A_{ld}[2,1] & A_{md}[2,2] & A_{ud}[2,3] & \dots & 0 & 0 & 0 \\ \vdots & \vdots & \vdots & \ddots & \vdots & \vdots & \vdots \\ \vdots & \vdots & \vdots & \ddots & \vdots & \vdots & \vdots \\ 0 & 0 & 0 & \dots & A_{ld}[m-1, m-2] & A_{md}[m-1, m-1] & A_{ud}[m-1, m] \\ 0 & 0 & 0 & \dots & 0 & A_{ld}[m, m-1] & A_{md}[m, m] \end{bmatrix}$$

$$\mathbf{h} = \begin{bmatrix} h[1] \\ h[2] \\ \vdots \\ h[m-1] \\ h[m] \end{bmatrix}, \quad \mathbf{b} = \begin{bmatrix} b[1] \\ b[2] \\ \vdots \\ b[m-1] \\ b[m] \end{bmatrix}$$

Figure D.1: Structure of matrix \mathbf{A} , and vectors \mathbf{h} and \mathbf{b} in tridiagonal method.

Appendix E: Examples of the hillslope unsteady equations

E.1 Dynamic Dupuit equation

For the dynamic Dupuit equation, its transformed form in time and space becomes:

$$0 = \frac{\partial}{\partial x} \left(K_s(x) w(x) h(\hat{t}, x) \frac{\partial h}{\partial x}(\hat{t}, x) \right) + N(\hat{t}, x, h(\hat{t}, x)) w(x) - f w(x) \frac{h(\hat{t}, x) - h(t_n, x)}{\hat{t} - t_n} \quad (E.1)$$

The fluxes, Q_{nl} and N_{nl} in terms of a_1, a_2 and a_3 take the form:

$$Q_{nl}(a_1, a_2, a_3) = -K_s(a_1) w(a_1) a_2 a_3 \quad (E.2)$$

$$N_{nl}(a_1, a_2) = N(a_1, a_2) w(a_1) - f w(a_1) \frac{a_2 - h_n(a_1)}{\hat{t} - t_n} \quad (E.3)$$

where h_n is the known state variable from previous time step t_n .

E.2 Dynamic Boussinesq equation

The transformed form of the unsteady Boussinesq equation in time and space becomes:

$$0 = \frac{\partial}{\partial x} \left(K_s(x) h(\hat{t}, x) \left(\cos^2(\beta) \frac{\partial h}{\partial x}(\hat{t}, x) + \sin(\beta) \right) \right) + N(\hat{t}, x, h(\hat{t}, x)) - f \frac{h(\hat{t}, x) - h(t_n, x)}{\hat{t} - t_n} \quad (\text{E.4})$$

The fluxes, Q_{nl} and N_{nl} in terms of a_1, a_2 and a_3 take the forms:

$$Q_{nl}(a_1, a_2, a_3) = -K_s(a_1) a_2 (\cos^2(\beta) a_3 + \sin(\beta)) \quad (\text{E.5})$$

$$N_{nl}(a_1, a_2) = N(a_1, a_2) - f \frac{a_2 - h_n(a_1)}{\hat{t} - t_n} \quad (\text{E.6})$$

E.3 Dynamic extended Boussinesq equation

The unsteady extended Boussinesq equation can be written as:

$$0 = \frac{\partial}{\partial x} \left(K_s(x) w(x) h(\hat{t}, x) \left(\cos^2(\beta) \frac{\partial h}{\partial x}(\hat{t}, x) + \sin(\beta) \right) \right) + N(\hat{t}, x, h(\hat{t}, x)) w(x) - f w(x) \frac{1}{\cos(\beta)} \frac{h(\hat{t}, x) - h(t_n, x)}{\hat{t} - t_n} \quad (\text{E.7})$$

The fluxes, Q_{nl} and N_{nl} in terms of a_1, a_2 and a_3 for the extended Boussinesq equation take the forms:

$$Q_{nl}(a_1, a_2, a_3) = -K_s(a_1) w(a_1) a_2 (\cos^2(\beta) a_3 + \sin(\beta)) \quad (\text{E.8})$$

$$N_{nl}(a_1, a_2) = w(a_1) N(a_1, a_2) - f w(a_1) \frac{1}{\cos(\beta)} \left(\frac{a_2 - h_n(a_1)}{\hat{t} - t_n} \right) \quad (\text{E.9})$$

E.4 Dynamic extended Boussinesq equation based on the slanted Dupuit assumption

The unsteady extended Boussinesq equation based on the slanted Dupuit assumption is written as:

$$0 = \frac{\partial}{\partial x} \left(\frac{K_s(x) w(x) h(\hat{t}, x) \cos(\beta(x))}{\cos(\beta(x) - \omega)} \left(\cos(\omega) \frac{\partial h}{\partial x}(\hat{t}, x) + b'(x) \right) \right) + N(\hat{t}, x, h(\hat{t}, x)) w(x) - f w(x) \frac{1}{\cos(\beta(x))} \left(\frac{h(\hat{t}, x) - h(t_n, x)}{\hat{t} - t_n} \right) \quad (\text{E.10})$$

As in the previous example, the fluxes in terms of a_1, a_2 and a_3 can be presented as:

$$Q_{nl}(a_1, a_2, a_3) = \frac{-K_s(a_1) w(a_1) \cos(\beta(a_1)) a_2 ((\cos(\omega) a_3) + b'(a_1))}{\cos(\beta(a_1) - \omega)} \quad (\text{E.11})$$

$$N_{nl}(a_1, a_2) = N(a_1) w(a_1) - f w(a_1) \frac{1}{\cos(\beta(a_1))} \left(\frac{a_2 - h_n(a_1)}{\hat{t} - t_n} \right) \quad (\text{E.12})$$

E.5 Dynamic extended Boussinesq equation based on the curved Dupuit assumption

The unsteady extended Boussinesq equation under the curved Dupuit assumption can be written as:

$$\begin{aligned}
 0 = & -\frac{\partial}{\partial x} \left(\frac{K_s(x) w(x) \cos(\beta(x))}{\kappa_B(x)} \ln(1 - h(\hat{t}, x) \kappa_B(x)) \right. \\
 & \left. \cdot \left(\cos(\beta(x)) \frac{\partial h}{\partial x}(\hat{t}, x) + b'(x) - \sin(\beta(x)) \kappa_B(x) h(\hat{t}, x) \right) \right) + N(\hat{t}, x, h(\hat{t}, x)) w(x) \quad (\text{E.13}) \\
 & - f w(x) \frac{1}{\cos(\beta(x))} (1 - \kappa_B(x) h(\hat{t}, x)) \left(\frac{h(\hat{t}, x) - h(t_n, x)}{\hat{t} - t_n} \right)
 \end{aligned}$$

The fluxes, Q_{nl} and N_{nl} in terms of a_1, a_2 and a_3 take the forms:

$$\begin{aligned}
 Q_{nl}(a_1, a_2, a_3) = & \frac{K_s(a_1) w(a_1) \cos(\beta(a_1))}{\kappa_B(a_1)} \ln(1 - a_2 \kappa_B(a_1)) \\
 & \cdot (\cos(\beta(a_1)) a_3 + b'(a_1) - \sin(\beta(a_1)) \kappa_B(a_1) a_2) \quad (\text{E.14})
 \end{aligned}$$

$$N_{nl}(a_1, a_2) = N(a_1, a_2) w(a_1) - f w(a_1) \frac{1}{\cos(\beta(a_1))} (1 - \kappa_B(a_1) a_2) \left(\frac{a_2 - h_n(a_1)}{\hat{t} - t_n} \right) \quad (\text{E.15})$$

References

- Anderson, M., and S. Brooks (1996), *Advances in Hillslope Processes*, 2 vols., 1306 pp., John Wiley, Hoboken, N. J.
- Anderson, M., and T. Burt (1978), The role of topography in controlling throughflow generation, *Earth Surf. Processes*, 3, 331–344.
- Akylas, E., A. D. Koussis, A. N. Yannacopoulos (2006), Analytical solution of transient flow in a sloping soil layer with recharge, *Hydrol. Sci. J.*, 51(4), 626-641.
- Basha, H. A., and S. F. Maalouf (2005), Theoretical and conceptual models of subsurface hillslope flows, *Water Resour. Res.*, 41(7), W07018, doi: 10.1029/2004WR003769.
- Bates, P.D., M. G. Anderson, D. A. Price, R. J. Hardy, and C. N. Smith (1996), Analysis and development of hydraulic models for floodplain flows, In *Floodplain Processes*, M. G. Anderson, D. E. Walling, P. D. Bates (eds). John Wiley & Sons, Chichester, 215-254.
- Bear, J. (1972), *Dynamics of Fluids in Porous Media*, Dover, Mineola, New York.
- Bear, J., and A. Verruijt (1987), *Modeling Groundwater Flow and pollution*, D. Reidel, Dordrecht.
- Berne, A., R. Uijlenhoet, and P. Troch (2005), Similarity analysis of subsurface flow response of hillslopes with complex geometry, *Water Resour. Res.*, 41(9), W09410, doi: 10.1029/2004WR003629.
- Beven, K., and P. Germann (1982), Macropores and water flow in soils, *Water Resour. Res.*, 18(5), 1311–1325.
- Bogaart, P. W., and P. A. Troch (2006), Curvature distribution within hillslopes and catchments and its effect on hydrological response, *Hydrol. Earth Syst. Sci.*, 10, 925-936.
- Boussinesq, J. (1877), Essai sur la theorie des eaux courantes. *Mem. Acad. Sci. Inst. Fr.*, 23(1): 252-60.
- Brammer, D., J. McDonnell (1995), An evolving perceptual model of hillslope hydrology at the Maimai catchment. In M. G. Anderson, S. Brooks and T. Burt (eds). *Advances in Hillslope Hydrology*, John Wiley and Sons, pp. 35-60.
- Brammer, D., J. McDonnell, C. Kendall, and L. Rowe (1995), Controls on the downslope evolution of water, solutes and isotopes in a steep forested hillslope. *EOS, Trans. AGU*, 76(46), 268.

-
- Burden, R., and D. Faires (1997), *Numerical Analysis*, Brooks/Cole, Pacific Grove, 811pp.
 - Chapman, T. (2005), Recharge-induced groundwater flow over a plane sloping bed: Solutions for steady and transient flow using physical and numerical models, *Water Resour. Res.*, 41(7), W07027, doi: 10.1029/2004WR003606.
 - Chapman, T., and G. Ong (2006), A new equation for shallow groundwater flow over a curved impermeable boundary: Numerical solutions and laboratory tests, *Water Resour. Res.*, 42(3), W03427, doi: 10.1029/2005WR004437.
 - Childs, E. (1971), Drainage of groundwater resting on a sloping bed, *Water Resour. Res.*, 7(5), 1256-1263.
 - Dunne, T., and R. Black (1970), An experimental investigation of runoff production in permeable soils, *Water Resour. Res.*, 6(2), 478–489.
 - Dunne, T., T. Moore, and C. Taylor (1975), Recognition and prediction of runoff - producing zones in humid regions, *Hydrological Sciences Bulletin*, 20, 305-327.
 - Dupuit, J. (1863), *Etudes Theoretiques et Pratiques sur le Mouvement des Eaux*, Dunod, Paris.
 - El-Hames, A. S., and K. S. Richards (1998), An integrated, physically based model for arid region flash flood prediction capable of simulating dynamic transmission loss, *Hydrol. Processes*, 12:1219-1232.
 - Fan, Y., and R. Bras (1998), Analytical solutions to hillslope subsurface storm flow and saturated overland flow, *Water Resour. Res.*, 34(4), 921–927.
 - Freer, J., J. McDonnell, K. Beven, D. Brammer, D. Burns, R. Hooper, and C. Kendal (1997), Topographic controls on subsurface storm flow at the hillslope scale for two hydrologically distinct small catchments. *Hydrol. Processes*, 11, 1347–1352.
 - Freer, J., J. McDonnell, K. Beven, N. Peters, D. Burns, R. Hooper, and B. Aulenbach (2002), The role of bedrock topography on subsurface stormflow, *Water Resour. Res.*, 38(12), 1269, doi: 10.1029/2001WR000872.
 - Freeze, R. (1972), The role of subsurface flow in generating surface runoff 2. Upstream source areas, *Water Resour. Res.*, 8(5), 1271–1283.
 - Hewlett, J., and A. Hibbert (1967), Factors affecting the response of small watersheds to precipitation in humid areas, in *Forest Hydrology*, edited by W. Sopper and H. Lull, pp. 275–290, The Pennsylvania State University, Pergamon Press, University Park, PA.

- Hilberts, A., E. van Loon, P. Troch, and C. Paniconi (2004), The hillslope-storage Boussinesq model for non-constant bedrock slope, *J. Hydrol.*, 291, 160-173.
- Hilberts, A (2006), *Low-dimensional modeling of hillslope subsurface flow Processes: Developing and testing the hillslope-storage Boussinesq model*, PhD thesis, Wageningen University, Wageningen, The Netherlands.
- Hilberts, A., P. Troch, C. Paniconi, and J. Boll (2007), Low-dimensional modelling of hillslope subsurface flow: the relationship between rainfall, recharge, and unsaturated storage dynamics, *Water Resour. Res.*, 43(3), W03445, doi: 10.1029/2006WR004964.
- Horton, R. (1933), The role of infiltration in the hydrologic cycle, *Eos, Trans. AGU*, 14, 446–460.
- Huff, D., R. O’Neill, W. Emanuel, J. Elwood, and J. Newbold (1982), Flow variability and hillslope hydrology, *Earth Surf. Processes Landforms*, 7, 91–94.
- Hutchinson, D., and R. Moore (2000), Throughflow variability on a forested hillslope underlain by compacted glacial till, *Hydrol. Process.*, 14(10), 1751-1766.
- Kirkby, M. (Ed.) (1978), *Hillslope Hydrology*, John Wiley, New York.
- Koninkrijk Nederlands Meteorologisch Instituut. Daily weather data. (<http://www.knmi.nl/klimatologie>)
- Koussis, A. D. (1992), A linear conceptual subsurface storm flow model, *Water Resour. Res.*, 28(4), 1047-1052.
- Kreyszig, E. (1983), *Advanced Engineering Mathematics*, 5th Edition, John Wiley, New York.
- McDonnell, J. (1990), A rationale for old water discharge through macropores in a steep, humid catchment, *Water Resour. Res.*, 26(11), 2821–2832.
- McDonnell, J., J. Freer, R. Hooper, C. Kendall, D. Burns, K. Beven, and J. Peters (1996). New method developed for studying flow on hillslopes. *EOS, Trans. AGU*, 77(47): 465-472.
- McDonnell, J., D. Brammer, C. Kendall, N. Hjerdt, L. Rowe, M. Stewart, and R. Woods (1998), Flow pathways on steep forested hillslopes: The tracer, tensiometer and trough approach, in *Environmental Forest Science*, edited by M. Tani, pp. 463-474, Springer, New York.
- Mehl, S. (2006), Use of Picard and Newton iteration for solving nonlinear water flow equations, *Ground Water*, 44(4), 583-594.

-
- Mikhaelides, K., and J. Wainwright (2002), Modelling the effects of hillslope-channel coupling on catchment hydrological response, *Earth Surf. Process. Landforms*, 27, 1441-1457.
 - Moore, R. D., and J. C. Thompson (1996), Are water table variations in a shallow forest soil consistent with the TOPMODEL concept? *Water Resour. Res.*, 32(3), 663-669.
 - Nutzmann, G., S. Mey, and B. Pftzner (2006), The 'coupling' of surface and subsurface watershed modeling approaches towards a better understanding of lowland hydrology, *Geophysical Research Abstracts*, Vol. 8, 07806.
 - O'Connell, P. E., and E. Todini (1996), Modeling of rainfall, flow and mass transport in hydrological systems: an overview, *J. Hydrol.*, 175, 3-16.
 - Paniconi, C., P. Troch, E. van Loon, A. Hilberts (2003), Hillslope-Storage Boussinesq model for subsurface flow and variable source areas along complex hillslopes: 2- Intercomparison with a 3D Richards equation model, *Water Resour. Res.*, 39(11), 1317.
 - Peters, D., J. Buttle, C. Taylor, and B. LaZerte (1995), Runoff production in a forested, shallow soil, Canadian Shield basin, *Water Resour. Res.*, 31(5), 1291-1304.
 - Polubarinova-Kochina, P. Y. A. (1962), *Theory of Groundwater Movement*, translated from Russian by R. J. M. DeWiest, 613 pp., Princeton Univ. Press, Princeton, N. J..
 - Seibert, J., K. Bishop, A. Rodhe, and J. McDonnell (2003), Groundwater dynamics along a hillslope: A test of the steady state hypothesis, *Water Resour. Res.*, 39(1), doi: 10.1029/2002WR001404.
 - Sloan, W. T. (2000), A physics-based function for modeling transient groundwater discharge at the watershed scale, *Water Resour. Res.*, 36(1), 225-241.
 - Tani, M. (1997), Runoff generation processes estimated from hydrological observations on a steep forested hillslope with a thin soil layer, *J. Hydrol.*, 200, 84-109.
 - Triana, E., J. W. Labadie, and T. K. Gates (2003), Stream-aquifer interaction modeling using artificial neural networks, *World Water and Environmental Resources Congress*, Philadelphia.
 - Triana, E., J. W. Labadie, and T. K. Gates (2004), Basin-scale stream-aquifer modeling of the lower Arkansas river, Colorado. *AGU Hydrology Days Conference*, Colorado.
 - Troch, P., C. Paniconi, and E. van Loon (2003), Hillslope-storage Boussinesq model for subsurface flow and variable source areas along complex hillslopes: 1- Formulation and characteristic response, *Water Resour. Res.*, 39(11), 1316.

- Troch, P., A. van Loon, and A. Hilberts (2004), Analytical solution of the linearized hillslope-storage Boussinesq equation for exponential hillslope width functions, *Water Resour. Res.*, 40(8), W08601, doi: 10.1029/2003WR002850.
- Tromp-van Meerveld, H. J., and J. J. McDonnell (2006), Threshold relations in subsurface stormflow: 1. A 147-storm analysis of the Panola hillslope, *Water Resour. Res.*, 42(2), W02410, doi:10.1029/2004WR003778.
- van Walsum, P., A. Veldhuizen, P. van Bakel, F. van der Bolt, P. Dik, P. Groenendijk, E. Querner, and M. Smit (2006), *SIMGRO 6.0.1: Theory and model implementation*, Alterra-report 913.1, Alterra, Wageningen.
- Verhoest, N., and P. Troch (2000), Some analytical solutions of the linearized Boussinesq equation with recharge for a sloping aquifer. *Water Resour. Res.*, 36(3), 793-800.
- Xiangjun, T., X. Zhenghui, Z. Shenglei, and L. Miaoling (2006), A subsurface runoff parameterization with water storage and recharge based on the Boussinesq-storage equation for a land surface model, *Science in China: Series D Earth Sciences*, 49(6), 622-631.
- Winter, T. C., J. W. Harvey, O. Lehn Franke, and W. M. Alley (1998), *Ground water and surface water: A single source*, USGS Circular 1139, Colorado, USA.
- Woods, R., and L. Rowe (1996), The changing spatial variability of subsurface flow across a hillside. *Journal of Hydrology (NZ)*, 35(1), 51-86.
- Woods, R. A., M. Sivapalan, and J. S. Robinson (1997), Modeling the spatial variability of subsurface runoff using topographic index, *Water Resour. Res.*, 33(5), 1061– 1073.

Curriculum Vitae

Kaka Shahedi, 06 September 1975, Aq-Qaleh, Iran

1989-1993:

High-school, Motahari School, Aq-Qaleh, Iran

1994-1998:

B.Sc. in Natural resources engineering (rangeland and watershed management), Gorgan Agricultural University, Gorgan, Iran

1998-2000:

M.Sc. in Watershed management engineering, Faculty of Natural Resources, Tehran University, Tehran, Iran

2001-2003:

Staff member, Faculty of Natural Resources, University of Mazandaran, Sari, Iran

2003-2008:

Ph.D. candidate in Hydrology and Quantitative Water Management group, Center for Water and Climate, Environmental Sciences Department, Wageningen University, Wageningen, the Netherlands

2008:

Netherlands Research School diploma for the Socio-economic and Natural Sciences of the Environment (SENSE)

Contact e-mail address:

kaka.shahedi@wur.nl

kaka.shahedi@gmail.com



Netherlands Research School for the
Socio-Economic and Natural Sciences of the Environment

CERTIFICATE

The Netherlands Research School for the
Socio-Economic and Natural Sciences of the Environment
(SENSE), declares that

Kaka Shahedi

Born on: *6 September 1975* at: *Aq Qaleh, Iran*

has successfully fulfilled all requirements of the
Educational Programme of SENSE.

Place: *Wageningen* Date: *18 June 2008*

the Chairman of the
SENSE board

Prof. dr. R. Leemans

the SENSE Director
of Education

Dr. C. Kroeze



The SENSE Research School declares that Mr. Kaka Shahedi has successfully fulfilled all requirements of the Educational PhD Programme of SENSE with a work load of 44 ECTS, including the following activities:

SENSE PhD courses:

- Environmental Research in Context
- Research Context Activity: "Writing of research proposal on 'Extreme hydrological response by physically hillslope model and extrapolation to ungauged catchments' and public communication of dissertation results"
- Techniques for Writing and Presenting Scientific Papers
- Art of Modelling
- Land science: land-use and landscape dynamics
- Uncertainty Analysis

Other Phd and MSc courses:

- Hydraulics and Hydrometry
- Introduction to Geo-information Science
- Hydrological modeling (theory and practice)
- Fluency speaking
- Academic writing I and II
- Scientific Writing

Poster Presentations:

- European Geosciences Union, General Assembly, 13 – 18 April 2008, Vienna Austria

Deputy director SENSE
Dr. A. van Dommelen

Samenvatting

Shahedi, K. 2008. *Hydrologisch modelleren van hellingen: de rol van de geometrie van de ondoorlatende laag en de helling-waterloop koppeling*, Proefschrift, Wageningen Universiteit, Wageningen, Nederland.

Dit proefschrift handelt over het hydrologische gedrag van hellingen als een belangrijk onderdeel van de hydrologische processen die ten grondslag liggen aan de reactie van stroomgebieden op neerslag. De meest fysische modellen hiervoor zijn drie-dimensionaal en omwille hiervan zeer complex in formulering en zeer moeilijk numeriek op te lossen. Daarom ligt de nadruk hier op ééndimensionale modellen van grondwaterstroming in hellingen. De kern van dit onderzoek is het bestuderen van hoe de gesimuleerde reactie van een helling op neerslag wordt beïnvloed door verschillende vereenvoudigende aannames over de geometrie van hellingen en over de randvoorwaarden.

Modellen van de hydrologische respons van hellingen zijn op verschillende wijzen aangepast om de complexiteit van de geometrie van de onderkant van de stroomvoerende laag mee te kunnen nemen. Om deze modellen op te lossen en om ze te kunnen vergelijken is een algemeen en flexibel numeriek algoritme ontwikkeld. Met deze opgestelde modellen en dit voorgestelde numerieke algoritme is een aantal vraagstukken onderzocht: (a) het onderzoeken van de rol die de benedenstroomse randvoorwaarde speelt in de respons van het grondwater, (b) het bestuderen van de invloed van de geometrie van de onderkant van de stroomvoerende laag op de hydrologische respons van een helling en (c) het nabootsen van de respons van een helling met een quasi-stationaire techniek. Evaluatie van het numerieke algoritme toont aan dat het flexibel is en kan omgaan met deze verschillende modellen, die voor verschillende doeleinden zijn toegepast, en dat de massabalans sluit.

De volgende conclusies kunnen worden getrokken uit het evalueren van de ontwikkelde modellen: (a) Een verband tussen de stijghoogte en de afvoer als benedenstroomse randvoorwaarde is een goed alternatief voor een gekoppeld helling-waterloop systeem; (b) Het recessiegedrag van hellingen hangt af van de geometrie van de onderkant van de stroomvoerende laag, en locale minima en maxima in het profiel van deze laag hebben invloed op de stijghoogte van het grondwater voor lage regenintensiteiten; (c) De quasi-stationaire benadering is een eenvoudige maar adequate methode (zowel in complexiteit als in vereiste rekentijd) om de dynamica van grondwater in hellingen te simuleren.

Samenvattend is dit proefschrift gericht op het verkrijgen van theoretisch inzicht in de manier waarop hydrologische processen in hellingen (grondwaterstroming en dynamica van de grondwaterspiegel) reageren op de geometrische complexiteit van de onderkant van de stroomvoerende laag en de benedenstroomse randvoorwaarde. Het gepresenteerde numerieke algoritme kan veel toepassingen vinden in onderzoeken op het gebied van de hellinghydrologie door de algemeenheid en flexibiliteit ervan.

Kernwoorden: *Hellinghydrologie, hydrologisch modelleren, geometrie van de onderkant van de stroomvoerende laag, randvoorwaarde, numerieke oplossing.*

در این رساله مطالعه عکس العمل هیدرولوژیکی دامنه‌ها بعنوان موضوعی مهم در کشف و درک فرآیندهای هیدرولوژیکی موثر در واکنش حوضه‌های آبخیز نسبت به وقایع بارندگی مورد تاکید است. بدلیل مشکلات (پیچیده بودن روابط و زمانبر بودن محاسبات) روابط ریاضی سه بعدی، تاکید این تحقیق بر روی مدل‌های فیزیکی یک بعدی جریان آب زیرزمینی می‌باشد که اطلاعات مورد نیاز آنها تا حد امکان از پارامترهای توپوگرافی مشتق می‌گردد. هدف عمده این تحقیق مطالعه چگونگی تاثیر فرضیه‌های ساده سازی شکل هندسی دامنه و شرایط مرزی بر روی شبیه سازی عکس العمل هیدرولوژیکی دامنه میباشد. تعمیم و ساده سازی های متعددی جهت لحاظ نمودن اشکال هندسی پیچیده سنگ بستر در مدل‌های عکس العمل هیدرولوژیکی دامنه انجام شده است. در این تحقیق به منظور مطالعه و مقایسه این مدل‌ها یک الگوریتم حل عددی پیشنهاد گردید. با استفاده از این الگوریتم، مدل‌های شبیه سازی عکس العمل هیدرولوژیکی برای شرایط (فرضیات) مختلف اجرا شدند تا: (1) نقش شرط مرزی پایین دست دامنه بر روی خروجی آب زیرزمینی بررسی شود، (2) نقش شکل هندسی سنگ بستر بر روی عکس العمل هیدرولوژیکی دامنه مطالعه گردد و (3) عکس العمل هیدرولوژیکی دامنه با استفاده از روش شبیه سازی نیمه ماندگار شبیه سازی شود.

ارزیابی الگوریتم حل عددی نشان میدهد که این الگوریتم منعطف بوده و قادر است که همه این مدل‌های مختلف را که برای اهداف مختلف بکار میروند ضمن رعایت قانون بقاء جرم حل نماید.

ارزیابی مدل‌های بسط داده شده در این تحقیق نتایج زیر را آشکار می‌سازد: (1) رابطه دبی-ارتفاع به عنوان شرط مرزی پایین دست دامنه گزینه ای مناسب جهت بررسی سیستم مرکب دامنه-آبراهه میباشد (2) خصوصیات بازدارندگی (تاخیری) دامنه بستگی به پروفیل سنگ بستر دامنه دارد و برای بارندگی های با شدت کم، پستی و بلندیهای کوچک در امتداد نیمرخ طولی سنگ بستر بر ارتفاع سطح ایستابی دامنه موثر است و (3) شبیه سازی نیمه ماندگار، روشی ساده (هم از نظر مدل و هم از نظر زمان لازم برای محاسبات) جهت شبیه سازی دینامیک آب زیرزمینی است.

بطور خلاصه هدف این رساله درک نظری واکنش فرآیند های هیدرولوژیکی (جریان زیرسطحی و دینامیک سفره آب زیرزمینی) به شکل پروفیل سنگ بستر و شرط مرزی پایین دست دامنه میباشد. الگوریتم حل عددی پیشنهادی بخاطر عمومیت و انعطاف پذیری می‌تواند در بسیاری از تحقیقات مربوط به هیدرولوژی دامنه بکار گرفته شود.

با تشکر از دوست گرامی آقای دکتر واحد بردی شیخ در ویراستاری چکیده فارسی



دانشگاه واخنینگن هند
دپارتمان علوم محیطی (مرکز مطالعات آب و اقلیم)
گروه هیدرولوژی و مدیریت کمی آب

رساله دکتری تخصصی (PhD)

مدل بندی هیدرولوژیک دامنه:
بررسی نقش شکل هندسی سنگ بسترو اثرات متقابل دامنه و آبراهه

کاکا شاهی
خرداد - 1387 (واخنینگن هند)

This research was financially supported by the Ministry of Science, Research and Technology (MSRT) of Iran.

Cover pages:

Back: Shows a hilly area in Iran.

Printed at:

Printing office Ponsen & Looijen b.v., Wageningen